

LUKAS KRIECHBAUM

# Storage Concepts and Transient Analysis of Solar Thermal Power Plants

Diploma Thesis

Graz University of Technology

Institute for Thermal Turbomachinery and Machine Dynamics

Head: Univ.-Prof. Dr.-Ing. Franz Heitmeir

Supervisor: Ao.Univ.-Prof. Dipl.-Ing. Dr.techn. Wolfgang Sanz

Graz, November 2012

This document was written with GNU Emacs, is set in Palatino, compiled with pdfL<sup>A</sup>T<sub>E</sub>X<sub>2</sub>ε and Biber.

The L<sup>A</sup>T<sub>E</sub>X template from Karl Voit is based on KOMA script and can be found online:  
<https://github.com/novoid/LaTeX-KOMA-template>

# Abstract

Solar thermal power plants are a good alternative to reduce the use of fossil fuels in power production. But power production is limited by the availability of solar irradiance. At night and during cloudy periods such a plant cannot be operated. By integrating a thermal energy storage system, power production can be decoupled from the availability of solar irradiance.

Performance prediction and annual yield analysis are important methods to determine optimum solar field size and storage capacity. The process simulation environment IPSEpro is a suitable and powerful tool for this kind of calculations. Nowadays time series simulations in IPSEpro are conducted in combination with MS Excel. A new approach is to carry out such calculations with IPSEpro and using an automation script instead of MS Excel.

A model of a solar thermal power plant with thermal energy storage is set up. The model consists of a transient solar field and thermal energy storage system model and a steady state model of the power block. Transient solar field components are developed from already existing steady-state models. Component models for a two-tank and a thermocline thermal energy storage system are created.

Several automation scripts are implemented. Performance predictions and annual yield analyses are conducted for different solar multiples and storage capacities. For a power plant with a two-tank storage system as well as for a power plant with a thermocline storage system.

# Kurzfassung

Solar-thermische Kraftwerke sind eine gute Alternative um fossile Brennstoffe in der Stromerzeugung zu ersetzen. Bei Solarkraftwerken ist die Stromerzeugung allerdings beschränkt auf Zeiten solarer Einstrahlung. Durch die Integration eines thermischen Speichers kann die Stromerzeugung von der solaren Einstrahlung entkoppelt werden.

Die Vorhersage der Performance und Jahresertragsrechnung sind wichtige Analyseverfahren um die optimale Solarfeldgröße Speicherkapazität eines solarthermischen Kraftwerks zu bestimmen. Für derartige Berechnungen ist die Prozesssimulationsumgebung IPSEpro eine geeignete und mächtige Software. Derzeit werden Zeitreihensimulationen in IPSEpro in Verbindung mit MS Excel durchgeführt. Ein neuer Ansatz ist nun, für solche Berechnungen ein Automatisierungsscript anstatt MS Excel zu verwenden.

Aus diesem Grund wurde ein Modell eines solarthermischen Kraftwerks mit thermischem Energiespeicher erstellt. Das Solarfeld und die Speichermodelle werden mit transienten Gleichungen modelliert, der kalorische Kraftwerksteil ist ein Modell mit stationären Gleichungen. Die transienten Modelle des Solarfeldes basieren auf schon existierenden stationären Modellen. Ein Zwei-Tank Speichermodell und ein Modell eines thermischen Schichtspeichers werden erstellt.

Mithilfe eines Automatisierungsscripts werden Performance-Vorhersagen und Jahresertragsrechnungen für verschiedene Solarfeld- und Speichergrößen für die Kraftwerksmodelle mit dem Zwei-Tank Speicher und dem Schichtspeicher durchgeführt.

## Statutory Declaration

I declare that I have authored this thesis independently, that I have not used other than the declared sources/resources, and that I have explicitly marked all material which has been quoted either literally or by content from the used sources.

Graz, \_\_\_\_\_  
Date

\_\_\_\_\_  
Signature

## Eidesstattliche Erklärung<sup>1</sup>

Ich erkläre an Eides statt, dass ich die vorliegende Arbeit selbstständig verfasst, andere als die angegebenen Quellen/Hilfsmittel nicht benutzt, und die den benutzten Quellen wörtlich und inhaltlich entnommene Stellen als solche kenntlich gemacht habe.

Graz, am \_\_\_\_\_  
Datum

\_\_\_\_\_  
Unterschrift

---

<sup>1</sup>Beschluss der Curricula-Kommission für Bachelor-, Master- und Diplomstudien vom 10.11.2008; Genehmigung des Senates am 1.12.2008



# Preface and Acknowledgement

Ever since starting my studies of mechanical engineering in 2006, I have been certain about my focus on energy and environmental engineering. My thermal engineering professor made me aware of the anthropogenic influence on climate change.

This topic caught my interest. I attended many lectures about renewable and sustainable energy systems. Therefore, I am finally finishing my studies with this thesis about storage concepts and transient analysis of solar thermal power plants.

I would like to thank my supervisor a.o.Univ.-Prof. Dipl.-Ing. Dr.techn. Wolfgang Sanz for thoroughly reading the final version of my thesis and for offering help during the past few months.

Special thanks goes to the staff at the company SimTech GmbH for the cooperation, support and the nice time there. Thank you Vera for helping me to draw the one or other sketch on the computer. Thank you Erhard for answering the all questions regarding IPSEpro nobody else could help me further with. Thank you Stefan for being patient with me and always having time to answer my questions. Thank you for all the awesome bike tours around Graz.

Furthermore, I want to thank my predecessor at SimTech GmbH Fritz Zaversky for implementing the solar irradiation and steady state solar collector component models into IPSEpro. Thanks also goes to Dr.-Ing. Jürgen Rheinländer. His RESYSpro model library gave inspired me a lot of inspiration for my own transient component models.

Finally I would like to thank all the trees which had to give their life for the paper this thesis is printed on.





# Contents

<b>1</b>	<b>Introduction</b>	<b>1</b>
1.1	Solar Thermal Power . . . . .	1
1.2	Solar Thermal Power with Thermal Energy Storage . . . . .	5
1.3	Objective . . . . .	7
1.4	Method . . . . .	7
1.5	Report Outline . . . . .	7
<b>2</b>	<b>Thermal Energy Storage for Solar Thermal Power Plants</b>	<b>9</b>
2.1	Thermal Energy Storage . . . . .	9
2.1.1	Sensible Heat Storage . . . . .	9
2.1.2	Latent Heat Storage . . . . .	10
2.1.3	Chemical Heat Storage . . . . .	11
2.2	High Temperature Thermal Energy Storage Materials . . . . .	12
2.2.1	Sensible Heat Storage Materials . . . . .	12
2.2.2	Latent Heat Storage Materials . . . . .	14
2.2.3	Chemical Heat Storage Materials . . . . .	15
2.3	Design Criteria . . . . .	15
2.3.1	Selection of Storage Type . . . . .	15
2.3.2	Sizing TES . . . . .	16
2.4	Thermal Energy Storage Concepts for Solar Thermal Power Plants . .	20
2.4.1	Multiple Tanks . . . . .	20
2.4.2	Single Tank . . . . .	23
2.4.3	Solid Media . . . . .	24
2.4.4	Latent Heat . . . . .	25
2.4.5	Thermo-Chemical . . . . .	25
2.5	Operation of a Solar Thermal Power Plant with TES System . . . . .	27
2.5.1	Operating Modes . . . . .	27
2.5.2	Operating Strategies . . . . .	28
<b>3</b>	<b>IPSEpro Design Suite</b>	<b>35</b>
3.1	Process Simulation Environment . . . . .	36
3.1.1	Solution Method . . . . .	37
3.1.2	Potential Problems During System Solution . . . . .	39

## Contents

3.2	IPSEpro's Scripting and COM Interface . . . . .	40
3.2.1	The Component Object Model and Windows Script Host . . . . .	41
3.2.2	Internal Scripts . . . . .	41
3.2.3	External Scripts . . . . .	42
<b>4</b>	<b>Solar Irradiation and Solar Field Modelling</b>	<b>43</b>
4.1	The Sun's Position and Solar Irradiation . . . . .	43
4.2	The Parabolic Trough Collector . . . . .	47
4.3	The Header and Mixer . . . . .	53
4.4	Pipes . . . . .	56
4.5	The Expansion Vessel . . . . .	58
4.6	Mass Flow Rate Prediction . . . . .	59
4.7	Solar Field Size and Layout . . . . .	60
4.8	The Solar Field Model . . . . .	61
<b>5</b>	<b>Modelling Thermal Energy Storage</b>	<b>63</b>
5.1	Two-Tank Model . . . . .	63
5.1.1	Basic Two-Tank Model . . . . .	65
5.1.2	Detailed Two-Tank Model . . . . .	66
5.2	Thermocline Model . . . . .	68
5.2.1	Design Model . . . . .	68
5.2.2	Off-Design Model . . . . .	69
<b>6</b>	<b>Modelling the Power Plant</b>	<b>73</b>
6.1	The Power Block . . . . .	73
6.1.1	Design Model . . . . .	73
6.1.2	Off-Design Model . . . . .	76
6.2	The Flow-Distributor . . . . .	79
6.2.1	PB Off and Warm-Up . . . . .	79
6.2.2	Solar-Only . . . . .	80
6.2.3	TES System and PB On . . . . .	80
6.3	PB, SF and TES Info and Power Plant Statistics . . . . .	81
6.4	Power Plant Model - Script Interaction . . . . .	83
6.4.1	Starting PSE and Initializing the Model . . . . .	83
6.4.2	Calculation Loop . . . . .	84
6.4.3	Report Results . . . . .	90
<b>7</b>	<b>Simulation Results</b>	<b>91</b>
7.1	Power Plant with Two-Tank TES System . . . . .	91
7.1.1	Power Plant with Basic Two-Tank TES System . . . . .	93
7.1.2	Power Plant with Detailed Two-Tank TES System . . . . .	97
7.2	Power Plant with Thermocline TES System . . . . .	104

<b>8</b>	<b>Conclusions and Outlook</b>	<b>113</b>
8.1	Conclusions . . . . .	113
8.2	Outlook . . . . .	114
	<b>Bibliography</b>	<b>115</b>

## List of Figures

1.1	Flow diagram of a typical solar thermal power plant (from Goswami and Kreith [GKo8]). . . . .	2
1.2	Schematic diagrams of the main four CSP systems (from Goswami and Kreith [GKo8]). . . . .	3
1.3	Extending operating hours of a 50 MWe CSP plant with thermal storage, to follow the demand curve of a normal mid-summer day in Spain. Demand curve derived from RED Electrica de España (2011) and CSP load from computer simulation (from European Academies Science Advisory Council [Eur11]). . . . .	6
2.1	Daily thermal power production for different solar field multiples (from Montes et al. [Mon+09]). . . . .	17
2.2	Achievable capacity factor as a function of solar multiple and storage capacity (from Geyer [Gey87]). . . . .	18
2.3	Qualitative energy flow in a solar thermal plant with storage. . . . .	19
2.4	Scheme of installation of a central receiver power plant (Planta Solar Tres), with direct two-tank storage system (from Plataforma Solar de Almeria [Plao7]). . . . .	21
2.5	Scheme of installation of a parabolic trough power plant, with an indirect two-tank active storage system (from Herrmann, Kelly, and Price [HKP04]). . . . .	22
2.6	Scheme of installation of a parabolic trough power plant, with indirect single-tank storage system (from Herrmann, Kelly, and Price [HKP04]). . . . .	23
2.7	Scheme of a parabolic trough power plant, with solid media storage system (from Herrmann, Kelly, and Price [HKP04]). . . . .	24
2.8	Scheme of installation of a parabolic trough power plant, with a modular PCM storage system (from Gil et al. [Gil+10]). . . . .	26
2.9	Ammonia dissociation and storage schematic. (from Dunn, Lovegrove, and Burgess [DLB12]). . . . .	26
2.10	Qualitative energy flow in a solar thermal plant with storage (from Geyer [Gey87]). . . . .	29
2.11	Flowchart describing the power plant system control strategy used for fixed-price and base-load operating strategy. . . . .	31

2.12	Flowchart describing the power plant control strategy used for variable-price and peak-load operating strategy. . . . .	33
3.1	IPSEpro architecture (from SimTech Simulation Technology [Simo2]).	36
3.2	Undamped Newton Raphson Method (from SimTech Simulation Technology [Sim11b]). . . . .	38
3.3	Damped Newton Raphson Method (from SimTech Simulation Technology [Sim11b]). . . . .	38
3.4	Structural singularities(from SimTech Simulation Technology [Sim11b]).	40
4.1	$\theta_z$ zenith angle, $\beta$ slope angle, $\gamma$ surface azimuth angle, $\gamma_s$ solar azimuth angle and $\alpha_s$ solar altitude angle for a tilted surface (from Duffie and Beckman [DBo6]). . . . .	44
4.2	An example of the effects of Raleigh scattering and atmospheric absorption on the spectral distribution of beam irradiance (from Duffie and Beckman [DBo6]). . . . .	44
4.3	$\tau_b$ as a function of zenith angle $\theta_z$ at sea level for a mid-latitude summer climate zone. . . . .	46
4.4	Comparison of measured ( $DNI_M$ ) and calculated ( $DNI_C$ and $DNI_{C+I}$ ) irradiance data. Values were measured at a location close to Prewitt, NM on 30 <sup>th</sup> of May 2012. . . . .	48
4.5	Comparison of measured ( $DNI_M$ ) and calculated ( $DNI_C$ and $DNI_{C+I}$ ) irradiance data. Values were measured at a location close to Golden, Colorado on 9 <sup>th</sup> of May 2012. . . . .	49
4.6	Principle of a PTC including optical parameters (from Goswami and Kreith [GKo8]). . . . .	49
4.7	A typical receiver tube of a PTC (from Goswami and Kreith [GKo8]). .	50
4.8	LS-3 collector dimension (from Goswami and Kreith [GKo8]). . . . .	51
4.9	Comparison of collector row outlet temperatures for the steady state (ss) and the transient (t) collector models. . . . .	52
4.10	Outlet temperature and flow comparison for controlled and non-controlled loops (from Cohen, Kearney, and Kolb [CKK99]). . . . .	54
4.11	Inlet and outlet header with the collector loops in an IPSEpro flow-sheet.	55
4.12	Influence of $h_i$ on $U$ for a pipe with two layers (pipe dimensions: $d_1 = 0.9$ m, $d_2 = 0.92$ m, $d_3 = 1.1$ m, $k_1 = 15$ W/(mK), $k_2 = 0.008$ W/(mK), $h_3 = 8$ W/(m <sup>2</sup> K)). . . . .	57
4.13	Solar field layouts for parabolic trough collectors (from Goswami and Kreith [GKo8]). . . . .	60
4.14	Flow sheet of the solar field in IPSEpro. . . . .	62

## List of Figures

5.1	The TES subsystem in an IPSEpro flow sheet with the two-tank storage system, the working fluid/storage fluid heat exchanger and the flow distributor. . . . .	64
5.2	Concept of the multi-node modelling approach. . . . .	69
5.3	Temperature distribution in the ten-node thermocline model when charging with constant inlet mass flow rate and temperature. . . . .	71
5.4	Temperature distribution in the twenty-node thermocline model when charging with constant inlet mass flow rate and temperature. . . . .	71
6.1	The flow sheet for the power block (PB) at design point. . . . .	74
6.2	Isentropic turbine efficiency at partial load as a function of $f(\psi) / f(\psi_0)$ . . . . .	78
6.3	Generator efficiency at partial load as a function of $P_{gen} / P_{gen,0}$ . . . . .	78
6.4	Basic flow sheet of the script procedure. . . . .	83
6.5	Basic flow sheet of the calculation loop. . . . .	85
6.6	Procedure for setting the time for the current time step. . . . .	86
6.7	Detailed flow-sheet of the convergence improvement measures. . . . .	87
6.8	Detailed flow sheet for selecting the appropriate operation profile. . . . .	88
7.1	Flow sheet of the power plant with a two-tank TES system. . . . .	92
7.2	Ramp for smoothing transition in operation mode change. . . . .	93
7.3	Simulation results for solar irradiation, heat-flow-rates and power output. . . . .	95
7.4	Simulation results for the HTF flow-rates through the SF and temperatures at SF and collector inlet and outlet. . . . .	96
7.5	Simulation results for the TES system temperatures and the charging state. . . . .	97
7.6	Heat and power flow rates for the $SM = 1.5, C_{FLH} = 7.5$ plant configuration on winter solstice. . . . .	101
7.7	Hot and cold storage tank temperatures $t_{hot}$ and $t_{cold}$ and storage capacity of the $SM = 2, C_{FLH} = 7.5$ plant configuration on equinox. . . . .	102
7.8	Heat and power flow rates for the $SM = 3, C_{FLH} = 9$ plant configuration on summer solstice. . . . .	103
7.9	Flow sheet of the power plant with a thermocline TES system. . . . .	105
7.10	Decreasing ramp when the TES system becomes full. . . . .	106
7.11	Decreasing ramp when the TES system becomes empty. . . . .	107
7.12	Simulation results of temperature profile throughout the thermocline tank of the $SM = 1.5, C_{FLH} = 7.5$ plant configuration on three days at the beginning of May. Node N20 is at the bottom of the tank and node N1 is at the top. . . . .	109
7.13	Predicted mass flow rates and temperatures in the SF of the $SM = 1.5, C_{FLH} = 7.5$ plant configuration on 4 <sup>th</sup> of May. . . . .	110

7.14 Predicted heat and power flow rates of the  $SM = 1.5$ ,  $C_{FLH} = 7.5$   
plant configuration on 15<sup>th</sup> of October. . . . . 111

# Acronyms

COM	Component Object Model
CRS	central receiver system
CSP	concentrated solar power
DII	direct incident irradiance
DNI	direct normal irradiance
HCE	heat collecting element
HTF	heat transfer fluid
MDK	Model Development Kit
NSRDB	National Solar Radiation Data Base
PB	power block
PCM	phase change material
PSE	Process Simulation Environment
PTC	parabolic trough collector
SEGS	solar energy generating system
SF	solar field
SM	solar multiple
TES	thermal energy storage
TIT	turbine inlet temperature
WSH	windows script host



## List of symbols

$A$	area, $\text{m}^2$
$\alpha$	molecular thermal diffusivity factor, $\text{m}^2 \text{s}^{-1}$
$c$	specific heat, $\text{J kg}^{-1} \text{K}^{-1}$ ; speed of light, $\text{m s}^{-1}$
$c_p$	specific heat at constant pressure, $\text{J kg}^{-1} \text{K}^{-1}$
$c_v$	specific heat at constant volume, $\text{J kg}^{-1} \text{K}^{-1}$
$D$	diameter, m
$G$	radiation, $\text{W m}^{-2}$
$H$	height, m
$h$	convection heat transfer coefficient, $\text{W m}^{-2} \text{K}^{-1}$ ; specific enthalpy, $\text{J kg}^{-1}$
$k$	thermal conductivity, $\text{W m}^{-1} \text{K}^{-1}$
$m$	mass, kg
$N$	number of nodes
$p$	power, W
$\psi$	pressure number
$Q$	heat, J
$\rho$	density, $\text{kg m}^{-3}$
$T$	temperature, K
$t$	time, s
$U$	overall heat transfer coefficient, $\text{W m}^{-2} \text{K}^{-1}$
$V$	volume, $\text{m}^3$
$v$	specific volume, $\text{m}^3 \text{kg}^{-1}$ ; velocity, $\text{m s}^{-1}$
$x$	distance, m



# 1 Introduction

In times of increasing fossil fuel prices and a huge anthropogenic contribution to global warming, alternative energy sources for power production are necessary. The CO<sub>2</sub> concentration in the atmosphere almost has doubled since 1906 because of burning fossil fuels like coal, oil or natural gas. The mean temperature on earth has risen by  $0.74 \pm 0.18$  °C in the meantime. Sea level measurements indicate an annual increase of 3 mm since 1991, almost twice as much as measured in the years before in the 20<sup>th</sup> century [KMS08].

To avoid further rapid changes and damages to our planet's climate, which endanger the world's economy and lifestyle, humankind has to reduce greenhouse gas emissions. Solar thermal power plants, frequently also called concentrated solar power (CSP) plants, can play an important role in reaching this goal. They emit hardly any greenhouse gases in operation and do not cause safety concerns like nuclear power plants do. The power is produced the same way as in any other conventional thermal power plant by driving a steam turbine, only the energy source is radiation coming from the sun. Solar thermal power plants are restricted to the availability of their energy source, the sun. In the night or during cloudy periods, in times without solar irradiance, solar thermal power plants cannot work. With a thermal energy storage (TES) system these limitations can be avoided.

## 1.1 Solar Thermal Power

Within six hours deserts receive more energy from the sun than humankind consumes within a year [KMS08].

The basic working principle of a solar thermal power plant is shown in Figure 1.1 Direct solar radiation is collected by an optical concentrator and focused onto a receiver where the temperature of a working fluid is increased. The hot working fluid is then used to operate a heat engine which produces electric energy. Or the heat is stored in a heat storage for later use.

## 1 Introduction

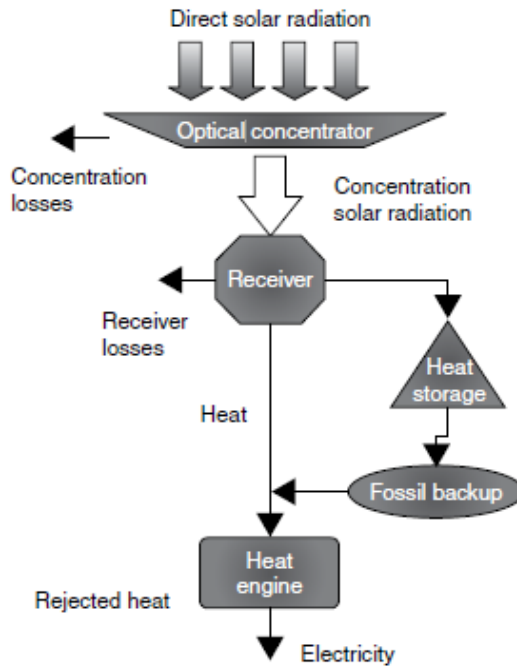


Figure 1.1: Flow diagram of a typical solar thermal power plant (from Goswami and Kreith [GKo8]).

Solar radiosity on the sun's surface is  $63 \text{ MW m}^{-2}$  at a blackbody equivalent temperature of  $5777 \text{ K}$ , and therefore has a high exergetic value. Because of sun-earth geometrical constraints available irradiance at earth surface is slightly above  $1 \text{ kW m}^{-2}$  and achievable temperatures are low [GKo8]. A non-concentrating, black coated flat plate collector can reach a temperature approximately  $100^\circ\text{C}$  above ambient temperature. For higher temperatures, the sunlight must be concentrated to a point (3D) or a line (2D). 3D focusing allows higher concentration ratios, the ratio of absorber to reflector area, than 2D focusing. The higher the concentration ratio, the higher temperatures can be achieved.

Nowadays, the most common design is the parabolic trough collector (PTC) concept. The collectors are parabolic shaped-mirrors which focus the sunlight to a line onto the absorber tube. The maximum reachable temperature with PTC is approximately  $500^\circ\text{C}$ . The working fluid in such plants can be water (direct steam generation) or a mineral oil. The mineral oil limits the maximum temperature to  $400^\circ\text{C}$  due to its thermal instability above this temperature. Some plants of this design, the SEGS I - VIII in the USA, using mineral oil as heat transfer fluid (HTF) have already been in operation for almost 30 years.

The linear Fresnel concept is a single axis tracking technology. It differs from the parabolic trough concept in that the absorber is fixed in space above the mirror

## 1.1 Solar Thermal Power

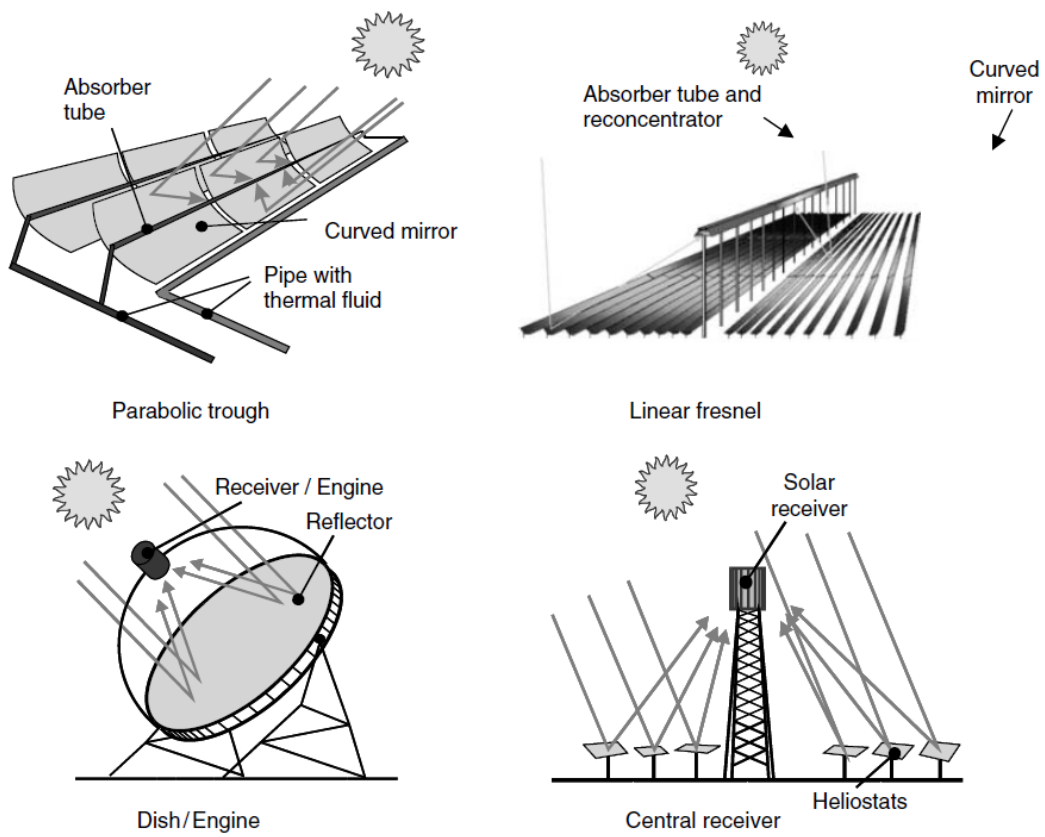


Figure 1.2: Schematic diagrams of the main four CSP systems (from Goswami and Kreith [GKo8]).

## 1 Introduction

field and the reflector is composed of many long row segments which focus collectively on an elevated long tower receiver running parallel to the reflector rotational axis [Milo4]. Power plants with Fresnel collectors usually work with direct steam generation and can reach working fluid temperatures of more than 500 °C. Compared to PTC linear Fresnel collectors are cheaper. To date some prototype plants with linear Fresnel collectors are in operation in Spain.

Power towers have a 3D focusing concept; higher concentration factors and temperatures than with PTC and linear Fresnel collectors can be reached. It is also called central receiver concept. Many mirrors, also called heliostats, are situated around a tower and focus the sunbeam onto the receiver placed on its top. Concentration factors are between 200 and 1000 and temperatures between 300 °C and 1000 °C are possible. The possible working fluids are water, molten salt mixtures or air [GKo8]. With air as a working fluid and due to the high temperatures, high efficiencies might be reached with a concept similar to combined cycle plants.

Another 3D concentrator with concentration ratios up to 4000 are parabolic dish collectors. Sterling engines or Brayton microturbines are located in the focal point for power generation [GKo8].

Schematic diagrams of these four concepts can be found in Figure 1.2. Only plants with the PTC design are in commercial operation to date. From the other three concepts, only pilot plants have been built.

Table 1.1: Characteristics of Concentrating Solar Power Systems (from Goswami and Kreith [GKo8]).

system	peak efficiency in %	annual efficiency in %	annual capacity factor in %
trough/linear Fresnel	21	10 - 18	24
power tower	23	14 - 19	25 - 70
dish/engine	29	18 - 23	25

Table 1.1 shows the characteristic peak and annual efficiencies and the annual capacity factors that can be reached. The annual capacity factor is the ratio of the actual output of a power plant over a year to its potential output if it had operated at rated power the entire year. The lower efficiencies and annual capacity factors pointed out in Table 1.1 for trough/linear Fresnel systems have already been demonstrated under real operation and market conditions. The higher efficiencies and all values for power tower and dish/engine systems are only projected based on pilot scale testing.

## 1.2 Solar Thermal Power with Thermal Energy Storage

Because of the high intermittency of solar radiation reaching the Earth's surface, solar thermal power plants have a limited capability of replacing fossil fuels for power production. Unstable weather conditions, diurnal and annual variation in insolation and the unavailability of solar irradiation during nighttime have a strong negative impact on the plant's power output. The average daily operating time of a solar thermal power plant, without auxiliary heater or TES system, throughout a year is approximately 6 hours only [Adi10].

Today fossil fuelled auxiliary heaters are used in most solar thermal power plants to stabilize power delivery and extend daily operating hours into periods without solar irradiance. In order to save fossil fuels and prolong operation time to periods after sunset, the power plant can be equipped with a TES system. Compared to a plant without TES system the solar field size must be increased to operate the power generation unit at rated power and charge the TES system simultaneously when solar irradiation is high. In times of low or no insolation heat can be retrieved from the TES system to maintain power production.

In solar only mode, without TES and auxiliary heater, solar thermal power plants can reach an annual capacity factor of approximately 20 %, with a TES the capacity factor can be increased [Gey87].

The highest power demand and the highest insolation usually occur at different times. As it can be seen in Figure 1.3 there are two electric power demand peaks over the day. The first one around lunchtime and the second one in the evening when people return home from work. The first peak overlaps with the daily insolation peak. The second one occurs after sunset. With heat from the thermal storage system the power plant can be operated at full load during this peak to meet the power demand with clean energy from the sun.

The first commercial solar thermal power plant equipped with a TES system was SEGS I in California. It had a two-tank storage system with a storage capacity of three full load hours. The three Andasol plants in Spain are also equipped with a two-tank TES system. Hot and cold fluid are stored in two separate tanks. When charging cold fluid is withdrawn from the cold tank, heated up and stored in the hot tank, when discharging the process is reversed. It has a storage capacity of 1010 MWh, this is enough to operate the turbine 7.5 hours at nominal load. The storage medium is a mixture of 60 % sodium nitrate and 40 % potassium nitrate.

## 1 Introduction

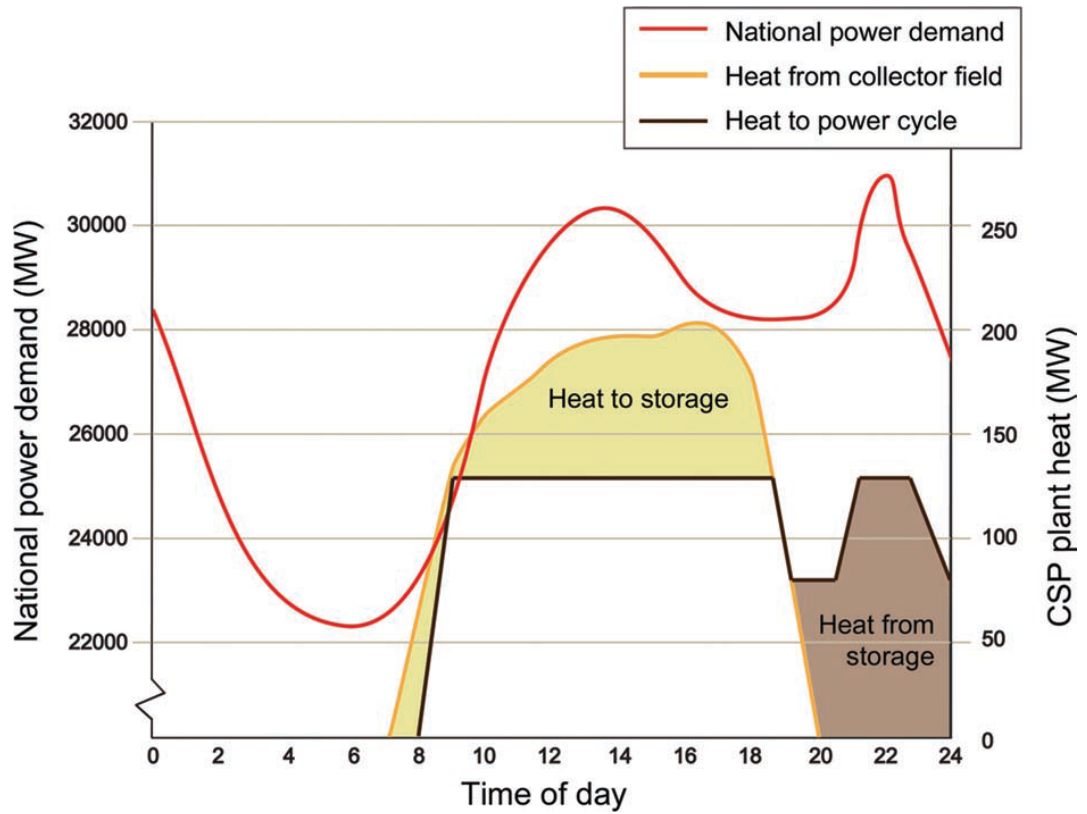


Figure 1.3: Extending operating hours of a 50 MWe CSP plant with thermal storage, to follow the demand curve of a normal mid-summer day in Spain. Demand curve derived from RED Electrica de España (2011) and CSP load from computer simulation (from European Academies Science Advisory Council [Eur11]).



## 1.3 Objective

The objective of this work is provided by the software company SimTech Simulation Technology. SimTech Simulation Technology provides state-of-the-art modelling tools and services for the power and process industries. Their main product is the IPSEpro heat balance and process simulation package. With its various modules it supports users throughout the entire life cycle of a process plant, from conceptual design to on-line plant performance monitoring and optimization. Due to its open modelling approach it is well suited for modelling non-conventional power plant concepts.

The main aim of this work is the development of a simulation tool for thermal energy storage systems, suitable for transient time series calculation of solar thermal power plants. An already existing solar thermal power plant component model library for IPSEpro shall be adapted for the use in transient analysis of solar thermal power plants with TES systems. With existing and new components a solar thermal power plant model with TES shall be created. Finally, a performance prediction and annual yield analysis shall be conducted to demonstrate the new simulation tool.

## 1.4 Method

To achieve the given objective, as a first task the possible TES concepts for solar thermal power plants are evaluated. Two of these concepts are chosen and the TES systems are modelled in IPSEpro. The already existing solar thermal power plant library is extended for the use in transient time series calculation. For both TES concepts solar thermal power plant models are set up. Design as well as off-design models are created. Finally, the off-design models are used to carry out a performance prediction and an annual yield analysis.

## 1.5 Report Outline

To illustrate the issues that come up when modelling solar thermal power plants with thermal energy storage it is important to understand the basic physical processes occurring. For this reason, Chapter 2 is dedicated to the principles of thermal energy storage, storage materials and different storage concepts found in the literature. Apart from that, operating strategies for solar thermal power plants with TES and some basic guidelines of sizing TES systems are pointed out. A short overview about IPSEpro is given in Chapter 3. In Chapter 4 the transient solar

## 1 Introduction

field (SF) component models are set up. The modelling of the two selected TES systems is described in Chapter 5. Chapter 6 describes setting up the PB and the “Flow-Distributor”, the connecting element between SF, PB and TES system. The implementation of the automation script for transient analyses is described there as well. The results of the conducted simulations with both TES concepts are presented in Chapter 7. Finally, in Chapter 8 concluding remarks are made and an outlook on further work is given.

## 2 Thermal Energy Storage for Solar Thermal Power Plants

This chapter provides some basic information about thermal energy storage for solar thermal power plants. In the first part the fundamentals of TES are explained and suitable storage materials for high temperature energy storage are presented. In the second part design criteria and different storage concepts for solar thermal power plants are expounded. At the end of this chapter operation modes and operation strategies for solar thermal power plants with TES systems are described.

### 2.1 Thermal Energy Storage

TES deals with the storing of energy by cooling, heating, melting, solidifying or vaporizing a material; the thermal energy becomes available when the process is reversed [DR02]. The main two forms of thermal energy storage are sensible and latent heat storage. Sensible heat can be stored in solids and liquids by the change of temperature. Latent heat is based on the phase change of some material (solid-liquid or liquid-vapor) without temperature change. Other storage methods of interest for solar thermal power plants are thermo-chemical storage and sorption heat storage, where heat is stored in reversible chemical reactions.

#### 2.1.1 Sensible Heat Storage

Sensible energy is stored by the temperature change of a solid, liquid or gaseous storage medium without any phase change. The amount of stored energy is proportional to the temperature change  $\Delta T$  in the medium (where  $\Delta T = T_{final} - T_{initial}$ ) and the mass  $m$ . Each medium has a certain ability to store heat, the heat capacity  $c$ . The stored heat  $Q$  in a medium is:

$$\Delta Q = mc\Delta T \quad (2.1)$$

## 2 Thermal Energy Storage for Solar Thermal Power Plants

For gases the specific heat  $c$  has to be substituted by the specific heat at constant volume  $c_v$  for stores with constant volume or specific heat at constant pressure  $c_p$  for stores with constant pressure. The volumetric thermal capacity is  $\rho c$ , where  $\rho$  is the density. It expresses the storage ability per  $\text{m}^3$ . With volume  $V$  the stored energy  $Q$  is

$$\Delta Q = \rho c V \Delta T \quad (2.2)$$

A high volumetric thermal capacity is of advantage in order to build compact stores and minimize the storage vessel surface. Thermal conductivity  $k$  and diffusivity  $\alpha$  have an influence on the rate heat can be released and added. For liquid storage media low vapor pressure is of advantage to avoid the need of pressurized storage vessels.

The most common sensible heat storage medium is water. It is used mostly for domestic hot water supply, building heating and cooling. It has a high heat capacity of  $c = 4.2 \text{ kJ kg}^{-1} \text{ K}^{-1}$  and its easy and cheap availability makes it a logical choice for such applications. Solid media like ceramics usually have a lower heat capacity, but larger temperature changes are possible.

### 2.1.2 Latent Heat Storage

Latent heat is stored due to a phase change in the storage material. The materials used are called phase change material (PCM). It might be a solid-solid, a solid-liquid or a liquid-gaseous phase change. For pure fluids the temperature stays constant during the whole process. The heat released or consumed is called the heat of phase change or latent heat  $\Delta Q_f$ .

The liquid-gaseous phase change releases the highest amount of latent heat (e.g. water to steam at atmospheric pressure and  $100 \text{ }^\circ\text{C}$ :  $\Delta q_f = 2257 \text{ kJ/kg}$ ), but volumetric heat storage capacity of gases is low. For the most part, latent heat storage is understood to be the storage of melting heat which involves only small volume changes. Sometimes the solid-liquid phase change is combined with a solid-solid phase change at a temperature somewhat below the melting point [BG84].

If sensible and latent heat storage are combined, the equation for a solid-liquid phase change is as follows:

$$\Delta q = c_{p,s}(T_f - T_1) + \Delta q_f + c_{p,l}(T_f - T_2) \quad (2.3)$$

## 2.1 Thermal Energy Storage

This formula is valid for  $T_1 < T_f$  and  $T_2 > T_f$ , constant pressure and mass. In this case heat storage and release are not at a constant temperature level any more.

Latent heat storage systems still need some research and development. Nevertheless, already in the 19<sup>th</sup> and 20<sup>th</sup> century ice from lakes was harvested and stored in cellars. The melting of the ice kept the cellar on constant temperature during the summer. The Hungarian parliament is still air-conditioned by ice from lake Balaton [DR02] and Sundsvall hospital in Sweden is cooled during the summertime by the help of a snow storage [NS07]. Ice has good properties for such applications. It can be harvested in winter, so it is cheap, has a high specific heat capacity in solid and liquid phase ( $c_s = 2.1 \text{ kJ/kg}$  and  $c_l = 4.2 \text{ kJ/kg}$ ), a good thermal conductivity ( $k_s = 2.2 \text{ W/mK}$ ) and an appropriate melting temperature ( $t_f = 0^\circ\text{C}$ ). The latent heat is rather low ( $\Delta q_f = 335 \text{ kJ/kg}$ ). Some other important properties for latent heat storage media are no tendency to segregation, low thermal expansion and low risk (no poisonous vapors, no dangerous reactions with working medium and heat transfer medium [BG84]). For solar thermal power there exist media with melting points from  $300^\circ\text{C}$  up to  $600^\circ\text{C}$  like  $\text{NaNO}_3$  or  $\text{KNO}_3$  [Hun94]. There are three different types of storage media: pure substances, binary and ternary mixtures. Binary and ternary mixtures have the advantage of high heat capacities, high heat of fusion and low melting temperatures.

### 2.1.3 Chemical Heat Storage

The change in binding enthalpy of reversible reactions of two or more media can also be used for TES. According to the chemical bond type one has to distinguish between sorption heat storage and thermo-chemical heat storage.

If it is possible to store the reaction partners separately, such systems are appropriate for long term-storage since the reaction participants can be stored close to ambient temperature. In case of liquid reaction media high energy densities are possible.

#### Sorption Heat Storage

To a mixture AB which can be liquid or solid the heat  $\Delta Q_V$  is added. This separates the mixture into its components A and B which may be solid, liquid or gaseous. Usually the mixture is solid or liquid and one component is solid or liquid and the other gaseous.



## 2 Thermal Energy Storage for Solar Thermal Power Plants

In most cases sorption enthalpy is higher than heat of evaporation. Energy density of stored gaseous components is low, demanding a compressed storage or huge store. The heat transfer in the bulk material is poor and reaching a good heat transfer for charging and discharging is challenging [BG84].

### Thermo-Chemical Heat Storage

Thermo-chemical storage makes use of the binding energy of reversible chemical reactions. Heat is used to excite an endothermic chemical reaction. With the reversed exothermic reaction the heat can be recovered. A catalyst may be involved in the reaction. The reaction partners are separated and stored separately.

## 2.2 High Temperature Thermal Energy Storage Materials

High temperature thermal energy storage materials have different requirements. They have to withstand the temperatures in the desired operation range. The storage material should have a high energy density and a good heat transfer between storage material and HTF. Mechanical and chemical stability and a long lifetime are further important points [Gil+10].

Sensible heat can be stored in solids, liquids or gases and latent heat in PCM. For thermo-chemical heat storage appropriate reversible reactions are available.

### 2.2.1 Sensible Heat Storage Materials

Sensible heat can be stored in solids, liquids or gases. Gases, which have a very low energy density, are not very suitable for heat storage and are not considered any more in this work.

For parabolic trough power plants using synthetic oil as the heat transfer medium, the application of solid media sensible heat storage is an attractive option regarding investment and maintenance costs [Lai+06]. Studies at DLR in Stuttgart and the Plataforma Solar de Almeria in Spain have evidenced that concrete and castable ceramics are good options.

The castable ceramic is based on a binder containing  $\text{Al}_2\text{O}_3$ . The binder is prepared on site under ambient conditions and reacts chemically to form a solid, stable matrix which encloses the aggregates. Iron oxides, accumulated as waste material in strip

## 2.2 High Temperature Thermal Energy Storage Materials

steel production, are the main aggregates. For the high temperature concrete, blast furnace cement is used as binder; iron oxides are used again as the main aggregate as well as flue ash and again a small amount of auxiliary materials [Lai+06]. The properties of both materials can be found in Table 2.1.

Table 2.1: Material properties of storage materials developed at DLR (from Laing et al. [Lai+06]).

Material	Castable ceramic	High temperature concrete
Density [kg/m <sup>3</sup> ]	3500	2750
Specific heat capacity at 350 °C [J/kg K]	866	916
Thermal conductivity at 350 °C [W/m K]	1.35	1.0
Coeff. of thermal expansion at 350 °C [10 <sup>-6</sup> /K]	11.8	9.3
Material strength	Low	Medium
Crack initiation	Hardly no cracks	Several cracks

The most common sensible heat storage materials for high temperature applications found in literature are presented in Table 2.2.

Table 2.2: Main characteristics of sensible heat storage solid materials (from Gil et al. [Gil+10]).

Storage medium	Temperature		Average density (kg/m <sup>3</sup> )	Average heat conductivity (W/m K)	Average heat capacity (kJ/kg K)	Volume specific heat capacity (kWh <sub>t</sub> /m <sup>3</sup> )	Media costs per kg (US\$/kWh <sub>t</sub> )	Media costs per kWh <sub>t</sub> (US\$/kWh <sub>t</sub> )
	Cold (°C)	Hot (°C)						
Sand-rock-mineral oil	200	300	1700	1.0	1.30	60	0.15	4.2
Reinforced concrete	200	400	2200	1.5	0.85	100	0.05	1.0
NaCl (solid)	200	500	2160	7.0	0.85	150	0.15	1.5
Cast iron	200	400	7200	37.0	0.56	160	1.00	32.0
Cast steel	200	700	7800	40.0	0.60	450	5.00	60.0
Silica fire bricks	200	700	1820	1.5	1.00	150	1.00	7.0
Magnesia fire bricks	200	1200	3000	5.0	1.15	600	2.00	6.0

Many liquid or gaseous materials have been investigated about their TES abilities, including water, air or oil, but eventually inorganic nitrate salt mixtures have proven to be superior. They offer a very favourable combination of density (1880 kg/m<sup>3</sup>), specific heat (1500 J/(kg K)), chemical reactivity (very low), vapour pressure (<0.01 Pa) and cost (\$0.40 – \$0.90/kg) [HKPo4]. Their operation temperature matches quite well with today's high pressure and high temperature steam turbines. A disadvantage are their high freezing temperatures of more than 100 °C.

The three leading candidates are solar salt, Hitec and HitecXL. Solar salt is a binary salt consisting of 60 % NaNO<sub>3</sub> and 40 % KNO<sub>3</sub>, the salt melts at 221 °C and is kept liquid at 288 °C in an insulated cold storage tank. HitecXL is a ternary salt consisting of 48 % Ca(NO<sub>3</sub>)<sub>2</sub>, 7 % NaNO<sub>3</sub>, and 45 % KNO<sub>3</sub>, and its properties were analysed in PSA and Themis plants. This salt was developed as a second tentative from Hitec,

## 2 Thermal Energy Storage for Solar Thermal Power Plants

an eutectic mixture of 40 %  $\text{NaNO}_2$ , 7 %  $\text{NaNO}_3$  and 53 %  $\text{KNO}_3$ , with 142 °C melt-freeze point [Gil+10].

Table 2.3: Main characteristics of sensible heat storage liquid materials (from Gil et al. [Gil+10]).

Storage medium	Temperature		Average density (kg/m <sup>3</sup> )	Average thermal conductivity (W/m K)	Average heat capacity (kJ/kg K)	Volume specific heat capacity (kWh <sub>t</sub> /m <sup>3</sup> )	Media costs per kg (US\$/kWh <sub>t</sub> )	Media costs per kWh <sub>t</sub> (US\$/kWh <sub>t</sub> )
	Cold (°C)	Hot (°C)						
HITEC solar salt	120	133	–	–	–	–	–	–
Mineral oil	200	300	770	0.12	2.6	55	0.30	4.2
Synthetic oil	250	350	900	0.11	2.3	57	3.00	43.0
Silicone oil	300	400	900	0.10	2.1	52	5.00	80.0
Nitrite salts	250	450	1825	0.57	1.5	152	1.00	12.0
Nitrate salts	265	565	1870	0.52	1.6	250	0.50	3.7
Carbonate salts	450	850	2100	2.0	1.8	430	2.40	11.0
Liquid sodium	270	530	850	71.0	1.3	80	2.00	21.0

Details about the characteristics of some liquid storage materials, including salt mixtures, can be found in Table 2.3. Solar salt is the storage material used in the Andasol I-III power plants. Molten salts are also proposed to act as heat transfer fluid in central receiver plants.

### 2.2.2 Latent Heat Storage Materials

Storage with PCM are considered to be a good alternative to sensible heat storage. They have a higher energy density compared to sensible heat storage materials and can provide heat at a constant temperature. For heat storage the solid-liquid phase change is preferred. The liquid-gaseous phase change involves the largest latent heat, but energy density of gases is rather low.

There exist organic and inorganic PCM. The organics are not corrosive, but compared to inorganics they have a lower phase change enthalpy and thermal conductivity. Another disadvantage is their inflammability. Inorganic PCM have a higher latent heat, but this is related with corrosion issues, phase separation and a lack of thermal stability [Zal+03]. A good overview of PCM suitable for high temperature energy storage can be found in Gil et al. [Gil+10]

To date PCMs still suffer from many issues like low thermal conductivity and solid deposits on heat transfer surfaces. Heat transfer in the PCM can be improved by adding objects with higher thermal conductivity (for example graphite) to the PCM. Another option is to improve it by convection. But there is still a lot of research and development required to use a PCM storage system in any application.



### 2.2.3 Chemical Heat Storage Materials

Thermo-chemical storage materials promise higher energy densities than sensible and latent heat storage materials. Many chemical reactions are known that could potentially be utilized to store solar energy. A short overview of the investigated reactions can be found in Hadorn [Hado6].

The two most relevant chemical reactions are metal oxide/metal reactions and the dissociation of ammonia. The reaction temperature for metal oxide/metal reactions is  $>2000$  K. By adding a reducing atmosphere or a reducing component it can be decreased to temperatures appropriate for solar thermal power. Forster [Foro4] proposes the dissociation of  $\text{SnO}_x$  as a possible reaction for thermochemical storage of solar energy. Dissociation temperatures of  $\text{SnO}_x$  without any reducing substances are above 2000 K at 1 bar. In the presence of  $\text{CH}_4$  or C the reaction temperature can be decreased to temperatures below 1250 K. For the ammonia process, also called "Haber-Bosch" process, there is more than 100 years of industrial experience available. For charging liquid ammonia ( $\text{NH}_3$ ) is dissociated in an endothermic reaction. For discharging the reaction products,  $\text{H}_2$  and  $\text{N}_2$ , release energy in an exothermic reaction. The reaction temperature is between  $400^\circ\text{C}$  to  $500^\circ\text{C}$ . In modern ammonia plants the heat from exothermic reaction is already used for superheated steam generation.

Chemical heat storage is still at an early stage of development, a critical point is still the reaction kinetics [Foro4]. For ammonia synthesis reactors, conventional industry practice suggests very slow ramp rates, limiting the capability to match varying loads [DLB12].

## 2.3 Design Criteria

TES for solar thermal power is a fairly new topic. There do not exist common design and sizing guidelines. Different technical and environmental, as well as financial criteria influence the selection of the appropriate storage system.

### 2.3.1 Selection of Storage Type

The main parameter when choosing the type of a storage system is the temperature range at which the system is operated. With this knowledge an appropriate storage material can be selected. The requirements on the storage material are a high energy density, and mechanical and chemical stability to allow sufficient charge and discharge cycles. For safety reasons the storage material must be compatible with

## 2 Thermal Energy Storage for Solar Thermal Power Plants

the HTF. To avoid huge impact on the environment in case of a disaster, the storage material must not be inflammable and poisonous.

The main influence factors on investment costs of a TES system are the storage material, the charging and discharging equipment and the storage vessel. The need of a heat exchanger, if HTF and storage fluid are different, increases the cost of a storage system. But this can be compromised by the use of a cheaper storage fluid.

### 2.3.2 Sizing TES

The accurate size of the TES system has an important influence on the economical success of the power plant. An oversize store has high investment costs and will be poorly utilized. An undersized store is cheaper, but its storage capacity is small, which results in poor utilization of SF and PB.

From a technical point of view the main influence factors for the size of a TES system, next to the operation strategy of the power plant, are the thermal power coming from the SF  $\dot{Q}_{th,SF}$  and the power consumption of the PB  $\dot{Q}_{th,PB}$ . Maximum load, maximum charge and discharge rate have to be considered as well.

There does not exist any approved method to size a TES for a solar thermal power plant. TES in previously built plants are rare or were built as prototypes and therefore sizing was done on an experimental basis.

In the following sections first some key parameters for solar thermal plants with a TES system will be described and then some guidelines to determine the proper storage capacity are presented.

#### Solar Multiple, Capacity Factor and Storage Utilization Factor

The solar multiple (SM) is the ratio of the delivered heat  $Q_{th,SF}$  by the solar field to the nominal heat load  $Q_{th,PB}$  of the power block at design point.

$$SM = \frac{\dot{Q}_{th,SF}}{\dot{Q}_{th,PB}} \quad (2.5)$$

The SM in the design point  $SM_{design}$  determines the solar field size depending on the power block size. Common design points for solar thermal power plants are at 12 AM at equinox, summer or winter solstice. At  $SM = 1$  the power block can be operated at nominal load. In times when the SM exceeds one, the excess energy

has to be either stored or dumped. This is shown in Figure 2.1, the grey area is the excess energy.

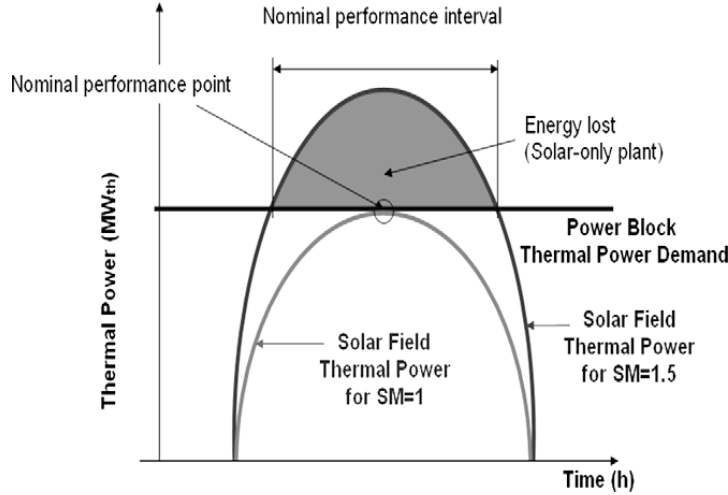


Figure 2.1: Daily thermal power production for different solar field multiples (from Montes et al. [Mon+09]).

The capacity factor  $c_{el}$  is the electric energy  $W_{el,a}$  produced by the plant over a period divided by the nominal electric power  $P_{el,nom}$  times the period length.

$$c_{el} = \frac{P_{el,a}}{P_{el,nom}t} \quad (2.6)$$

Peak load power plants have a low capacity factor, base load plant a high one. Solar thermal power plants with a  $SM = 1$  and no storage are limited by the availability of the energy source and have an annual capacity factor of approximately  $c_{el} \approx 0.2$ . This means 1750 hours of nominal power output over a year. With the help of a storage annual operation time can be increased and the capacity factor will rise.

The storage utilization factor  $\epsilon$  is the relation of the real energy output on discharge to its theoretical maximum value.

$$\epsilon = \frac{Q_{TES,D}}{Q_{TES,D,max}} \quad (2.7)$$

A low value means that only a small part of the storage capacity is used [DGT91].

## 2 Thermal Energy Storage for Solar Thermal Power Plants

### Storage Capacity

The heat capacity stored in the TES system  $C_{FLH}$  is expressed by the number of full-load hours for which the PB can be supplied with the required heat from the TES alone [RBEo8].

Geyer [Gey87] cites that preliminary storage layout calculations for a pilot plant in Albuquerque, New Mexico, using 1960 meteorological data, yield a linear increase of the capacity factor for the first 9 to 15 full-load hours. This data is not based on a specific plant, it was obtained by simple energy accounting. This is presented in Figure 2.2 for SM from 4 to 15. The abscissa shows the storage capacity in full-load hours and the ordinate the capacity factor. From a critical SM = 5 it is possible to achieve 100% of solar operation. This would require an enormous storage capacity which might not be practical. With the first 15 full-load hours a capacity factor of up to 90% can be achieved. Each full-load hour is utilized once a day and provides approximately 350 rated power hours. Each additional full-load hour only provides 11 rated power hours. The first 15 full-load hours compensate day and night cycles, the additional full-load hours are for seasonal changes. If the SM is increased above the critical SM, the storage capacity to achieve a capacity factor of 100% decreases. Then the seasonal insolation valleys are levelled by the solar field, but there will be an unused energy surplus in summer [DGT91].

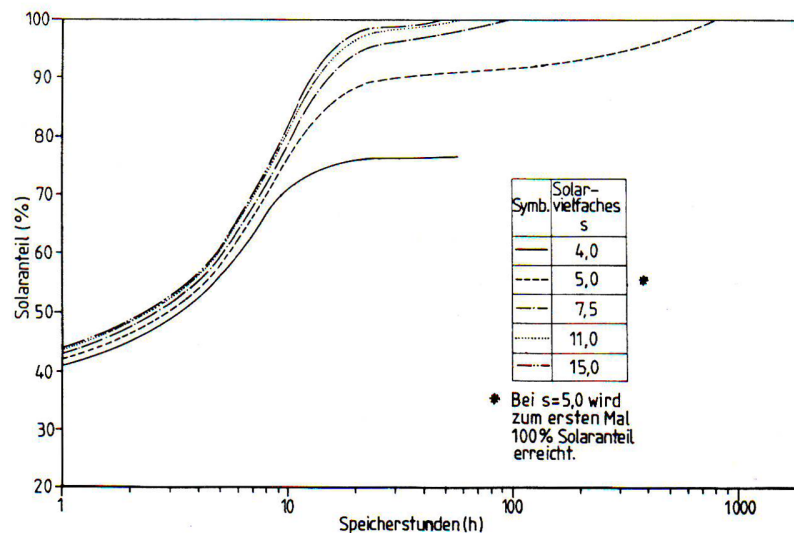


Figure 2.2: Achievable capacity factor as a function of solar multiple and storage capacity (from Geyer [Gey87]).

Figure 2.3 shows the qualitative energy flow for a solar thermal power plant with energy storage. If the thermal power from the SF  $\dot{Q}_{SF}$  exceeds the power consump-

tion of the PB  $\dot{Q}_{PB}$  the surplus energy  $Q_{TES,C}$  is stored. Only the receiver must be designed to be capable of peak loads, the PB can have another design point. If  $\dot{Q}_{SF}$  is lower than  $\dot{Q}_{PB}$ , the missing power is retrieved from the stored energy  $Q_{TES,D}$ . During charging, storing and then discharging there occur losses.

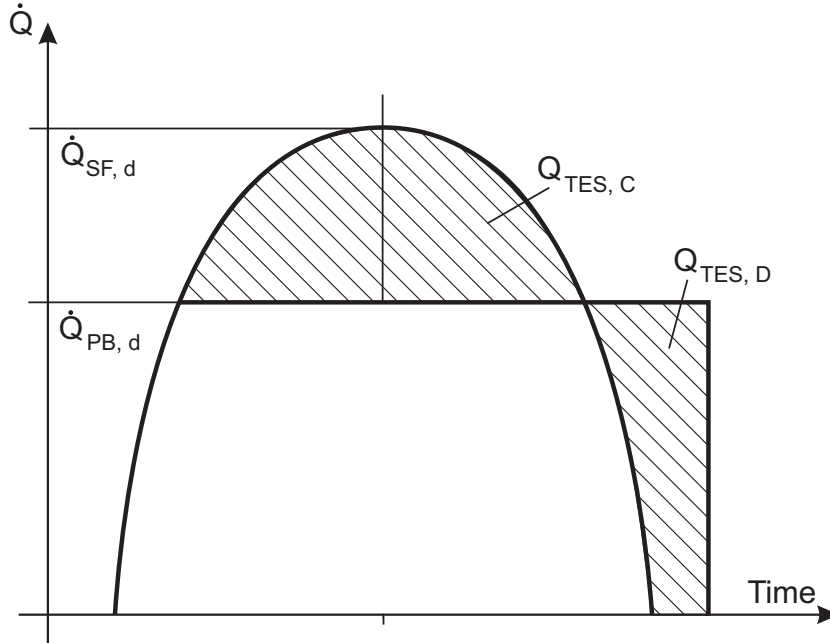


Figure 2.3: Qualitative energy flow in a solar thermal plant with storage.

The storage efficiency  $\eta_{TES}$  is the ratio between stored and retrieved energy.

$$\eta_{TES} = \frac{Q_{TES,D}}{Q_{TES,C}} \quad (2.8)$$

All in all less energy is transferred to the PB in a system including thermal storage than in the same-sized system without TES system. The fraction of energy from the SF  $Q_{SF}$  sent to the storage system, also called the storage factor  $\delta_{TES}$ , is

$$\delta_{TES} = \frac{Q_{TES}}{Q_{SF}} \quad (2.9)$$

The total SF output  $Q_{SF}$  is then reduced by the storage loss factor  $\gamma_{TES}$ .

$$\gamma_{TES} = 1 - \delta_{TES}(1 - \eta_{TES}) \quad (2.10)$$

## 2 Thermal Energy Storage for Solar Thermal Power Plants

That means if 50 % of the receiver output are charged into a TES system with  $\eta_{TES} = 90\%$ , then the total SF output is reduced by 5 % [DGT91].

But usually the averaged efficiency of the whole power plant is increased by avoiding partial load operation of the PB. From an economic point of view a TES system makes sense by shifting parts of power production to high tariff periods [Gey87].

In order to optimize the TES system it is important to find the optimum value of  $\delta_{TES}$  and the energy from the SF has to be utilized in a way to maximize the power output.

With these considerations it is obvious that aiming of a capacity factor of 100 % is not very practical. Either parts of the storage system or parts of the SF will be poorly utilized. Both components are two of the most expensive ones in a solar thermal power plant. Determining the optimum ratio of storage capacity to solar field size has to be part of an economic optimization, but this is not within the scope of this work.

### 2.4 Thermal Energy Storage Concepts for Solar Thermal Power Plants

Many concepts for solar thermal power plants with TES have previously been developed. Some of them have already been applied in operating power plants, some were realized in small scale as pilot plants and some were only investigated theoretically.

The TES systems can be divided into active and passive storage systems. In passive systems the storage medium is solid and a HTF passing through it charges or discharges the store. Active systems have a forced convection heat transfer to the storage fluid, mostly in a heat exchanger. They can be further subdivided into direct and indirect systems. In direct systems the storage material is also the HTF, in indirect systems both media are different.

In the following section a short overview of the most important storage concepts found in literature is given.

#### 2.4.1 Multiple Tanks

Storing heat in multiple tanks is probably the most advanced heat storage technology to date. The hot and the cold fluid are stored in separate tanks. When charging, cold fluid is taken from the cold tank, heated up and then stored in the hot tank. For

## 2.4 Thermal Energy Storage Concepts for Solar Thermal Power Plants

discharging the whole procedure is reversed. Mostly such systems consist of two tanks, one hot and one cold tank, but also multiple tanks are possible. There the empty space in the tanks is reduced, costs for space and enclosure can be decreased, but multiple charge and discharge equipments are necessary. Another disadvantage is the higher heat loss because of the larger surface area compared to a two-tank system.

Already SEGS I, a PTC solar thermal power plant built in 1984, was equipped with a 3 full-load hours two-tank thermal storage system. Is was an active direct storage system, the mineral oil used as HTF was also used as storage fluid [HKP04]. Figure 2.4 shows a scheme of the installation of "Solar Tres", a central receiver system (CRS) plant with a two-tank active direct storage system. There the HTF and storage material is molten salt.

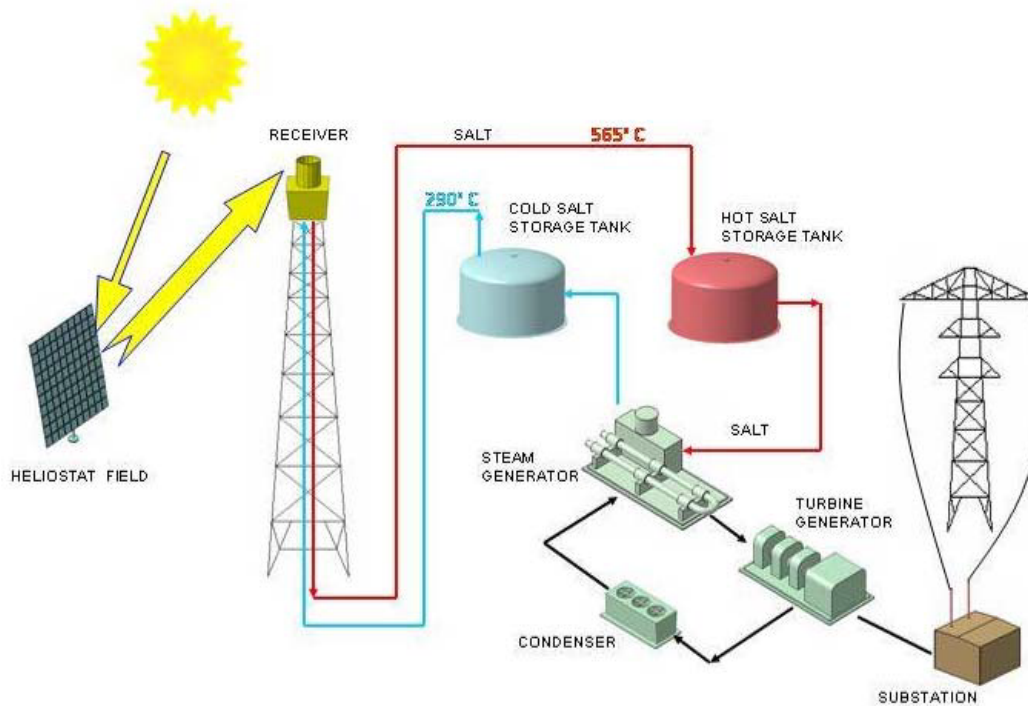


Figure 2.4: Scheme of installation of a central receiver power plant (Planta Solar Tres), with direct two-tank storage system (from Plataforma Solar de Almeria [Pla07]).

During a typical charge cycle of an indirect two-tank TES system, a portion of the oil from the collector field is directed to the oil-to-salt heat exchanger, where the oil cools from the nominal inlet temperature of 391 °C to an outlet temperature of about 298 °C. In a shell and tube heat exchanger the salt is heated from an inlet

## 2 Thermal Energy Storage for Solar Thermal Power Plants

temperature of  $291\text{ }^{\circ}\text{C}$  to an outlet temperature of  $384\text{ }^{\circ}\text{C}$ , and then stored in the hot storage tank. During the discharge cycle, the oil and salt flow paths are reversed. Heat is then transferred from the salt to the oil to provide the thermal energy for the steam generator [Gil+10]. A flow sheet for a plant with an indirect two-tank TES system is shown in Figure 2.5

Each of the Andasol I-III plants includes an indirect two-tank molten salt storage system. The storage capacity of the Andasol I solar plant is about  $1010\text{ MWh}$ , that means about 7.5 hour of full-load production of electricity. The storage temperature is  $291\text{ }^{\circ}\text{C}$  in the cold tank and  $384\text{ }^{\circ}\text{C}$  in the hot tank. The annual average efficiency converting from solar energy to electricity is  $14.7\%$  [Med+10]

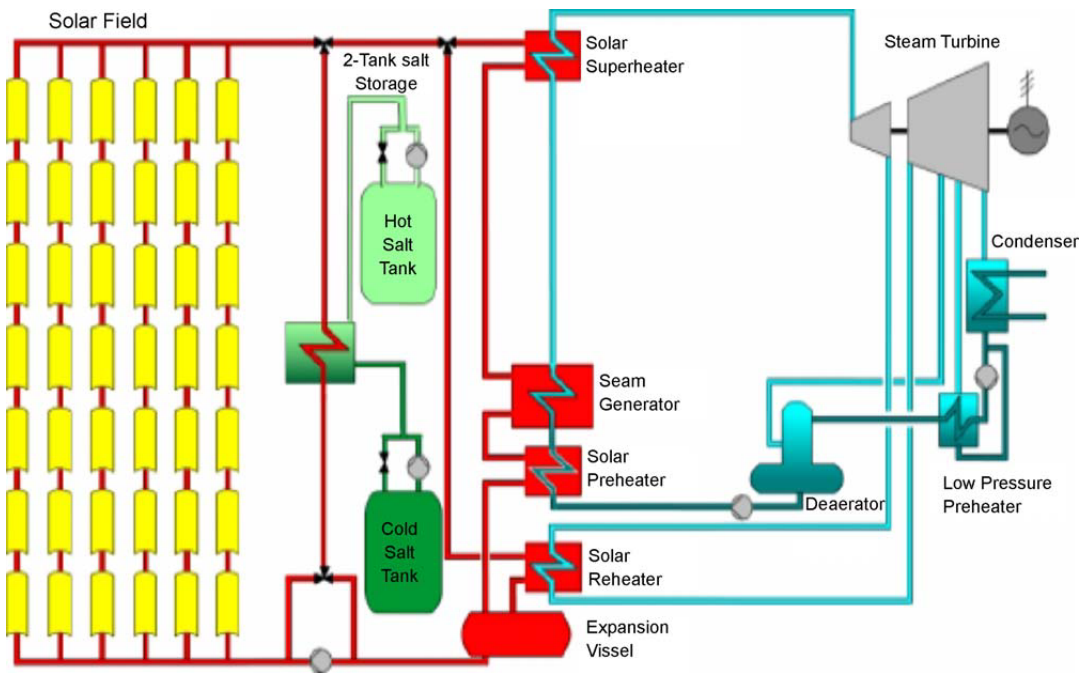


Figure 2.5: Scheme of installation of a parabolic trough power plant, with an indirect two-tank active storage system (from Herrmann, Kelly, and Price [HKP04]).

The main advantages of two-tank storage systems is their convenience and the fact that hot and cold fluid are stored separately. Disadvantages are the high cost of the storage equipment and the small temperature difference between hot and cold tank. In case of using molten salt as storage fluid there is a risk of solidification due to its high freezing point.



### 2.4.2 Single Tank

The hot and the cold storage fluid are stored in a single tank. It is predicted that such a design can reduce capital costs, compared to a two-tank approach, up to 33% [Kol11]. Space consumption is lower as well.

Because of buoyant forces, hot fluid stays on top and cold fluid at the bottom. The transition zone is called thermocline. When charging, cold fluid is withdrawn from the bottom and hot fluid added on top. The thermocline shifts down. When it reaches the bottom the storage system is fully charged. The inlet and outlet devices must be designed carefully to maintain thermal stratification and avoid mixing. For discharging the whole process is reversed.

Thermocline systems can be direct or indirect storage systems. Figure 2.6 shows the flow sheet of a parabolic trough power plant, with indirect single-tank storage system. Molten salt or mineral oil are used as storage media. One option to significantly reduce costs for the storage material is to replace a large share of the molten salt or mineral oil with low-cost filler materials. The filler material is used as the primary thermal storage medium, and molten nitrate salts as the direct heat transfer fluid. It also helps to maintain thermal stratification. Suitable filler materials are quartzite rock or silica sands [Bro+05].

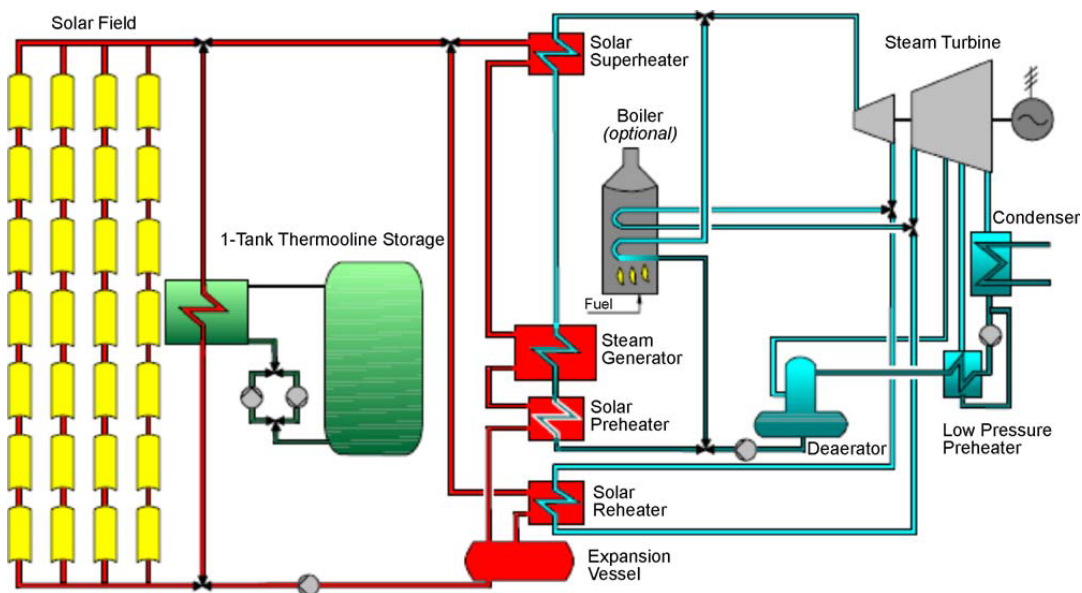


Figure 2.6: Scheme of installation of a parabolic trough power plant, with indirect single-tank storage system (from Herrmann, Kelly, and Price [HKP04]).

## 2 Thermal Energy Storage for Solar Thermal Power Plants

The Solar One CRS plant in California used a thermocline tank, with mineral oil as heat transfer fluid and a low cost filler material [PSK01]. After 4 years in operation Solar One was converted to Solar Two, which used a two-tank molten salt TES system.

Simulations performed by Kolb [Kol11] of the annual performance of 50 MW Andasol like parabolic trough plants that employ either a two-tank or a thermocline-type molten-salt thermal storage system predict that the annual performance of the thermocline plant is virtually identical to the two-tank plant.

### 2.4.3 Solid Media

Solid media storage systems are passive systems. Storage materials are mostly concrete or castable ceramics. The HTF circulates through pipes which are enclosed in the storage material. Figure 2.7 shows a flow sheet of a parabolic trough power plant, with a solid media storage system.

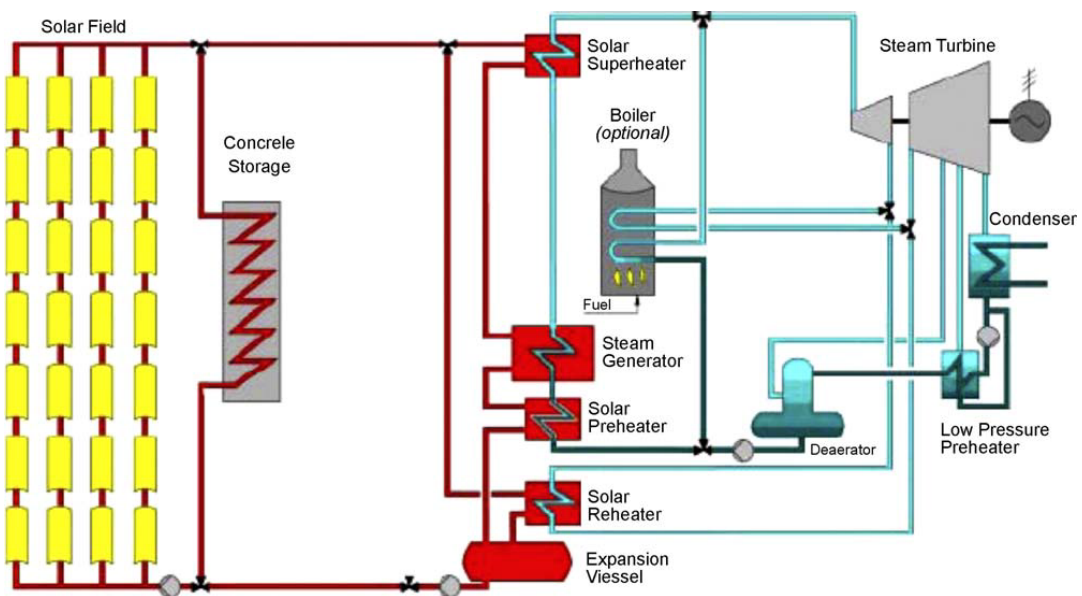


Figure 2.7: Scheme of a parabolic trough power plant, with solid media storage system (from Herrmann, Kelly, and Price [HKP04]).

To this day no solar thermal power plant with a solid media TES system has been operated. Already back in 1987 Geyer [Gey87] proposed a modular thermal ceramic storage system as a component of a gas-cooled receiver plant. The DLR built two storage units, one with castable ceramics and one with high temperature concrete

## 2.4 Thermal Energy Storage Concepts for Solar Thermal Power Plants

as heat storage material, at Plataforma Solar de Almeria. Various performance tests were performed. From both materials the high temperature concrete seems to be the more favourable material due to lower costs, higher material strength and easier handling [Lai+06].

With the acquired data the enhancement of heat transfer into the storage material through heat transfer structures was investigated. The additional costs for this measures outweighed by far the benefits. Simulation models for solid TES systems were created and different storage concepts in solar thermal power plants could be investigated. Compared to a plant with an integrated TES concept, the modular storage integration showed an increase of 100% storage capacity or a reduction of more than a factor of 2 in storage size and therefore investment costs [Lai+08].

### 2.4.4 Latent Heat

Latent heat storage systems are passive systems as well. The concept is similar to the concept for solid media. Finned tubes are enclosed in the PCM material. Figure 2.8 shows the scheme of installation of a parabolic trough power plant, with a modular PCM storage system. In another concept the PCM is encapsulated and used as a filler material in single-tank. Charging temperature has to be above the melting temperature of PCM, discharging temperature is below.

No latent heat storage system has been in operation in any solar thermal power plant until now. Solar thermal power plants with latent heat storage are still in conceptual design. One proposal is to use a cascaded PCM storage system to avoid superheating and supercooling of PCM. Another proposal is to use different PCM with different melting points for steam generation, superheating and reheating [DGT91].

### 2.4.5 Thermo-Chemical

Concepts for integrating thermo-chemical storage systems into solar thermal power plants are at a very early stage of development. When using ammonia as storage and working fluid a concept as shown in Figure 2.9 seems to be possible. It is a direct storage concept, the storage fluid and the working fluid are the same. In a reactor in the focal point of a solar collector ammonia is dissociated at 700 °C, the reaction products are cooled down, separated and stored. In another reactor ammonia synthesis produces large quantities of heat for steam generation. The liquid ammonia is either stored or returned to the dissociation reactor.

## 2 Thermal Energy Storage for Solar Thermal Power Plants

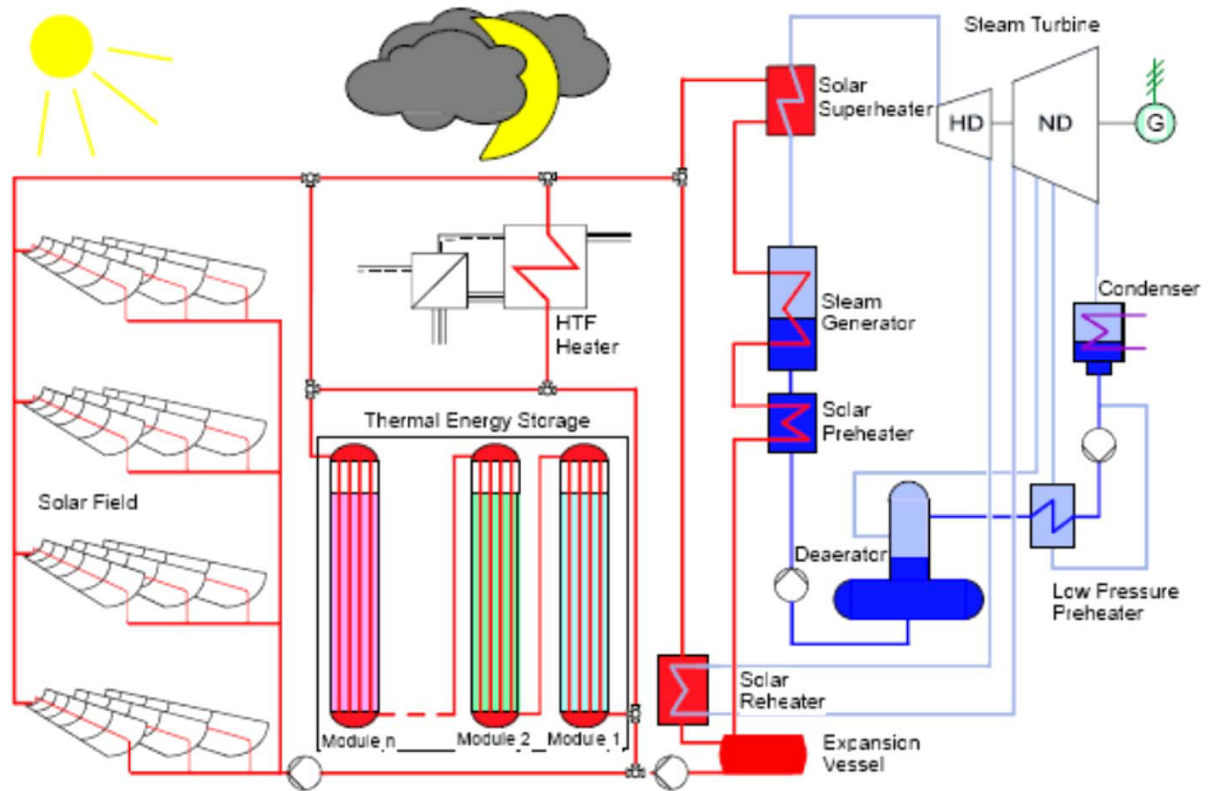


Figure 2.8: Scheme of installation of a parabolic trough power plant, with a modular PCM storage system (from Gil et al. [Gil+10]).

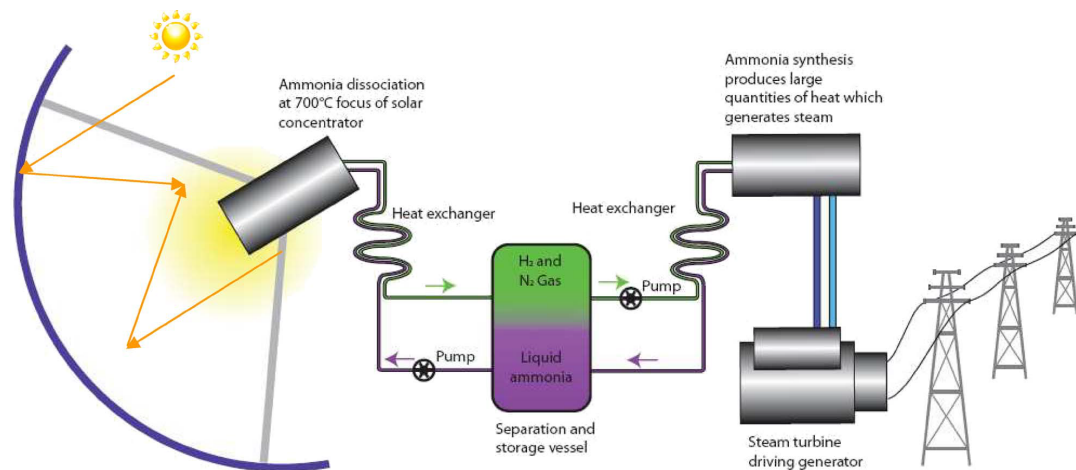


Figure 2.9: Ammonia dissociation and storage schematic. (from Dunn, Lovegrove, and Burgess [DLB12]).

## 2.5 Operation of a Solar Thermal Power Plant with TES System

To obtain maximum benefit from a TES system in a solar thermal power plant, storage operation strategies have a considerable influence. The plant has to be operated at the suitable operating modes and if necessary the operating mode has to be changed at the correct time. The possible operating modes and the two most obvious operating strategies are described in the following sections.

### 2.5.1 Operating Modes

An energy system involving TES usually consists of a production unit, e.g. the solar field or an auxiliary heater, a consumption unit, e.g. the power block and the thermal storage. There are six different ways to operate all these devices.

#### Charging TES System Only

In this operation mode the PB is shut down and the TES system is charged with heat from the SF. In parabolic trough solar thermal power plants heat is usually transferred to the HTF expansion vessel at start up. The power block is still not in operation, but the HTF fluid in the expansion vessel is heated to its determined temperature. Another case to only charge the TES system might be a PB failure or economical reasons.

#### Charging TES System and Serving PB

This happens at times when there is more power available from the sun than necessary to meet the power block's demand. The excess heat is stored in the TES system. If possible the solar field is operated at full load.

#### Solar Only Operation

If the TES system is full, charging must be stopped. The TES is resting and only heat losses to the surrounding occur. The production unit has to be adjusted to meet the consumption unit's demand. This means some mirrors in the solar field must be defocused to not overload the power block. If the TES system is empty and the

## 2 Thermal Energy Storage for Solar Thermal Power Plants

SF does not provide enough heat to reach rated power, the PB is only served by the available heat from the SF and is operated in partial load.

### Serving PB from SF and TES System

In times of little solar irradiance and available power in the TES system the power block is served by energy from the solar field and the TES system. This might happen after sunrise and before sunset when the solar irradiance is too little to operate the PB at rated power.

### Serving PB Only from TES System

Without any solar irradiance available the solar field cannot work. All the power for the power block has to come from the TES system. This is the case at night or when the sky is cloudy.

### PB and SF off, TES resting

During periods with no solar irradiance and low electricity price, the power block might be shut down. The energy in the TES system is saved for times when power production is economically more profitable. Of course, heat losses to the surrounding from the TES system occur during this time.

## 2.5.2 Operating Strategies

Choosing the appropriate operating mode described in Section 2.5.1 is part of the operating strategy. It depends on the type of the power plant, if base-load or peak-load plant, and the pricing scheme for the produced electric energy, if fixed-rate pricing or variable-rate pricing.

Figure 2.10 shows a possible operation scenario for a base load plant at an ideal day (no clouds) and a storage system that is not fully charged. At  $t_{SR}$  the sun rises and the SF and the PB start to heat up. When  $t_{ON}$  is reached the warm-up procedure is finished and power production starts at partial load, since the SF power  $\dot{Q}_{SF}$  is still too low to reach rated power.  $\dot{Q}_{SF}$  increases and when at  $t_{DC}$  rated power is reached and charging of the TES system begins. After  $t_{DD}$   $\dot{Q}_{SF}$  is too low, the difference to maintain rated power output is retrieved from the TES system. After sunset  $t_{SS}$  all

## 2.5 Operation of a Solar Thermal Power Plant with TES System

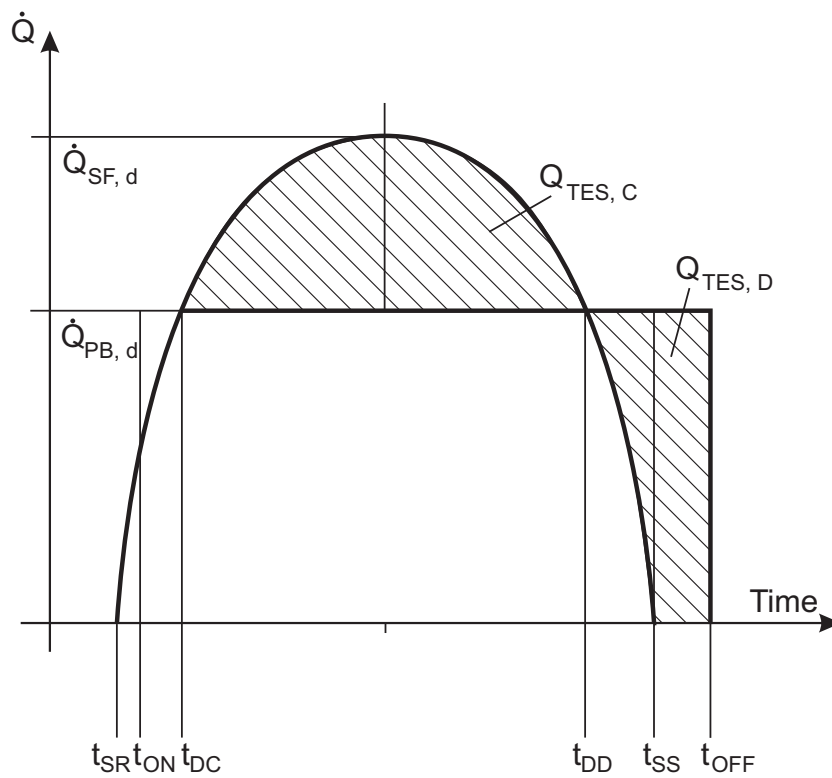


Figure 2.10: Qualitative energy flow in a solar thermal plant with storage (from Geyer [Gey87]).

## 2 Thermal Energy Storage for Solar Thermal Power Plants

the thermal power comes from the TES system until it is empty. At  $t_{OFF}$  the PB is shut down.

The strategies for base-load and fixed-rate pricing are the same. Also peak-load and variable rate pricing have the same operation strategy. Variable-pricing scheme means the price depends on demand and supply. High demand and little supply imply a high price and the other way round it implies a low price. Fixed-pricing is independent of demand and supply.

### Base-Load - Fixed Price

In this case the most economic way to operate the power plant is to maximize power output over the day. This is possible if the available energy is used to maintain the plant at a state of its highest efficiency. Frequent start-ups and shut-downs should be avoided, since they are consuming a lot of energy. In times of high solar insolation the plant is operated at maximum efficiency point and the excess energy is stored in a TES system. If the solar field cannot provide the energy demand of the power-block, the stored energy is used to maintain the power block at a point of high efficiency. During times of no solar irradiance all the energy is taken from the storage if available. In Figure 2.11 the structure of this operation mode is presented. Dependent on the temperature and energy in the HTF coming from the solar field it is decided whether the TES system is charged, discharged or detached.

### Peak-Load - Variable-Price

Peak-load or variable-pricing operation is more complex. Usually there are several smaller and higher peaks in electric power demand over the day. During the night power consumption and prices are low. In the morning when people get up and production sites start to work, demand and price are rising. Around noon there is a "lunch" peak. The highest electric power demand and the highest utility prices occur in the evening after people have come home from work, prepare dinner and switch on their TV sets. This peak is also called "TV-peak".

Figure 2.12 visualizes the control strategy for peak-load or variable-pricing power plant operation. It is best to operate the plant having the highest possible power output when the highest electricity prices occur. During periods of cheaper electricity the power block might operate at lower power output or is shut down while the storage is charged. For this purpose a TES system is really important for the plant since highest insolation and highest electricity prices usually do not occur at the same time. But several start-ups and shut-downs during one day should be avoided



## 2.5 Operation of a Solar Thermal Power Plant with TES System

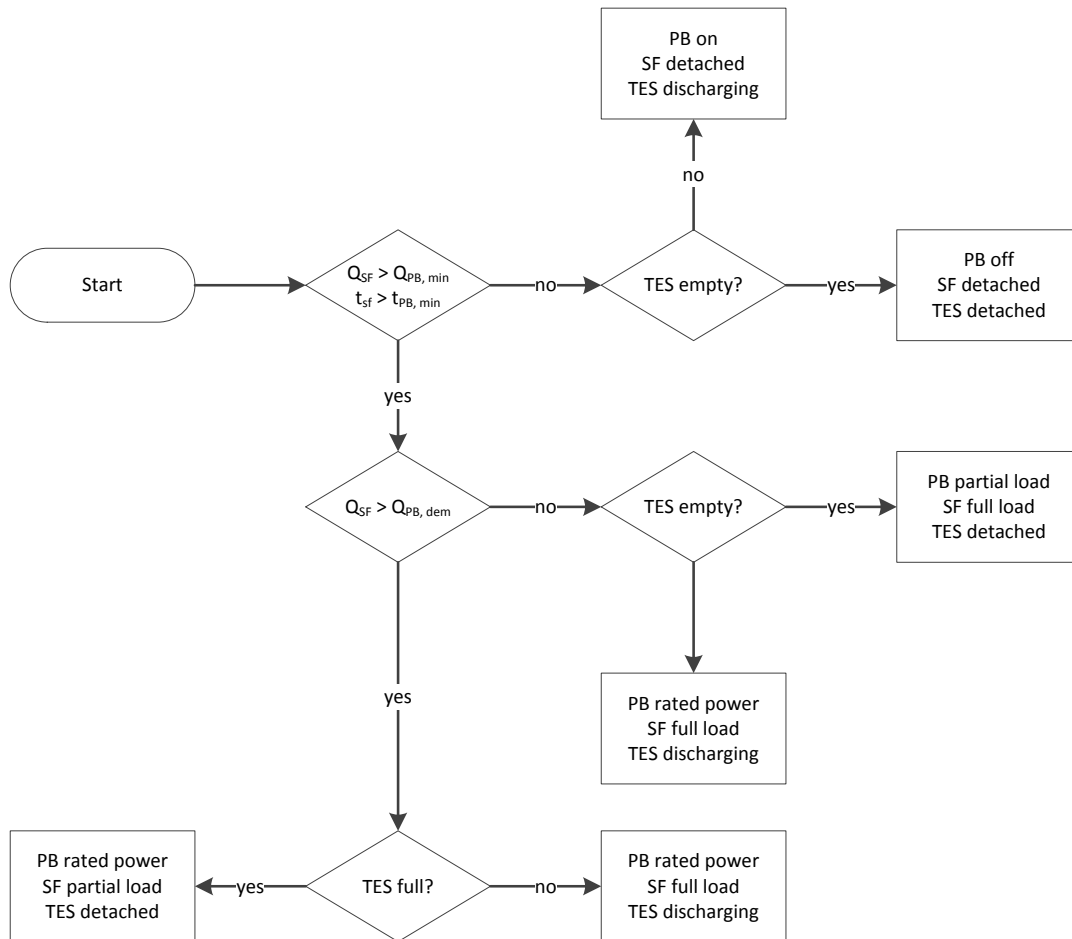


Figure 2.11: Flowchart describing the power plant system control strategy used for fixed-price and base-load operating strategy.

## 2 Thermal Energy Storage for Solar Thermal Power Plants

since they consume a lot of energy and increase the plant's maintenance costs. The plant needs the ability to react very quickly to price fluctuations.

## 2.5 Operation of a Solar Thermal Power Plant with TES System

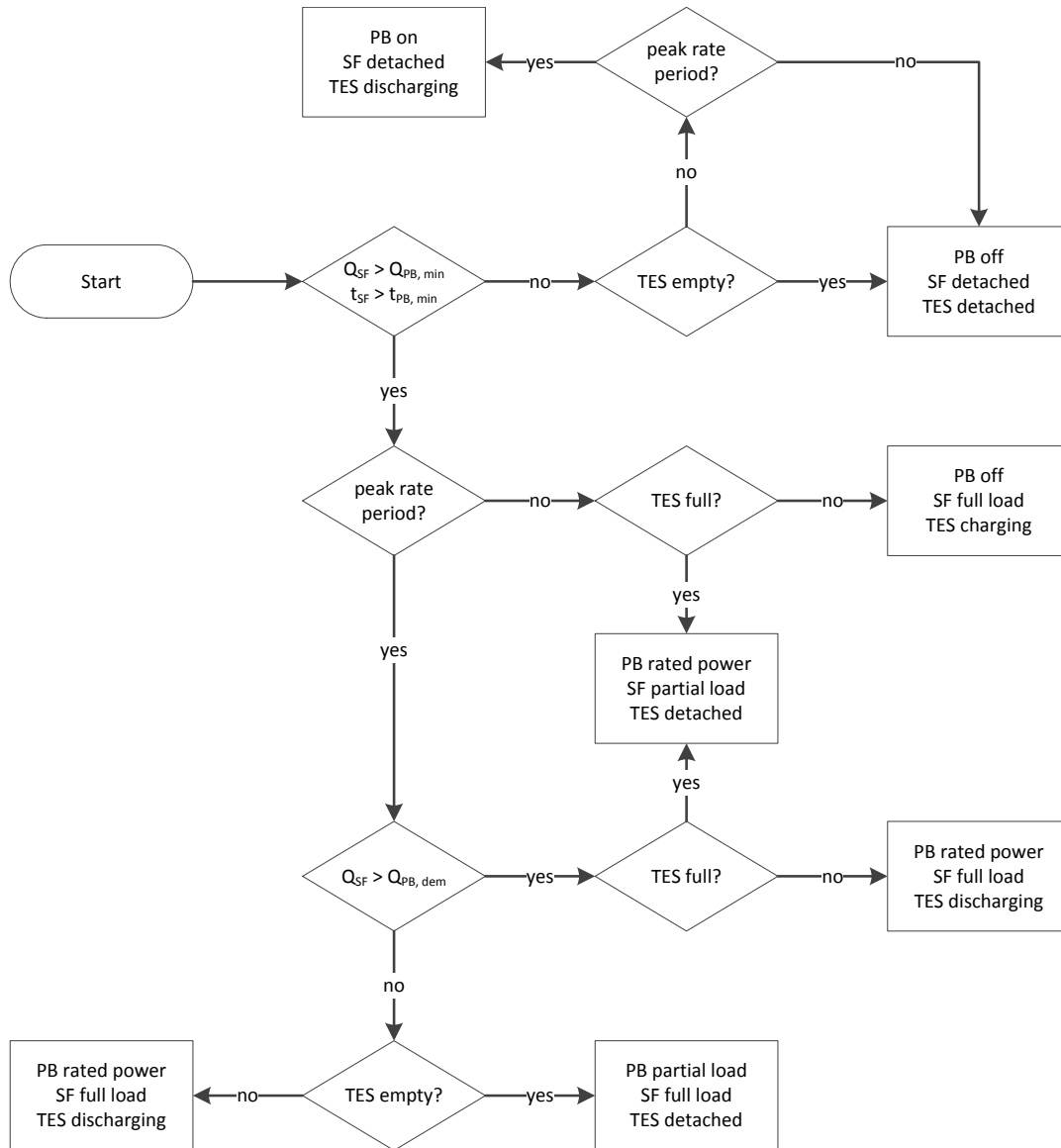


Figure 2.12: Flowchart describing the power plant control strategy used for variable-price and peak-load operating strategy.



## 3 IPSEpro Design Suite

The simulation environment used is the IPSEpro Design Suite. Originally IPSE stood for Integrated Process Simulation Environment and was a standalone desktop application. Today the software consists of several modules which will be described in the following.

The IPSEpro Design Suite is a highly flexible software environment for calculating thermodynamic processes. It is used in various fields of application like power plant engineering, chemical engineering and other related areas. Using the IPSEpro Design Suite, users can create process models graphically by appropriately connecting component models from a library. IPSEpro provides efficient data management, powerful mathematical methods and an intuitive graphic user interface, so one can fully concentrate on the technical aspects of the models. IPSEpro offers virtually unlimited flexibility: It supports users to modify existing component models or to create their own ones in order to meet exactly their modelling requirements. For a growing number of fields of application, ready-to-use standard model libraries are available. This includes libraries for thermal power processes, refrigeration processes and desalination processes [Sim02].

At the core of the software package is the capability to build process models from components, typically representing individual pieces of equipment, like heat exchangers, pumps, etc. IPSEpro is a software framework. It strictly distinguishes between the actual program and the application-specific component models. The user is not limited by built-in component models: The component models are organized in model libraries, which contain all component specific information, from graphical appearance to the equations that describe the behaviour of the components. The user can modify existing model libraries and create new ones. This makes it possible to adjust IPSEpro to new fields of application without modifying the program itself. [PBo6]

The Process Process Simulation Environment (PSE) is used to model and solve thermodynamic processes based on components from a library. PSE provides a graphic flow sheet editor for setting up process models. The user selects the required components from the library menu and arranges them appropriately. All process data is entered directly in the flow sheet. PSE generates output protocols automatically and displays the results in the flow sheet, at the end of a simulation run. [PBo6]

### 3 IPSEpro Design Suite

IPSEpro's Model Development Kit (MDK) provides the capabilities that are required to define new models and to translate them into a form that can be used by PSE. MDK consists of two functional units:

- Model editor
- Model compiler

The model editor allows the user to design icons that represent the models and to describe the model behaviour mathematically in the form of model equations. [PBo6]

In Figure 3.1 the architecture of IPSEpro is visualized. The program modules PSEasy, PSWeb and PSServer are not used in this work and therefore not described here.

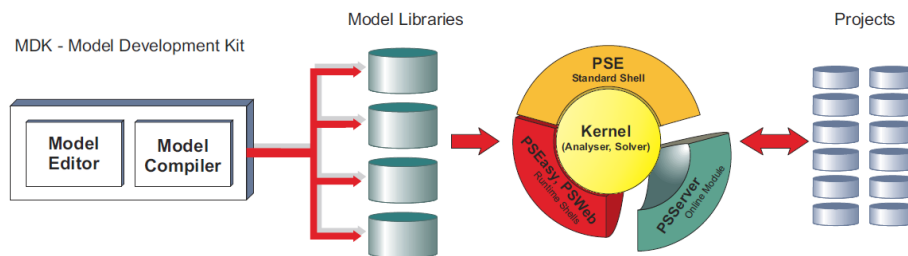


Figure 3.1: IPSEpro architecture (from SimTech Simulation Technology [Simo2]).

PSE gathers the equations behind the icons to form a system of equations. The equations are solved employing a Newton-Raphson Method. Usually this is quite a fast solution method, but sometimes no solution can be found for the equations. More about this in Section 3.1.

For repetitive tasks a scripting module is available. For communication with other programs a Component Object Model (COM) interface is available. This allows to start PSE from any other program supporting COM interface and also allows data exchange. These two features will be described in Section 3.2

## 3.1 Process Simulation Environment

In this section the standard solution method of PSE is explained. Problems that might occur during the solution are described as well.

### 3.1.1 Solution Method

For an equation-oriented simulation software like IPSEpro, running a steady-state simulation requires the solution of a nonlinear algebraic equation system. All solution methods for systems of nonlinear equations are based on some iterative algorithm, iterating an initial value as long as reaching an abort criterion. So the initial value has an important influence on the convergence.

When starting a simulation, as a first step PSE analyzes the system and groups the variables together in such a way that the groups can be calculated one after the other and that the group-size is minimized. Small groups mean little computational effort to solve the system of equations.

To solve a system, PSE adopts a two-phase approach [Sim11b]:

- **System analysis.** In the analysis phase PSE determines the optimum solution method for the equation system. It analyses the order in which it can treat the variables of a model. If PSE must solve several equations simultaneously, it combines them into groups. During the analysis phase PSE also chooses the optimum numerical method for each group.
- **Numerical solution.** When calculating the numerical solution of the system, PSE solves the equations in the order pre-established by the analysis, and uses the numerical methods that also have been chosen in the analysis phase.

IPSEpro uses the Newton-Raphson method to solve the equations:

$$x_{n+1} = x_n - \frac{f(x_n)}{f'(x_n)} \quad (3.1)$$

Starting with an initial value  $x_n$  and linearizing the system, a value  $x_{n+1}$  is calculated which should be closer to the solution.  $x_{n+1}$  becomes  $x_n$  and the whole step is repeated until a sufficiently accurate solution is reached.

The PSE-solver offers two different methods, an undamped and a damped method. The undamped method works as described before. The value  $\Delta x = x_n - x_{n+1}$  is the correction value added to the starting value to obtain the next value (see Figure 3.2). For the damped method  $\Delta x$  is calculated the same way, but before adding it, it is multiplied by a damping factor  $\alpha$  ( $\alpha \in ]0; 1]$ ). This is shown in Figure 3.3. The first simulation step is always undamped. Only if it fails, a decreasing damping factor is applied until the step is successful or the minimum damping factor is reached.

During the numerical solution the variables of the system are iterated until one of the following two criteria is satisfied [Sim11b]:

### 3 IPSEpro Design Suite

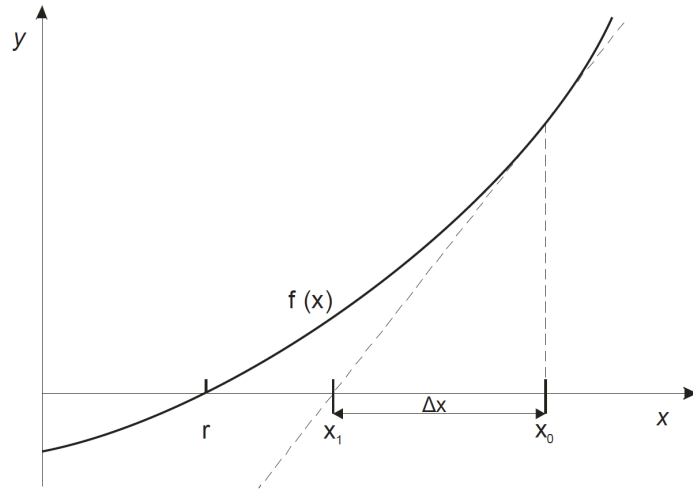


Figure 3.2: Undamped Newton Raphson Method (from SimTech Simulation Technology [Sim11b]).

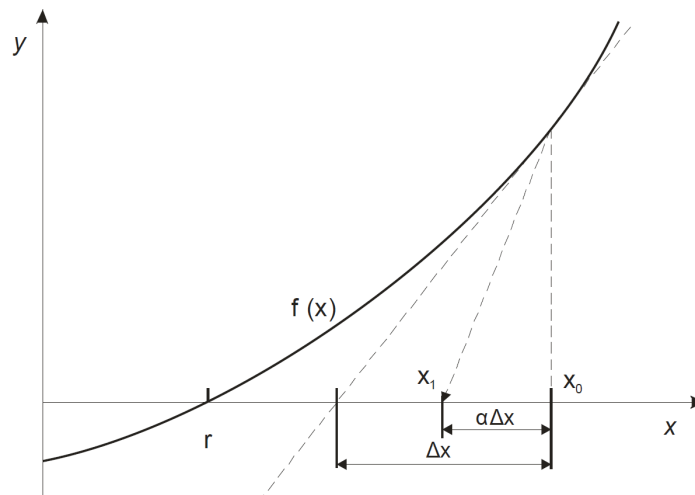


Figure 3.3: Damped Newton Raphson Method (from SimTech Simulation Technology [Sim11b]).



- The relative change in each variable is less than a certain threshold.
- The difference between the left and the right side of each equation, also called the function residual, is less than a certain threshold.

PSE uses a total error for all variables, the  $x$ -tolerance  $E_x$ , and a total error for all equations, the  $y$ -tolerance  $E_f$ . Based on the assumption that each variable contributes equally to the system solution and the total number of variables in the system  $n$ , the error permitted for a single variable is:

$$\epsilon_x = \frac{E_x}{\sqrt{n}} \quad (3.2)$$

The error permitted for a single equation is

$$\epsilon_f = \frac{E_f}{\sqrt{n}} \quad (3.3)$$

In PSE both tolerances can be set by the user in the range of  $10^{-1}$  to  $10^{-6}$ .

#### 3.1.2 Potential Problems During System Solution

When solving groups of equations several errors can occur. First of all the number of unknown variables and the number of equations has to be the same, otherwise the system is either undefined or over-determined. Some groups of equations cannot be solved completely. Further errors are described in [Sim11b]:

- The system of equations is structurally singular. Structural singularities are the consequence of invalid prescribed values. To fix this problem you have to check those variables that you have prescribed.
- The system of equations is numerically singular. The reason for numerical singularity is most frequently the fact that particular equations become singular. For example, the function  $t = f(p, h)$ , which determines the temperature, has a horizontal tangent for wet steam. Applying the Newton method, this causes an error.
- The system of equations does not converge within the given number of solution steps.
- Errors in the built-in or external numerical functions. For example, the attempt to calculate the square root of a negative value causes such an error.

### 3 IPSEpro Design Suite

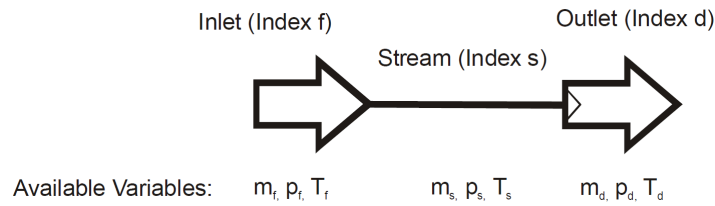


Figure 3.4: Structural singularities(from SimTech Simulation Technology [Sim11b]).

If the system does not converge in the given number of steps, it very often oscillates. In some cases it also diverges. Oscillating systems are usually caused by invalid prescribed values or if the exit criteria  $\epsilon_x$  and  $\epsilon_f$  described above are set too precise.

Imagine a process model containing a source and a sink connected by a stream (see Figure 3.4). In each of them the mass flow  $m$ , the pressure  $p$  and the temperature  $T$  can be set. The system has three undefined variables. So three of the possible nine variables must be prescribed. Prescribing all values in either the source or sink or the stream is possible. Or prescribe the pressure  $p_f$  in the source, the temperature  $T_s$  in the stream and the mass flow rate  $m_d$  in the sink. But prescribing one of the variables  $p, T, m$  in more than one unit leads to a structural singularity of the system. They are not independent from each other. PSE cannot tell which variables to prescribe, but already this simple system allows 27 valid and 57 invalid combination of prescribed values.

Written as a mathematical equation this would look like this:

$$\begin{aligned} f_1 : x_1 + x_2 &= 2 \\ f(x_1, x_2, x_3) = f_2 : x_1 &= 1 \\ f_3 : \quad + x_2 &= 1 \end{aligned} \quad (3.4)$$

As seen in Equation 3.4  $x_3$  cannot be obtained from this system of equations.  $x_1$  and  $x_2$  are determined by  $f_2$  and  $f_3$ , equation  $f_1$  is not necessary [Sim11c].

## 3.2 IPSEpro's Scripting and COM Interface

Scripting is used for repetitive tasks in PSE. You can, for instance, carry out calculation procedures which need multiple evaluations of the simulation model or which consist of a step by step evaluation of different simulation models [Sim11a]. PSE allows internal and external scripts. For internal scripts the script-host is PSE, and they will be described in Section 3.2.2. External scripts offer much more possibilities,

they communicate with PSE over the COM-interface and are hosted in programs like Matlab or the windows script host (WSH).

### 3.2.1 The Component Object Model and Windows Script Host

The Microsoft COM is a platform-independent, distributed, object-oriented system for creating binary software components that can interact. It was introduced by Microsoft in 1993. COM specifies an object model and programming requirements that enable COM objects (also called COM components, or sometimes simply objects) to interact with other objects. These objects can be within a single process, in other processes, and can even be on remote computers. They can be written in different languages, and they may be structurally quite dissimilar, which is why COM is referred to as a binary standard; a standard that applies after a program has been translated to binary machine code [Mic12]. The COM- interface enables the access to a wide range of IPSEpro capabilities from a client application [Sim11c].

WSH is an environment for hosting scripts. That is, when a script arrives at your computer, WSH plays the part of the host, it makes objects and services available for the script and provides a set of guidelines within which the script is executed. Among other things, WSH manages security and invokes the appropriate script engine. It is language-independent for WSH-compliant scripting engines. It allows you to run scripts from both the Windows desktop and the command prompt. WSH is ideal for noninteractive scripting needs, such as logon scripting, administrative scripting, and machine automation [Mic12]. By default the WSH interprets VBScript and JScript, for other scripts like Perl, Python or Ruby the corresponding scripting engine has to be installed. Codes from different script files can be mixed in a windows script file. The code does not need to be of the same language. There are also other Script hosts available, like the PSE-in-built or the one provided by Matlab.

### 3.2.2 Internal Scripts

Internal scripts run in a host provided by PSE. The PSE script interpreter supports scripts written in JScript, Python, Perl, PHP and VBScript. The script communicates with PSE via the COM-interface. For the syntax please check SimTech Simulation Technology [Sim11a]. The main aim of internal scripts is the automation of repetitive tasks. They can perform a sequence of tasks with one single command. You can manipulate data in an existing project, and change values of parameters and variables. This makes scripts a quite useful tool when working with PSE. Data exchange with external sources is not possible. For this purpose external scripts are available. Changing the structure of a PSE project model is also not possible.

### 3.2.3 External Scripts

As mentioned above, external scripts are hosted in another program but PSE. Well-known are WSH or Matlab. Communication takes place similarly to internal scripts, via the COM-interface. External scripts can be written in each language working together with COM. They can start PSE, allow coupling two PSE-projects or linking a PSE-project to Matlab for external optimization. Data exchange with other programs, reading input data from a source or storing calculation data in a file are also possible. They can even run internal scripts, but they have to be written in one of the five languages pointed out in 3.2.2. Communication with internal scripts is not possible. Except from that they offer more or less the same functionality as internal scripts.

A JScript and VBScript script interpreter is installed by default when installing WSH. It is available for all currently available Microsoft Windows operating systems. In JScript the code for starting PSE and displaying the window looks like this:

```
var PSE = new ActiveXObject("PSE.Application");
PSE.showServer(3)
```

The `PSE.showServer(3)` command is necessary to show the PSE window. The number in the command determines the size and position of the window. For Python the code looks similar. First the Python COM client must be started, then PSE can be started:

```
import win32com.client
PSE = win32com.client.Dispatch("PSE.Application")
PSE.ShowServer(3)
```

In a Matlab-script the code looks a little different. Since methods and properties of PSE's COM-interface are not public, you must call `get`, `set` and `invoke` explicitly, like shown below. Also accessing properties that take arguments require explicit calls [Mat12].

```
IPSEpro=actxserver('PSE.Application');
invoke(IPSEpro, 'showServer', '3');
```

JScript and VBScript have the advantage of usually running out of the box on any up-to-date Microsoft Windows operating system. Writing the script can be done in any text-processor.

## 4 Solar Irradiation and Solar Field Modelling

The SF harvests the solar radiation and provides it to the PB and the TES system. A parabolic trough collector design with mineral oil as HTF are investigated in this work. The main parts of the SF are the collectors, the header and mixer, the SF mass flow rate prediction component, the expansion vessel and the piping.

Zaversky [Zav10] has developed a solar irradiation and a steady state parabolic trough collector model. These models have to be adapted for the use in a transient time series simulations. The modification of these two models and the modelling of the other components will be described in the following sections.

### 4.1 The Sun's Position and Solar Irradiation

The sun is the energy source of a solar thermal power plant. It provides the energy needed to operate the plant. Beam and diffuse radiation reach the earth surface, both together are the total solar radiation. Only beam radiation can be focused and therefore utilized for concentrated solar thermal power applications. For this reason it is essential to know the sun's position and the amount of beam radiation onto earth surface.

The sun's position and the direction of the beam radiation relative to a plane for a certain location are dependent on time and date. This can be described by several angles which are shown in Figure 4.1. The most important angles used here in this work are the zenith angle  $\theta_z$ , the angle between the vertical and the line to the sun, and the altitude angle  $\alpha_s$ , which is the complement of the zenith angle.

The solar constant  $G_{sc}$  is the energy from the sun per unit time received on a unit area of a surface perpendicular to the direction of propagation of the radiation at mean earth sun distance outside the atmosphere [DBo6]. It has a value of  $G_{sc} = 1367 \text{ W m}^{-2}$ . Variations of sun-earth distance over the year lead to variations

## 4 Solar Irradiation and Solar Field Modelling

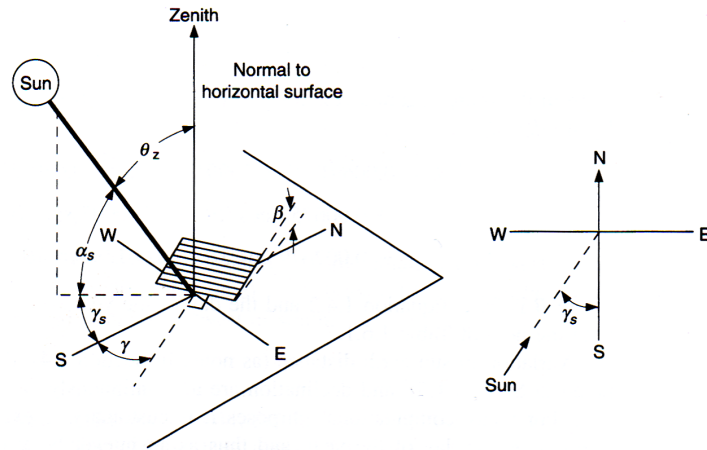


Figure 4.1:  $\theta_z$  zenith angle,  $\beta$  slope angle,  $\gamma$  surface azimuth angle,  $\gamma_s$  solar azimuth angle and  $\alpha_s$  solar altitude angle for a tilted surface (from Duffie and Beckman [DBo6]).

of extraterrestrial radiation  $G_{on}$  of  $\pm 3.3\%$  around  $G_{sc}$ . On its way through the atmosphere radiation diminishes by reflection at the entry, absorption at water, ozone and  $\text{CO}_2$  molecules and Raleigh- and Mie-scattering (see Figure 4.2).

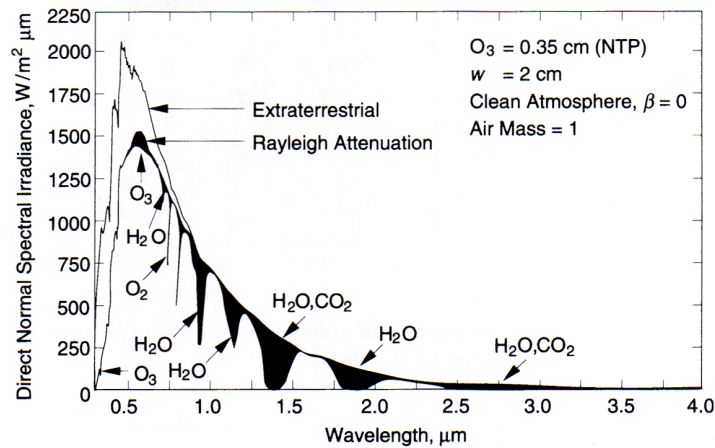


Figure 4.2: An example of the effects of Raleigh scattering and atmospheric absorption on the spectral distribution of beam irradiance (from Duffie and Beckman [DBo6]).

Solar radiation data can be either obtained from measurements, databases or analytical models. Radiation measurements for some location are time-consuming and costly. Databases, like glsTMY3 from the National Solar Radiation Data Base (NSRDB), which provides radiation data for 1020 different locations throughout the US [Nat05], require a high effort to utilize their data. Therefore some analytical

#### 4.1 The Sun's Position and Solar Irradiation

models have been developed. Usually they are easy to use and do not require plenty of input data. Their accuracy is limited, but they are sufficient for first estimations or if no more accurate data is available.

One of these simple models to estimate beam radiation reaching the earth surface through a clear atmosphere has been developed by Hottel [Hot76]. It is presented in Duffie and Beckman [DB06]. This radiation, measured in a plane normal to the incident radiation is also called direct normal irradiance (DNI) and is also the maximum available radiation under clear sky conditions.

$$DNI = G_{on}\tau_b \quad (4.1)$$

$$\tau_b = a_0 + a_1 \exp\left(\frac{-k}{\cos\theta_z}\right) \quad (4.2)$$

$\tau_b$  is the atmospheric transmittance for beam radiation.  $a_0$ ,  $a_1$ , and  $k$  are constants for a standard atmosphere with 23 km visibility. They can be determined by using Equations 4.3. The altitude  $A$  is in km and has to be below 2.5 km.

$$\begin{aligned} \dot{a}_0 &= 0.4237 - 0.00821(6 - A)^2 \\ \dot{a}_1 &= 0.5055 + 0.00595(6.5 - A)^2 \\ \dot{k} &= 0.2711 + 0.01858(2.5 - A)^2 \end{aligned} \quad (4.3)$$

To allow the use for other climate types the following correction factors have to be applied:

$$r_0 = \frac{a_0}{\dot{a}_0} \quad r_1 = \frac{a_1}{\dot{a}_1} \quad r_k = \frac{k}{\dot{k}} \quad (4.4)$$

$r_0$ ,  $r_1$ , and  $r_k$  for different climate types can be found in Table 4.1.

A model calculating the sun's position, the direction of the beam radiation and the clear sky DNI as a function of extraterrestrial radiation  $G_{on}$  according to Hottel [Hot76] has been implemented in IPSEpro by Zaversky [Zav10]. Using the position data in Hottel's clear sky radiation model, a discontinuity of  $\tau_b$  at sunrise and sunset

## 4 Solar Irradiation and Solar Field Modelling

Table 4.1: Correction Factors for Climate Types (from Hottel [Hot76]).

Climate Type	$r_0$	$r_1$	$r_k$
Tropical	0.95	0.98	1.02
Midlatitude summer	0.97	0.99	1.02
Subarctic summer	0.99	0.99	1.01
Midlatitude winter	1.03	1.01	1.00

occurs. At these times the zenith angle is  $\theta_z = \pm\pi/2$ , which causes a division by zero in Equation 4.2. The limes of  $\tau_b$  with  $\theta_z \rightarrow \pm\pi/2$  is calculated as following:

$$\lim_{\theta_z \rightarrow \pm\pi/2} a_0 + a_1 \exp\left(\frac{-k}{\cos\theta_z}\right) = a_0 \quad (4.5)$$

A plot of  $\tau_b$  for a mid-latitude summer climate at sea level can be seen in Figure 4.3. Determining DNI in the morning and evening with Equation 4.1, leads to inaccurate results.

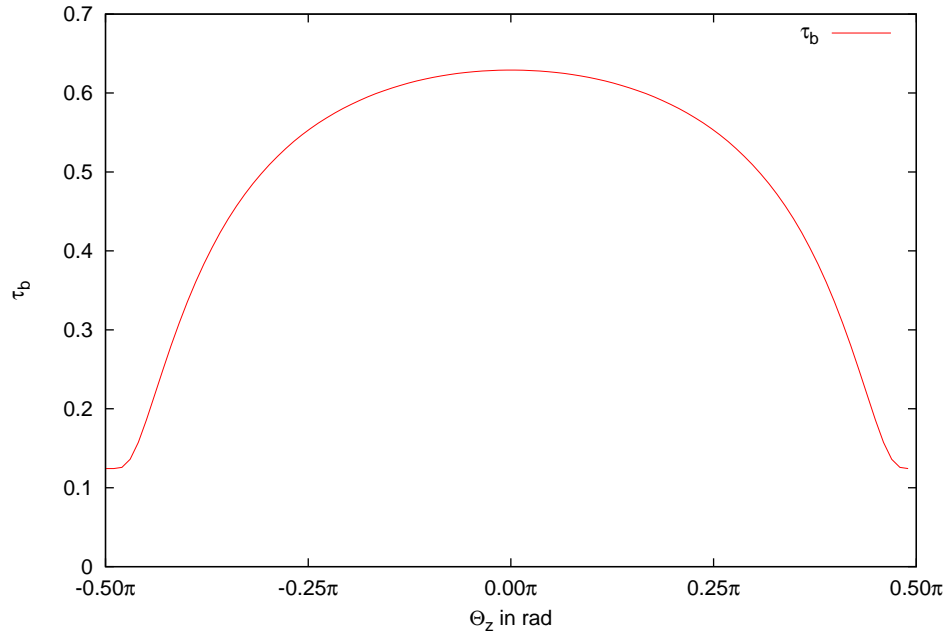


Figure 4.3:  $\tau_b$  as a function of zenith angle  $\theta_z$  at sea level for a mid-latitude summer climate zone.

To avoid this,  $\tau_b$ -values are linearly interpolated between a critical altitude angle  $\alpha_c$  and an altitude angle of  $\alpha = 0^\circ$  at sunrise and sunset. Thus, between  $\alpha = 0^\circ$  and  $\alpha_c$  atmospheric transmittance  $\tau_b$  is calculated according to:



$$\tau_b = \frac{a_0 + a_1 \exp\left(\frac{-k}{\sin \alpha_c}\right)}{\alpha_c \alpha} \quad (4.6)$$

$\alpha_c = 8^\circ$  was found to be a good value and is used in all further simulations but it can be set as desired.

Figure 4.4 shows a comparison of measured and calculated DNI values for Prewitt, New Mexico (Latitude: 35.42 North, Longitude: 108.09 West, Elevation: 2106 meters AMSL). The measurements were performed on the 30<sup>th</sup> of May 2012. The sky was clear except for a few clouds attenuating radiation before sunset. The clear sky DNI for a standard atmosphere according to Hottel is obtained by the model implemented by Zaversky [Zav10] ( $DNI_C$ ) and the model with interpolation at low altitude angles ( $DNI_{C+I}$ ). For both models results are identical except for low altitude angles.  $DNI_M$  and  $DNI_{C+I}$  values match at the best. Further details about the location and the used measuring instruments can be found in [Nat12a].

Similar results can be observed for measurements and calculations performed for location at the Solar Radiation Research Laboratories in Golden, Colorado (Latitude: 39.742 North, Longitude: 105.18 West, Elevation: 1828.8 meters AMSL) on the 9<sup>th</sup> of May 2012 [Nat12b].

## 4.2 The Parabolic Trough Collector

The main parts of a PTC are a parabolic shaped mirror, a steel structure where the mirrors are mounted on and a receiver tube. All rays parallel to the parabola's axis are reflected by the mirror to the focal point of the parabola where the receiver tube is placed. This heats up the HTF circulating through the absorber tubes. The basic working principle and the direction of the rays can be seen in Figure 4.6.

A drive unit rotates the collector to direct the parabola's axis always to the sun. The sun's position can either be measured by sensors or calculated by an astronomical algorithm.

For high temperature applications the reflectors are back-silvered glass mirrors. The receiver tube is a steel tube, coated with a high absorptivity layer and surrounded by a glass tube to reduce convection losses. For receiver temperatures higher than 250 °C the glass tube is evacuated. At the end of each tube there is an expansion bellow to compensate for the different thermal expansion of glass and steel. Figure 4.7 shows the two most common receiver designs from Solel and Schott.

## 4 Solar Irradiation and Solar Field Modelling

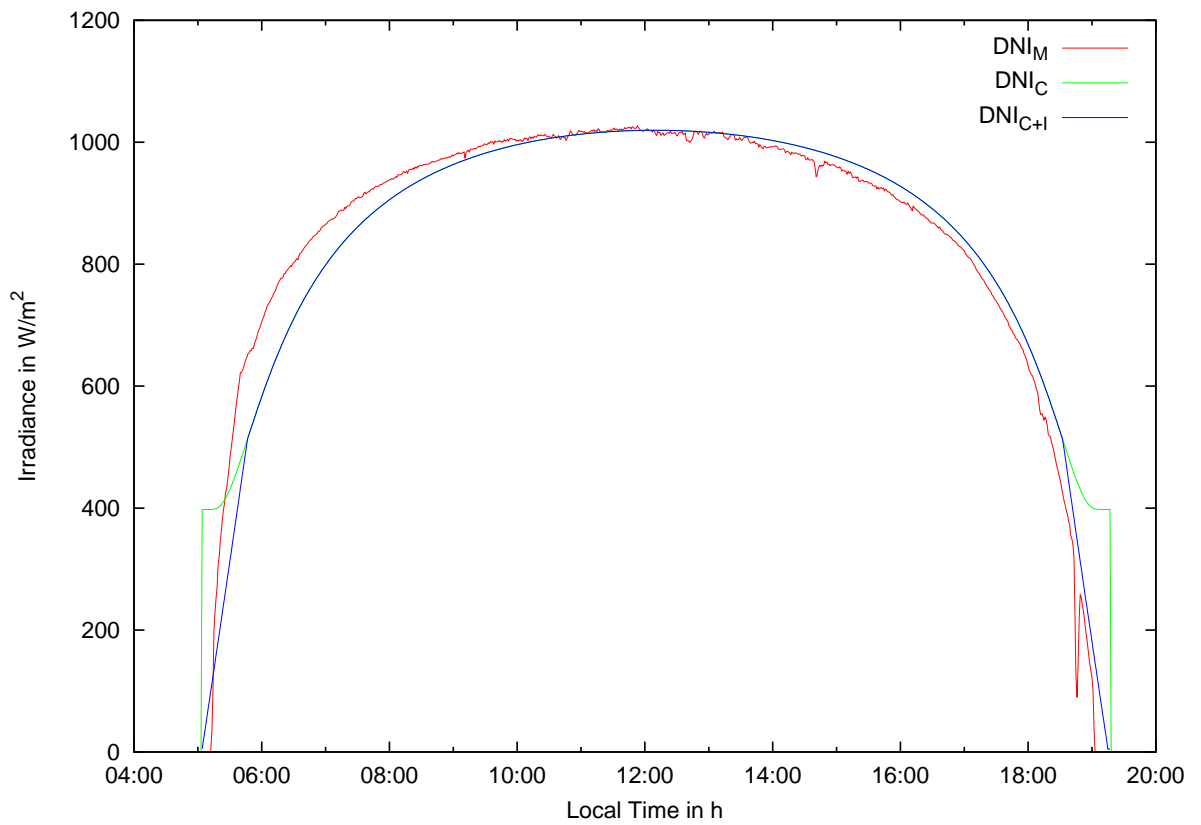


Figure 4.4: Comparison of measured ( $DNI_M$ ) and calculated ( $DNI_C$  and  $DNI_{C+I}$ ) irradiance data. Values were measured at a location close to Prewitt, NM on 30<sup>th</sup> of May 2012.

## 4.2 The Parabolic Trough Collector

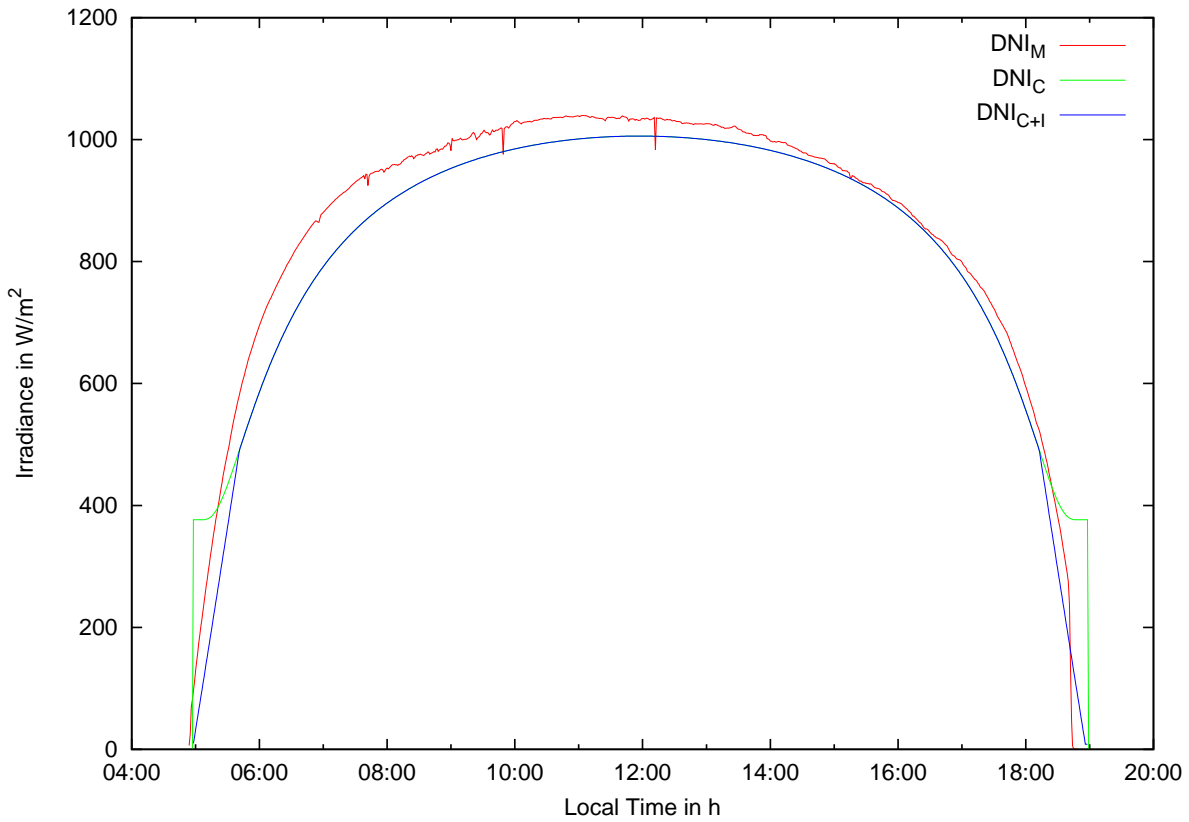


Figure 4.5: Comparison of measured ( $DNI_M$ ) and calculated ( $DNI_C$  and  $DNI_{C+I}$ ) irradiance data. Values were measured at a location close to Golden, Colorado on 9<sup>th</sup> of May 2012.

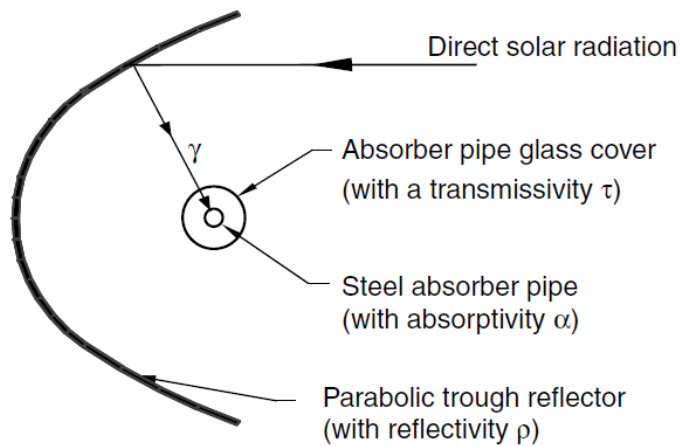


Figure 4.6: Principle of a PTC including optical parameters (from Goswami and Kreith [GKo8]).

## 4 Solar Irradiation and Solar Field Modelling

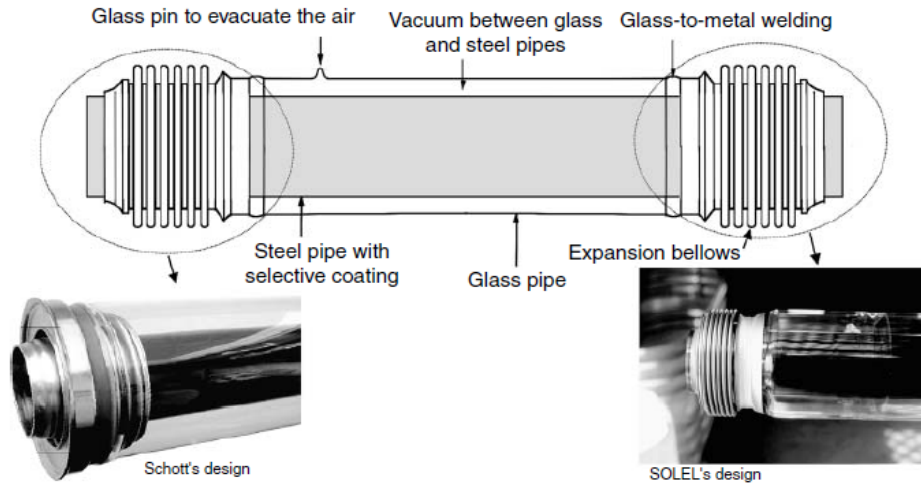


Figure 4.7: A typical receiver tube of a PTC (from Goswami and Kreith [GKo8]).

Today the most commonly used collectors are the LS-3 design from LUZ Industries and the ET-100 and ET-150 developed by the EuroTrough Consortium. Figure 4.8 shows the main LS-3 collector dimensions. This collector design is used for all simulations carried out in this work.

A steady state collector component model using thermal oil as HTF has been developed by Zaversky [Zav10]. The harvested heat is calculated based on physical and empirical relations. Geometric dimensions and characteristics of LS-1, LS-2, LS-3 and ET-100 collectors are implemented, but also a manual mode is available for other collector designs. The heat transferred to the HTF  $\dot{Q}_{fluid}$  is then

$$\dot{Q}_{fluid} = \dot{Q}_{DII} - \dot{Q}_{loss} \quad (4.7)$$

where  $\dot{Q}_{DII}$  represents the heat collected by the heat collecting element (HCE) and  $\dot{Q}_{loss}$  the convective losses from the absorber tube. Three different correlations for convective heat losses from the absorber tubes are available, one based on physical relations and two empirical models, one from [RZo7] and one including the wind speed from [OMB96].

The collector model is extended to a transient model, also considering the thermal capacity of the absorber tube. The energy balance for the absorber tube filled with HTF is

$$\frac{d(Q_{HTF} + Q_{wall})}{dt} = \dot{Q}_{DII} - \dot{Q}_{fluid} - \dot{Q}_{loss} \quad (4.8)$$

## 4.2 The Parabolic Trough Collector

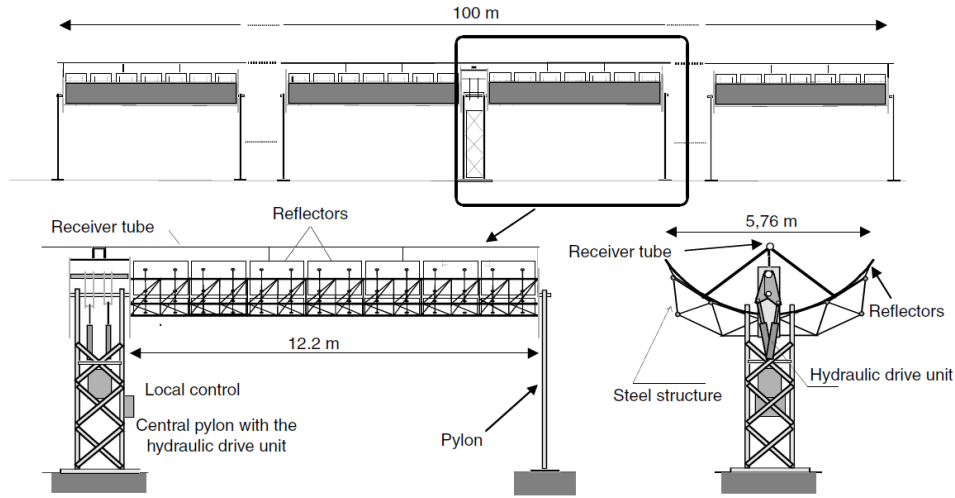


Figure 4.8: LS-3 collector dimension (from Goswami and Kreith [GK08]).

Assuming constant heat capacities for the absorber pipe  $c_{wall}$  and the HTF  $c_{HTF}$  Equation 4.8 can be written:

$$(c_{HTF} + c_{wall}) \frac{dT}{dt} = \dot{Q}_{DII} - \dot{Q}_{fluid} - \dot{Q}_{loss} \quad (4.9)$$

For the use of finite temperature and time steps  $dT$  and  $dt$  have to be replaced by  $\Delta T$  and  $\Delta t$ . This leads to the transient energy balance for an absorber pipe proposed by Rheinländer, Erbes, and Bergmann [REB10].

SF-start-up simulations of SEGS VI plant with such a transient collector model showed quite a good matching between simulated and measured data. Figure 4.9 shows a comparison of a collector loop with steady state and transient collector models. Each loop consists of six LS-3 collectors. The mass flow rate is determined by the help of a mass flow prediction. It will be described later. For the transient model the inlet temperature into the loops is 100 °C if the outlet temperature is below 100 °C. It is 290 °C if the outlet temperature is above 290 °C. In all other cases the outlet and inlet temperatures are identical. For the steady state model the the inlet temperature into the loops is 290 °C if the outlet temperature is higher than 290 °C, it is 200 °C if the outlet temperature is below 290 °C and higher than 200 °C. In all other cases the inlet temperature is 100 °C.

The differences between the steady state and the transient model occur during heat up and cool down phases. Compared to the steady state collector loop, the loop with the transient collector models reaches the nominal outlet temperature with some delay. After sunset it takes much longer for the outlet temperature in the transient

#### 4 Solar Irradiation and Solar Field Modelling

model to drop. The energy stored in the heat-up phase is released now in the cool-down phase. In times with little changes in solar irradiation and mass flow rate there is almost no difference between both collector models. The little fluctuations in the mass flow rate in the loop with the transient collector models are caused by the mass flow prediction.

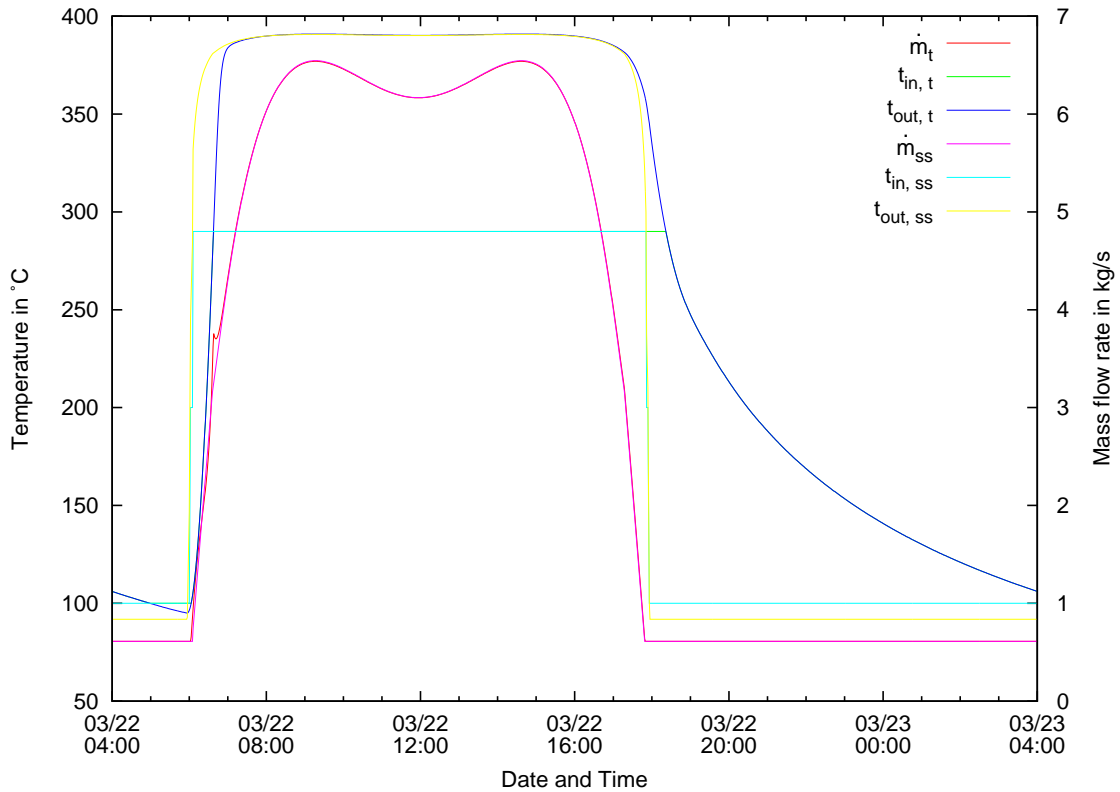


Figure 4.9: Comparison of collector row outlet temperatures for the steady state (ss) and the transient (t) collector models.

It is assumed that the absorber pipe and the fluid have the same temperature. The heat  $Q_{wall}$  stored in the pipe can be calculated as follows:

$$Q_{wall} = m_{wall}c_{wall}T_{fluid} \quad (4.10)$$

## 4.3 The Header and Mixer

The HTF enters the collector array from the inlet header. The outlet header collects the fluid coming from the collector rows and mixes it. In an ideal case each collector loop has the same outlet temperature. In a real SF this usually never happens. Broken or dusty mirrors, defocused collectors or some other irregularity in a collector loop have an influence on the flow rate and the loop outlet temperature.

In the Kramer Junction solar energy generating system (SEGS) plants a flow control valve on each loop sets the flow in each loop under varying header conditions. Even in a solar field with identical collectors, flow maldistribution between loops at varying flow rates can occur because of the settings of these valves. Flow distribution can be readjusted by manually changing the setting of the loop flow control valves [CKK99].

Another option would be to use automatic flow-control-valves to maintain a uniform outlet temperature over all loops. The outlet temperature of each loop is measured and used to adjust the mass flow rate. Compared to the manual flow-control valves, equipment costs are much higher and the equipment might be less reliable [CKK99].

A comparison of both methods was performed at the SEGS V plant. Two loops with automatic flow control valves were compared to two adjacent loops with manual control valves. Start-up tests showed a substantial quicker temperature increase to the desired temperature in the automatic controlled loops. This is shown for the 5<sup>th</sup> November 1997 in Figure 4.10. The loop outlet temperature is more stable on days with varying DNI in the automatically controlled loops and the loops reacted smoother on quick decreases in solar radiation (see Figure 4.10, 14<sup>th</sup> November 1997) [CKK99].

In IPSEpro modelling each loop of a header would require a lot of effort. Such a model would not be very convenient and user-friendly. For this reason the modelling attempt was to build an easy model which still represents reality quite well. Similar loops are grouped together and represented by a single loop. With only one representing loop, the SF's thermal power output can only be adjusted by closing down whole collector loops or defocusing the same collector in all loops. This is not very convenient. Two representing loops allow some more flexibility. Single collectors in both representing loops can be defocused. And it can be set how many loops are represented by each representative loop. Figure 4.11 shows the header model with the collector loops as it is implemented in IPSEpro.

From an energetic point of view it is best to defocus collectors at the cold end of the loop. So the heat losses can be minimized. Even though defocusing of collectors in both loops is possible, in this work, only collectors in the outer loop are defocused.

## 4 Solar Irradiation and Solar Field Modelling

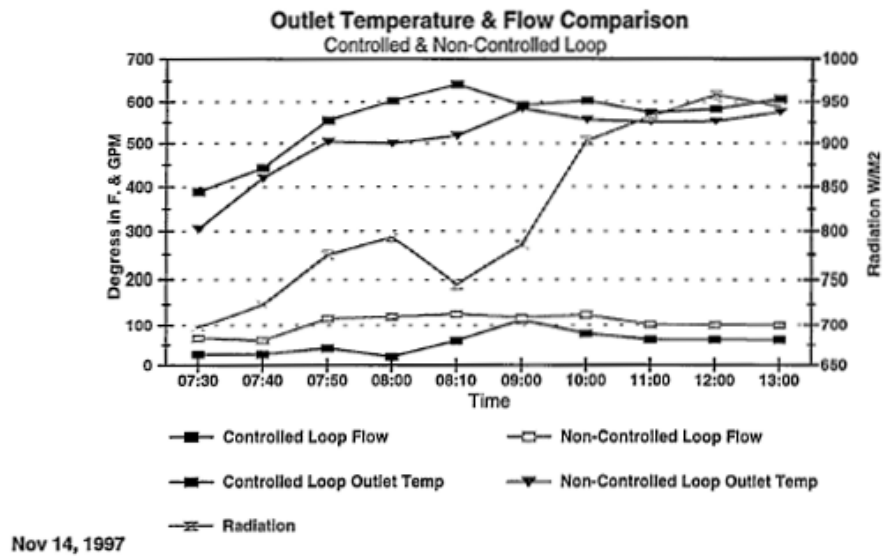
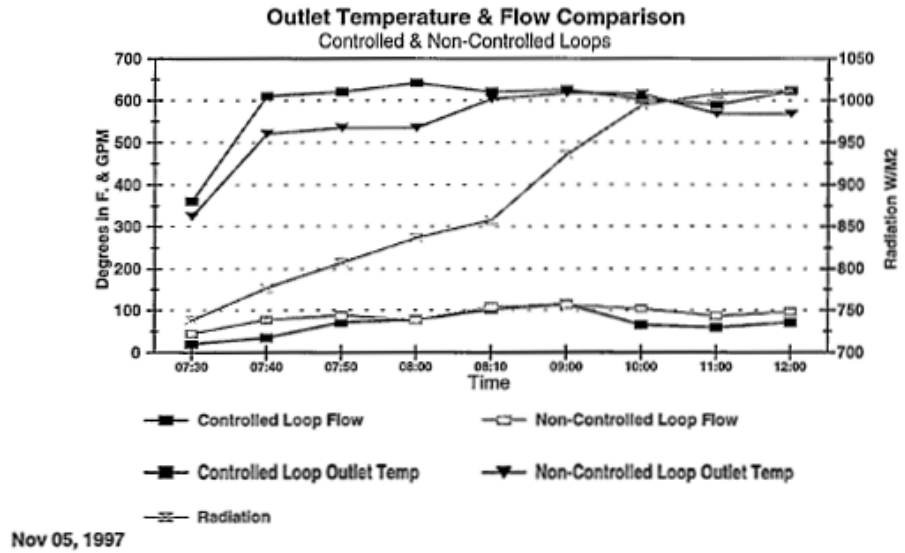


Figure 4.10: Outlet temperature and flow comparison for controlled and non-controlled loops (from Cohen, Kearney, and Kolb [CKK99]).



### 4.3 The Header and Mixer

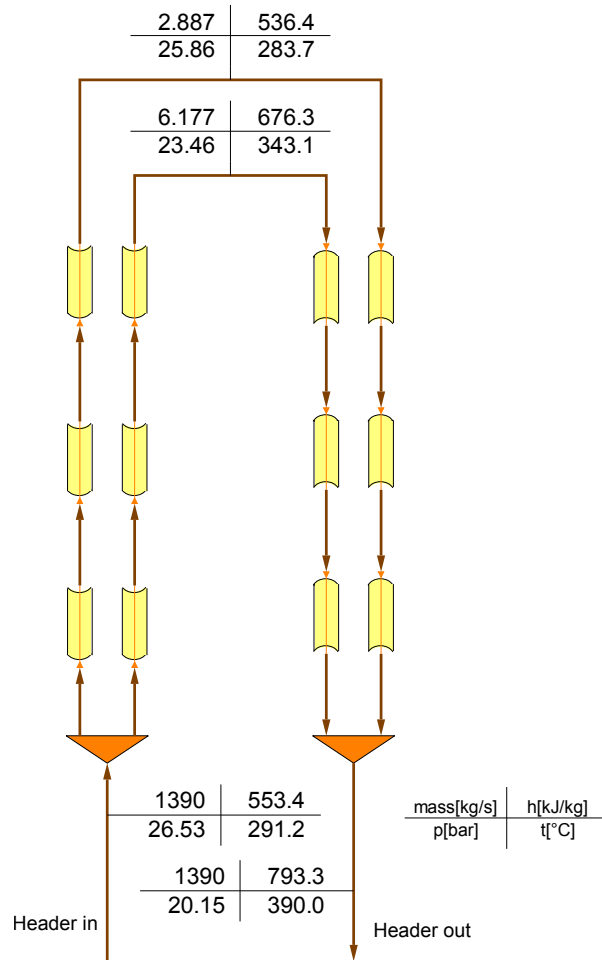


Figure 4.11: Inlet and outlet header with the collector loops in an IPSEpro flow-sheet.

## 4 Solar Irradiation and Solar Field Modelling

The inner loop is used as reference loop to calculate the maximum possible heat that can be collected by the SF.

Header models with automatic and manual flow control valves are developed. With automatic flow control valves the mass flow rate in each row is adjusted to reach a uniform outlet temperature.

With manual control flow valves, similar to the Kramer Junction SEGS solar field headers, the mass flow rate balances itself by the pressure loss. Fluid temperature has a strong influence on the pressure loss along the collector loops. In rows with defocused collectors pressure loss is lower, the mass flow increases. Outlet temperature of loops with defocused collectors drops, as well as header outlet temperature.

Heat losses and thermal capacities of the header are neglected. At very low HTF mass flow rates through the SF the same mass flow rate is guided to every loop, to avoid numerical issues with the solver if the mass flow rate in a loop tends to zero.

### 4.4 Pipes

Pipes are leading the hot HTF from the outlet header to the PB and TES system as well as the cold HTF back to the inlet header. Pipes usually consist of a metal inner tube, enclosed by insulation material which is covered by a thin protective metal layer. A steady-state design model and a transient off-design model are established.

For the design case the pressure loss  $p_{loss}$  and the inner convective heat transfer coefficient  $h_i$  are calculated the same way as for absorber tubes. Thermal conductivities  $k_i$  of the pipe layers, the outer convective heat transfer coefficient  $h_o$  and geometric dimensions have to be provided. The heat loss  $Q_{loss}$  can be expressed with the help of an overall heat transfer coefficient  $U$ :

$$Q_{loss} = UA(t_{mean} - t_{ambient}) \quad (4.11)$$

$U$  is dependent on thermal conductivities and convective heat transfer coefficients. For cylindrical surfaces it is usually defined in terms of a surface  $A$ , in this case the inner surface area.

$$U = \left( h_i^{-1} + \sum_{i=1}^{i=n} \frac{r_1}{k_i} \ln \left( \frac{r_{i+1}}{r_i} \right) + h_o^{-1} \frac{r_1}{r_n} \right)^{-1} \quad (4.12)$$

In partial load  $h_i$  might change because of changing fluid temperature and mass flow rate. Thermal conductivities and  $h_o$  remain constant. For an insulated pipe with fluid at the inner side and ambient conditions at the outer side thermal resistances through insulation and outer convection are much higher than thermal resistances through the piping material and inner convection. Figure 4.12 shows  $U$  for a varying inner convective heat transfer coefficient  $h_i$  for a given pipe. The maximum variation, is approximately 0.5%. Therefore the changes in  $U$  with the change of  $h_i$  are insignificant. With this knowledge a simple off-design heat loss model can be derived:

$$\frac{Q_{loss}}{Q_{loss,0}} = \frac{t_{mean} - t_{ambient}}{t_{mean,0} - t_{ambient,0}} \quad (4.13)$$

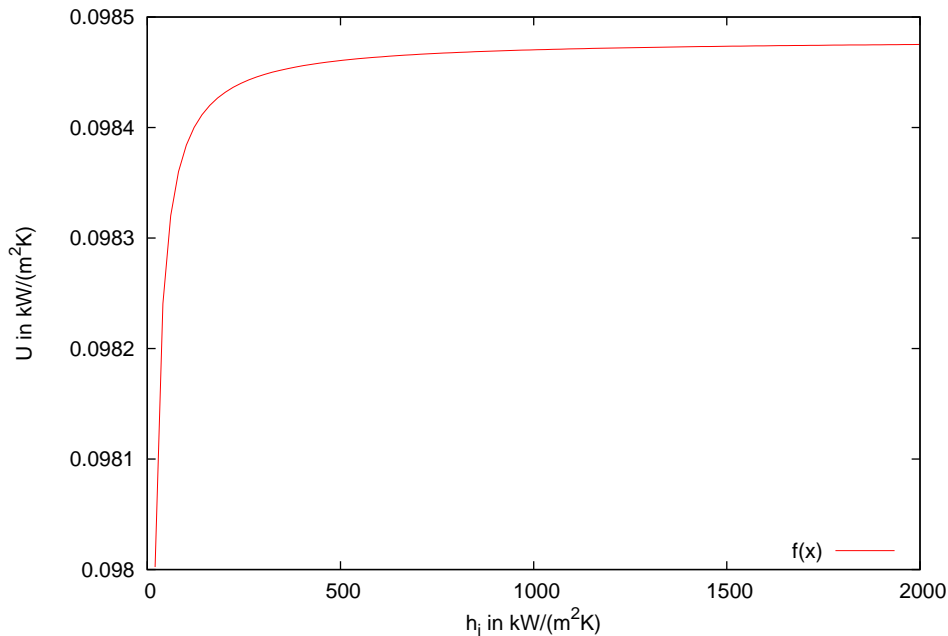


Figure 4.12: Influence of  $h_i$  on  $U$  for a pipe with two layers (pipe dimensions:  $d_1 = 0.9$  m,  $d_2 = 0.92$  m,  $d_3 = 1.1$  m,  $k_1 = 15$  W/(mK),  $k_2 = 0.008$  W/(mK),  $h_3 = 8$  W/(m<sup>2</sup>K)).

The pressure loss is proportional to the square of the mass flow rate, so that the loss at off design is:

$$\frac{\Delta p}{\Delta p_0} = \left( \frac{\dot{m}}{\dot{m}_0} \right)^2 \quad (4.14)$$

## 4 Solar Irradiation and Solar Field Modelling

This is valid since the friction factor for high Reynolds numbers stays constant.

The transient energy balance (see Equation 4.9, with  $\dot{Q}_{DII} = 0$ ) and the heat stored in the pipe are calculated the same way as for the absorber pipe (see Equation 4.10). Heat storage in the insulation and pipe protection is neglected because of low temperatures and heat capacities.

### 4.5 The Expansion Vessel

The HTF density is strongly temperature dependent. Before sunrise the fluid in the SF usually has its coldest temperature. Almost the whole fluid is circulating through pipes and collector rows. When the sun heats up the fluid, it expands and the excess fluid must be stored in an expansion tank. When the fluid cools down, it contracts and is released from the expansion tank. During periods of solar operation almost 25 % of the total HTF-mass are stored in the expansion vessel [REB10].

In IPSEpro the expansion vessel is modelled as a pressurized, ideally mixed tank. Inlet and outlet flow velocities are rather high. Ideally mixing conditions are possible. The vessel itself has a cylindrical shape. A design and an off-design model are implemented. In the steady-state design model the vessel volume, the heat loss and the thermal energy stored in the vessel equipment are calculated.

The volume of the vessel  $V_{vessel}$  is determined by the total HTF-mass  $m_{HTF,tot}$  in the system and the specific volumes  $v$  at maximum and minimum temperatures,  $t_{max}$  respectively  $t_{min}$ , of the fluid.

$$V_{vessel} = m_{HTF,tot} (v(t_{max}) - v(t_{min})) \quad (4.15)$$

The heat loss and the heat stored in the vessel are calculated the same way as for the pipes and the absorber tubes. Expansion tanks are usually long conical vessels. The surface area at the flat ends is usually small compared to the cylindrical area. For this reason heat losses through these areas are neglected, as well as thermal capacities in these walls. The transient energy balance is also the same as for the pipes and the absorber tubes.

The amount of fluid in the expansion vessel is determined as following. The total fluid in the SF  $m_{HTF,tot}$  stays constant. The fluid mass stored in each component of the SF can be calculated quite simply. The fluid mass in the expansion  $m_{HTF,vessel}$  vessel is the mass which cannot be stored in the pipes  $m_{HTF,pipe}$  and the absorber tubes  $m_{HTF,abs}$ .

$$m_{HTF,tot} = m_{HTF,vessel} + m_{HTF,pipe} + m_{HTF,abs} \quad (4.16)$$

The expansion vessel can be placed after the SF outlet or before SF inlet. At SF outlet it avoids fast temperature changes in the HTF which is sent to the PB. But it must be designed to withstand higher pressures and temperatures, which makes it more expensive compared to a expansion vessel placed at SF inlet. Heat losses at SF outlet are also higher compared to SF inlet.

## 4.6 Mass Flow Rate Prediction

During non-solar operation and early start-up it is not possible to achieve the target temperature at the SF outlet. This is obvious when  $DII = 0$ , but it also occurs after sunrise when irradiance may still be so low that only small HTF mass flows rates could reach the target temperature. In this situation, the warming of the equipment downstream of the SF loops would be slow, and collector temperatures might exceed the allowed limit [REB10].

Rheinländer, Erbes, and Bergmann [REB10] suggest the following correlation to estimate an appropriate HTF mass flow rate through the SF:

$$\frac{\dot{m}}{\dot{m}_0} * \frac{h_{out,0} - h_{in}}{h_{out,0} - h_{in,0}} = \frac{DII}{DII_0} \cdot \frac{\sum Q_0}{\sum Q} \quad (4.17)$$

$\dot{m}$  is the mass flow through the SF,  $h_{out}$  and  $h_{in}$  are the specific enthalpies at the outlet and inlet of the SF,  $DII$  is the direct incident irradiance (DII) into the collector aperture and  $\sum H$  is the thermal energy stored in the components. Index 0 indicates values at the power plant's design operating conditions. Extension factor with stored energy content ratio accelerates distribution of solar heat during start-up.

If the predicted HTF mass flow rate drops below a certain minimum mass flow rate, usually 10% of the design mass flow rate, the mass flow rate is set to this minimum value. This corresponds to real practice and prevents the HCEs from cooling down too much at night, as the heat remaining in the large insulated equipment after sunset is redistributed along the HTF circuit through the SF [REB10].

## 4.7 Solar Field Size and Layout

A SF consists of a number of parallel rows with collectors connected in series. The design mass flow rate and the desired temperature increase in the working fluid determine the number of collectors in a row. The desired rated thermal power determines the number of rows. The collector rows are connected to the feed and drain piping via the headers. The layout of the piping and the header depends on the size and purpose of the SF.

Figure 4.13 shows the three most common solar field piping layouts, direct return (a), inverse return (b) and centre feed (c) with their advantages and disadvantages. In all three options the drain piping with the hot fluid is shorter than the feed piping to minimize thermal losses.

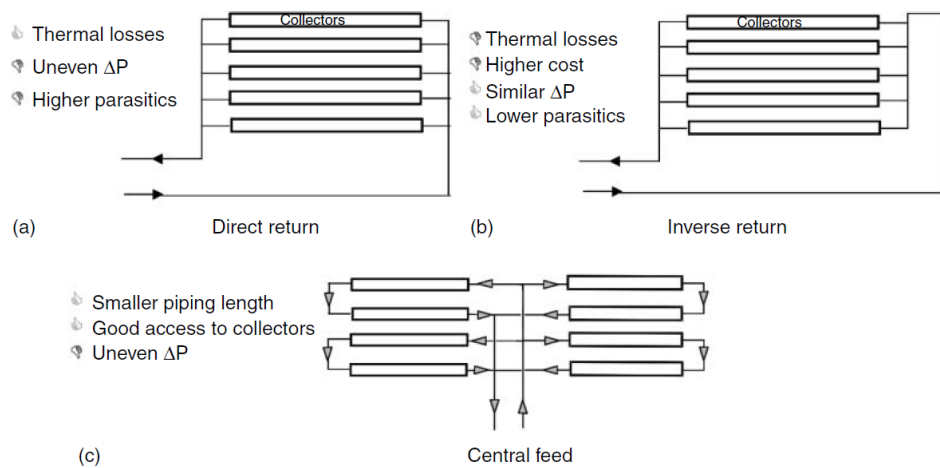


Figure 4.13: Solar field layouts for parabolic trough collectors (from Goswami and Kreith [GKo8]).

Direct return is the simplest configuration and most commonly used layout for small solar fields. It demands flow control valves to achieve a uniform flow rate in each row. This causes a significant pressure drop and increases parasitic pump power. Parasitics are tried to be minimized by pipe headers with different diameters, but investment costs for such headers are high. Compared to the inverse return configuration the piping is shorter and the thermal losses are lower [GKo8].

The inverse return has a better balanced flow and compared to the direct return configuration, lower pressure losses. Balancing valves might still be necessary. Another option would be header pipes that step down at the feed and step up at the drain to reach a uniform flow rate in the collector loops. This is the configurations with the longest piping that results in higher costs for piping, insulation and fluid. The longer feed piping might also increase thermal losses [GKo8].

The centre feed configuration is widely used for large SFs. Because pressure losses are uneven, balancing valves or stepping up and down headers are required. These headers minimize pressure losses. Of all three layouts this one has the shortest piping length, no pipe has to run along the collector rows. Collectors are easy to access since no pipes are along the sides of the SF [GKo8].

### 4.8 The Solar Field Model

Figure 4.14 shows the SF model in IPSEpro. The cold HTF, TherminolVP1, enters the SF at the bottom. The expansion vessel is placed at the cold end before the solar field pump. The orange bar where the SF feed and drain streams are passing through is the mass flow rate prediction. The header regulates the mass flow rates in each loop so a uniform outlet temperature can be achieved. Like in the SEGS XI SF six LS-3 collectors are connected in series. Through the outlet header and the piping the fluid is led to the consumers.

In the design point the fluid enters the solar field at 290 °C and leaves it at 390 °C. The number of loops is determined by the thermal rated power. It has to be ensured that the fluid temperature does not exceed 400 °C and does not fall below the freezing point of the HTF. Because of the low vapour pressure of TherminolVP1 a minimum pressure of 14 bar must be maintained in the HTF.

## 4 Solar Irradiation and Solar Field Modelling

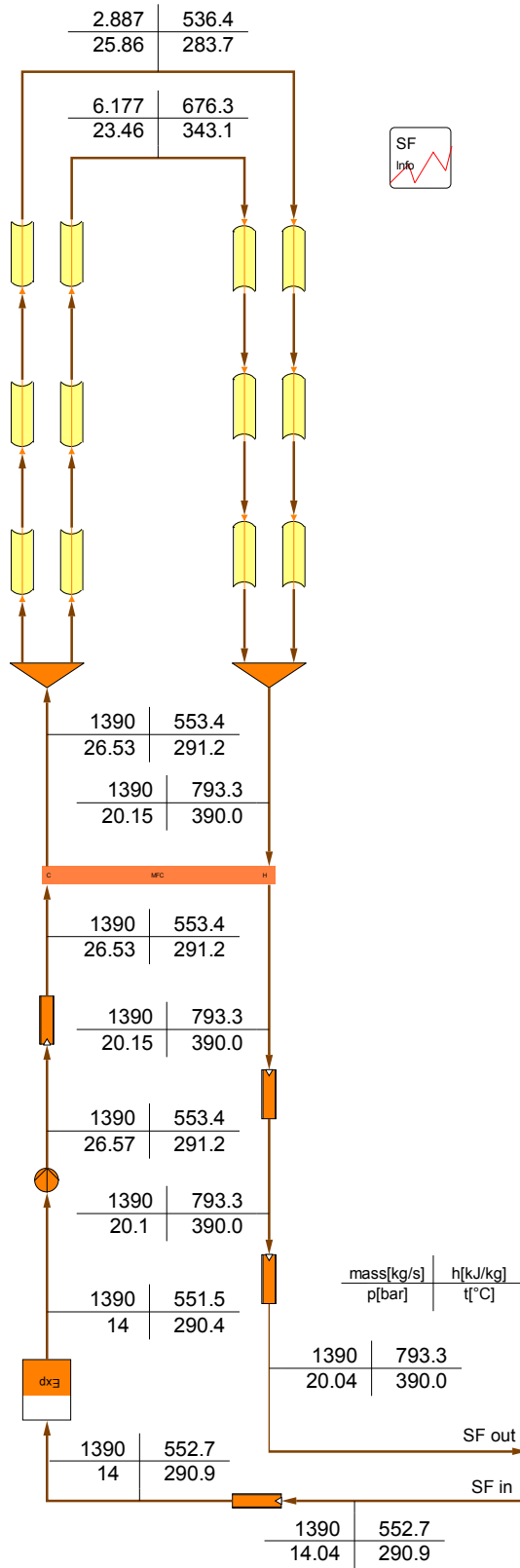


Figure 4.14: Flow sheet of the solar field in IPSEpro.



# 5 Modelling Thermal Energy Storage

In the following sections the modelling of a two-tank and a thermocline TES system is described. The main aim in this work is to study the performance of a solar thermal power plants involving a TES system. It is tried to keep the models as simple as possible and as detailed as necessary. Detailed models require a lot of computational effort in terms of input and output data reduction and calculation time. Calculation time is a critical point.

## 5.1 Two-Tank Model

Two different two-tank TES system models are created. A basic one, only considering the heat and mass balances with a simple heat loss model, and a more detailed one also considering geometrical dimensions of the tanks and with a more detailed heat loss model.

A two-tank storage system consists of the two storage tanks, the charge and discharge equipment and in case of an indirect storage system a working fluid/storage fluid heat exchanger.

As shown in Figure 5.1 the charging and discharging stream are modelled as two separate streams. In practice, for charging and discharging usually the same piping and heat exchanger is used, only the flow direction is reversed. The HTF passes through the working fluid/storage fluid heat exchanger which is modelled as a counter-flow heat exchanger. Usually for applications where thermo oil is used as HTF and molten salt as storage material, a tube and shell heat exchanger is used. The HTF is running through the tubes while the molten salt is passing on the shell side.

Very often the heat exchanger operates at off-design conditions because of fluctuations in solar irradiance. A good part load behaviour is necessary in order to collect as much surplus energy as possible. Here the same part load characteristic is used as for all other heat exchangers. Zaversky et al. [Zav+12] propose another part load performance characteristic for a shell and tube heat exchanger. At very low load heat transfer between oil and salt is quite poor. Therefore Zaversky et al. [Zav+12]

## 5 Modelling Thermal Energy Storage

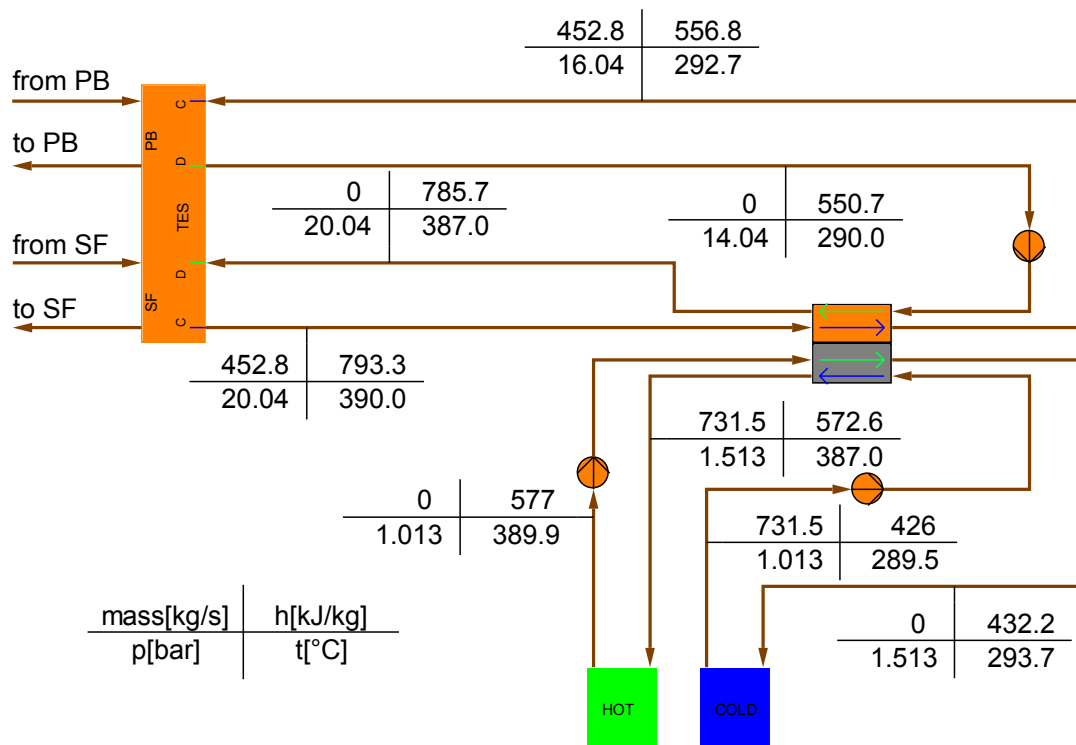


Figure 5.1: The TES subsystem in an IPSEpro flow sheet with the two-tank storage system, the working fluid/storage fluid heat exchanger and the flow distributor.

suggest to use two separate heat exchanger trains in parallel where one train can be switched off.

The tank itself is usually cylindrically shaped. At the outer surface insulation material is applied to reduce heat losses. Charge and discharge equipment is located at the bottom of each tank. This zone in the tank is also called pump sump and has to be covered by the storage material all the time. Therefore the fluid in the pump sump cannot be utilized for charging and discharging. The rest of the tank can be filled with active working fluid.

Both tanks are modelled as a fully-mixed tank, that means the entire fluid in a tank has the same temperature. The transient energy balance for such a tank is

$$\frac{dQ}{dt} = \dot{Q}_c - \dot{Q}_d - \dot{Q}_{loss} \quad (5.1)$$

where  $\dot{Q}_c$  and  $\dot{Q}_d$  are the charge and discharge power.  $\dot{Q}_{loss}$  is the rate of heat losses. For the use in an IPSEpro model Equation 5.1 has to be discretized and so it can be written:

$$(m_s h)^n - (m_s h)^{n-1} = [(\dot{m}h)_c^n - (\dot{m}h)_d^n - \dot{Q}_{loss}] \Delta t \quad (5.2)$$

$m_s$  is the mass and  $h$  the enthalpy of the storage material. The superscript  $n - 1$  indicates values from a time step  $\Delta t$  before. The values indicated with  $n$  are to calculate. This equation is used in the basic and the more detailed model, together with the mass balance

$$(m_s)^n - (m_s)^{n-1} = (\dot{m}_c^n - \dot{m}_d^n - \dot{m}_{leakage}) \Delta t \quad (5.3)$$

to determine mass and temperatures of the stored liquid for each tank. The pressure of the fluid entering and leaving the tank is equal the pressure in the atmosphere on top of storage fluid.

### 5.1.1 Basic Two-Tank Model

In the basic model the active storage mass  $m_{act}$  and the mass in the pump sumps of both tanks  $m_{ps}$  have to be prescribed. The total mass of fluid in one tank is then half of  $m_{ps}$  and the share of  $m_{act}$  in this tank. Heat and mass balance are used as presented in Equations 5.2 and 5.3. The heat loss rate  $\dot{Q}_{loss}$  is calculated with

## 5 Modelling Thermal Energy Storage

$$\dot{Q}_{loss} = (m_s h)^{n-1} k_{loss} \quad (5.4)$$

where  $k_{loss}$  is the heat loss factor per unit of time.

The stored energy in the TES system is the specific enthalpy difference of the hot and cold tank  $h_{hot}$  and  $h_{cold}$  times the active mass  $m_{act,hot}$  in the hot tank.

$$H_{TES} = (h_{hot} - h_{cold}) m_{act,hot} \quad (5.5)$$

The charging status of the TES system  $C_{TES}$  is the ratio of active mass in the hot tank to total active mass.

$$C_{TES} = \frac{m_{act,hot}}{m_{act}} \quad (5.6)$$

### 5.1.2 Detailed Two-Tank Model

The detailed two-tank model consists of a design and a transient off-design model. In the design model tank dimensions and storage capacity are determined. The off-design model is used for transient performance calculation.

#### Design Model

The active storage mass is determined by the desired energy stored  $H_{TES}$  and the enthalpy drop from the hot to the cold tank.

$$H_{TES} = m_{act} (h_{hot} - h_{cold}) \quad (5.7)$$

Storage capacity in full load hours  $C_{FLH}$  is the stored heat divided by the nominal thermal power consumption of the PB  $\dot{Q}_{PB,0}$ :

$$C_{FLH} = \frac{H_{TES}}{\dot{Q}_{PB,0}} \quad (5.8)$$

Tank dimensions are determined by the fluid density and the maximum mass in each tank. The inner tank volume is determined by the volume necessary for the active mass  $V_{act}$  and a volume fraction necessary for the pump sump  $f_{PS}$  and some fraction of empty room  $f_{empty}$  on the top.

$$V_{act} = (1 - f_{PS} - f_{empty}) V_{tank} \quad (5.9)$$

The volume in the cold tank can be smaller because of lower density of the fluid at the lower temperature. The inactive mass stored in the pump sump in each tank is

$$m_{PS} = f_{PS} V_{tank} \rho \quad (5.10)$$

and the total mass  $m_{tot}$  in both tanks is

$$m_{tot} = m_{PS,hot} + m_{PS,cold} + m_{act} \quad (5.11)$$

The heat losses are calculated based on the conduction and convection heat transfer coefficients in tank walls, insulation and at the outer surface. It is assumed that the temperature of the inner wall is identical to the fluid temperature. The overall heat transfer coefficient for the cylindrical parts of the tank is calculated according Equation 4.12. For the flat areas the overall heat transfer coefficient  $U_{flat}$  with the wall thickness of a certain layer  $x_i$  is:

$$U_{flat} = \left( h_i^{-1} + \sum_{i=1}^{i=n} \frac{x_i}{k_i} + h_o^{-1} \right)^{-1} \quad (5.12)$$

The heat loss from a tank is then calculated:

$$Q_{loss} = \left[ (UA)_{flat} + (UA)_{cyl} \right] (t_s - t_{ambient}) \quad (5.13)$$

The cylindrical areas are the walls of the tank, the flat areas are on top and at the bottom. The same heat loss is assumed of top and bottom even though there occurs convection heat transfer on the outer surface and conduction heat transfer to the ground through the bottom area.

### Off-Design Model

The off-design model works almost the same way as the easy two-tank model, except for the heat loss calculation. Active and pump sump mass for both tanks are taken from the design model. Off-design heat loss is calculated relative to design heat loss according Equation 4.13.

### 5.2 Thermocline Model

A multi-node approach is used for the thermocline TES system model. The tank is divided into  $N$  nodes (see Figure 5.2). All of them act as a fully mixed store.

Dependent on the storage capacity the number of nodes has to be chosen. With too many nodes  $N$  this model represents a high level of stratification in the tank that may not be achievable in actual reality [DBo6]. Too few nodes might not represent stratification at all. De-stratification over time due to diffusion and axial conduction in the tanks walls is not considered.

If the storage and working fluid are different, a heat exchanger like the one described in Section 5.1 has to be used. Like for the two-tank model the charging and discharging stream are modelled as two separate streams. In practice, for charging and discharging usually the same piping and heat exchanger is used, only the flow direction is reversed.

Again this model consists of a design model and a transient off-design model. In the design model the geometric dimensions and the storage mass necessary for the desired storage capacity are determined. With the off-design model charge and discharge procedures can be simulated.

#### 5.2.1 Design Model

Storage mass necessary for a desired storage capacity can be calculated with the specific enthalpies  $h_{hot}$  and  $h_{cold}$  of the hot and cold section at the design temperatures  $t_{hot}$  and  $t_{cold}$  using Equations 5.7 and 5.8. The inner tank volume  $V_{tank}$  can be calculated:

$$V_{tank} = \frac{m_{TES}}{\rho(t_{hot})} \quad (5.14)$$

The inner tank dimensions with the inner diameter  $D_i$  and the inner tank height  $H_i$  are then:

$$V_{tank} = \frac{D_i^2}{4} \pi H_i \quad (5.15)$$

The wall and insulation thickness,  $x_{wall}$  and  $x_{ins}$ , thermal conductivity of the material and the convection heat transfer coefficient at the outer surface area are used to calculate the overall heat transfer coefficient  $U$  according Equation 4.12.

### 5.2.2 Off-Design Model

Figure 5.2 shows the concept of the multi-node modelling approach. When charging, fluid with the mass flow rate  $\dot{m}_c$  and the temperature  $t_c$  enters the node  $N_{i-1}$ . At the same time fluid with the same mass flow rate and the temperature  $t_{N_{i-1}}$  is shifted from node  $N_{i-1}$  to  $N_i$ . The same happens from node  $N_i$  to  $N_{i+1}$  and so further down until the fluid exits at the last node to be heated up again. In case of discharging the whole process is reversed.

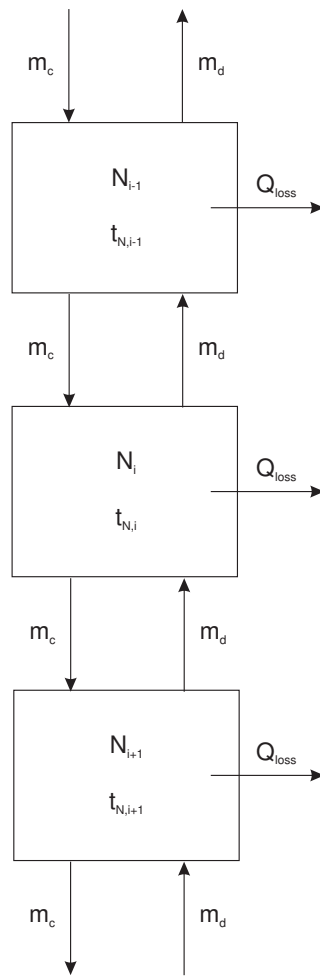


Figure 5.2: Concept of the multi-node modelling approach.

The mass in the tank is divided into  $N$  sections with the mass  $m_N$

$$m_N = \frac{m}{N} \quad (5.16)$$

## 5 Modelling Thermal Energy Storage

The mass balance is steady-state. For a node  $N_i$  the energy balance can be expressed as

$$\frac{m_N}{\Delta t} \left( h_{N_i}^n - h_{N_i}^{n-1} \right) = \dot{m}_c \left( h_{N_{i-1}}^{n-1} - h_{N_i}^{n-1} \right) + \dot{m}_d \left( h_{N_{i+1}}^{n-1} - h_{N_i}^{n-1} \right) - A_s U \left( t_{N_i}^n - t_{ambient} \right) \quad (5.17)$$

where the last term on the right hand side accounts for the losses to the environment.

Very important for this model is the stability criterion:

$$\dot{m}_c \Delta t \leq m_N \quad \& \quad \dot{m}_d \Delta t \leq m_N \quad (5.18)$$

The product of flow rate and timestep must not exceed the mass stored in a single node if inconsistent results for the node temperatures shall be avoided.

The energy stored  $H_{TES}$  in the thermocline tank is the sum of stored energy in the single nodes.

$$H_{TES} = m_N \sum_{i=1}^N (h_{N_i} - h_{cold,0}) \quad (5.19)$$

Finally, the charging status of the TES  $C_{TES}$  is calculated:

$$C_{TES} = \frac{H_{TES}}{H_{TES,0}} \quad (5.20)$$

Two thermocline TES off-design models are created, a ten- and a twenty-node model. Figure 5.3 and 5.4 show calculation results for the same thermocline tank system, one performed with the ten-node model and one with the twenty-node model. The twenty-node model is suitable for thermocline systems with higher degrees of stratification.



## 5.2 Thermocline Model

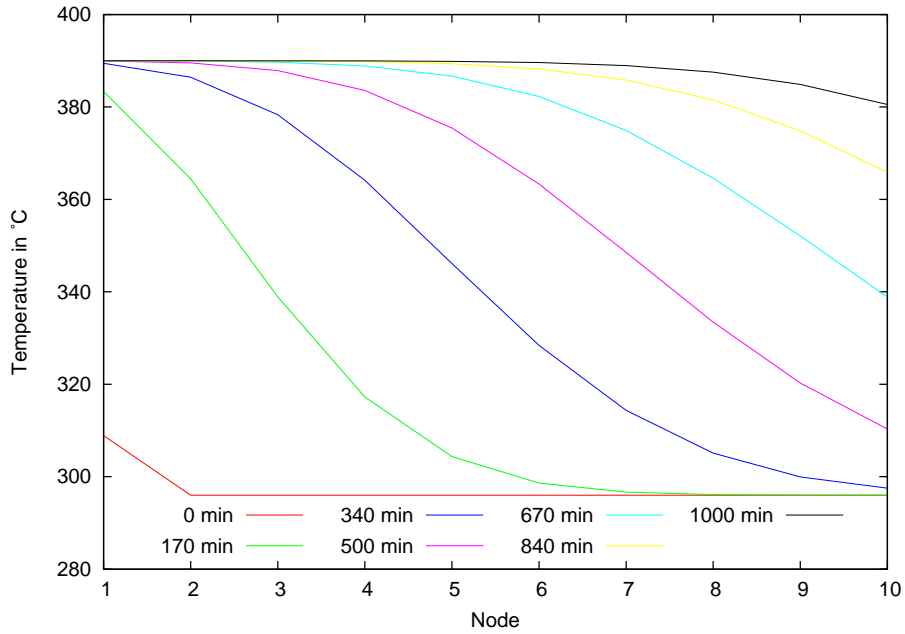


Figure 5.3: Temperature distribution in the ten-node thermocline model when charging with constant inlet mass flow rate and temperature.

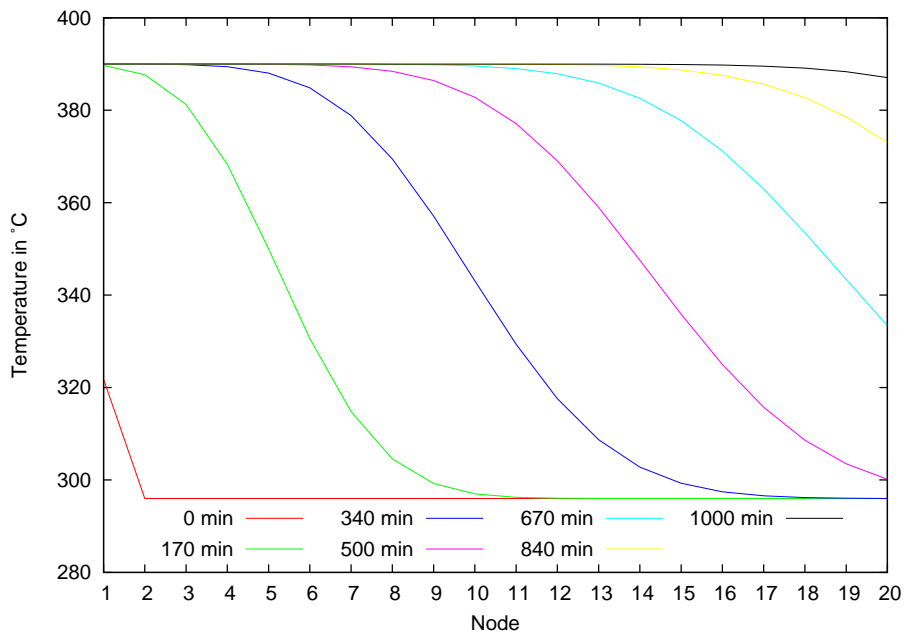


Figure 5.4: Temperature distribution in the twenty-node thermocline model when charging with constant inlet mass flow rate and temperature.



## 6 Modelling the Power Plant

The PB model is a conventional Rankine steam cycle. A component called Flow-Distributor connects the PB, SF and TES system. As last modelling task in PSE for the PB, the SF and the TES system information component models are created. They provide an overview over the most important and interesting values of each section. The last part of this chapter is about the interactions of the power plant model with the automation script.

### 6.1 The Power Block

The PB converts the thermal energy from the solar field and the TES to electricity. The plant layout is similar to the one of SEGS VIII. It is a conventional Rankine power cycle, which is commonly used in steam power plants like a coal-fired power plants. Steam and feed water parameters have been obtained from a flow sheet of the SEGS VIII plant found in Ratzesberger [Rat95]. An overview of steam and HTF-parameters of the SEGS plants can be found in Goswami and Kreith [GKo8]. The PB consists of the steam generator, a high- and low-pressure turbine, a condenser and six feed water heaters including one deaerator.

A design and an steady-state off-design model of the PB are set up.

#### 6.1.1 Design Model

Figure 6.1 shows the PB set up in PSE at design point. The HTF comes from the SF at  $t_{SF,out} = 390\text{ }^{\circ}\text{C}$  (up left) and is split into two streams. One is led to the reheater and the other one is led through the superheater, evaporator and economizer. After this they are mixed and led back to the SF at  $t_{SF,in} = 293\text{ }^{\circ}\text{C}$  (bottom left). The feedwater enters the economizer at  $t_{eco,in} = 235\text{ }^{\circ}\text{C}$ . The evaporator is operated under forced circulation conditions. In the superheater saturated steam from the drum is heated up to the turbine inlet temperature (TIT) of  $t_{TIT} = 371\text{ }^{\circ}\text{C}$ . The hot steam enters the high-pressure turbine with a pressure of  $p_{TIT} = 104\text{ bar}$ . After the high pressure turbine the steam is reheated to  $t_{TIT,RH} = 371\text{ }^{\circ}\text{C}$  and enters the low-pressure turbine at

## 6 Modelling the Power Plant

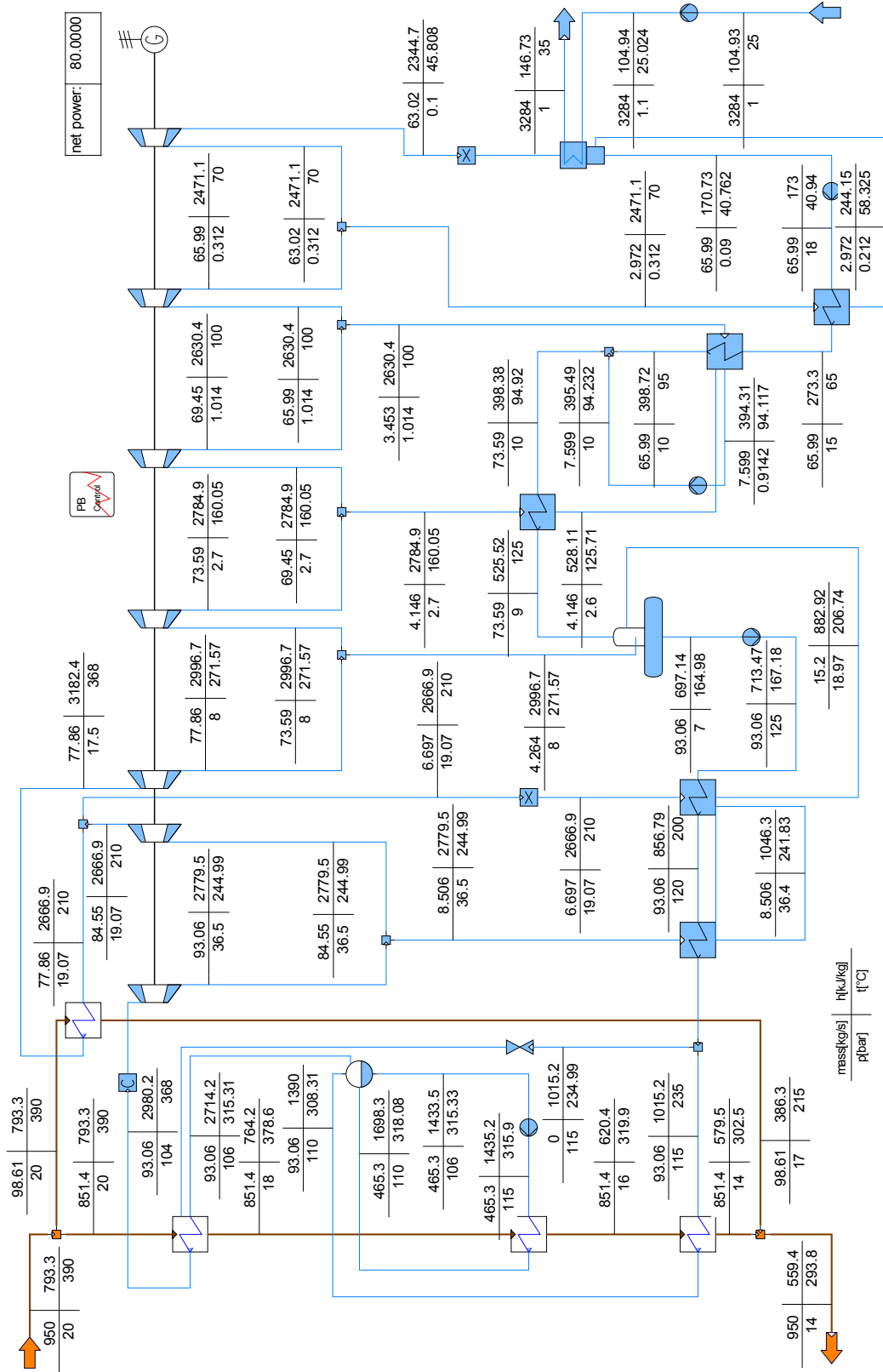


Figure 6.1: The flow sheet for the PB at design point.

$p_{RH} = 17.5$  bar. The steam exits the last turbine stage with a condensation pressure of  $p_{cond} = 0.1$  bar. Steam saturation should be higher than  $x = 0.9$ . In the condenser the steam is subcooled by  $\Delta t_{sub} = 3$  °C. The condensate is directed through a cascade of five feed water heaters, one deaerator and three pumps back to the economizer. Extracted steam from the turbines is condensed in the feed water heaters and mixed to the feedwater. Subcooling temperature in the feedwater heaters is  $\Delta t_{sub} = 3$  °C .

Table 6.1: Guidelines for isentropic efficiencies  $\eta_{is}$  for high pressure (HP), medium pressure (MP) and low pressure steam turbines (from Beckmann [Bec09]).

Blocksize	HP	MP	LP
100 MW	0.82	0.85	0.84
500 MW	0.85 - 0.90	0.90	0.86
700 MW	0.90	0.92 - 0.94	0.85

Table 6.2: Guidelines for mechanical efficiencies  $\eta_m$  of steam turbines at 3000 rpm (from Beckmann [Bec09]).

Power in MW	5	10	20	50	100
$\eta_m$	0.985	0.991	0.993	0.994	0.997

Table 6.3: Guidelines for generator efficiencies  $\eta_{gen}$  for different generator sizes (from Beckmann [Bec09]).

Power in MW	20	50	100	200	500
$\eta_{gen}$	0.975	0.978	0.982	0.985	0.99

Isentropic turbine efficiency is assumed to be  $\eta_{is} = 0.85$  for all stages (see Table 6.1). Generator efficiency is estimated to  $\eta_{gen} = 0.97$ . This is below the value suggested in Table 6.3 but also includes the mechanical efficiency of the generator and all turbine stages. For this reason mechanical efficiencies for all turbines are set to  $\eta_{m,turb} = 1$ . Guidelines for mechanical efficiencies of steam turbines can be found in Figure 6.2. Pump efficiency in the design point is  $\eta_{mech} = 0.71$  including all electro-mechanic losses of the pump and its motor. Isentropic pump efficiencies are set to  $\eta_{pump,is} = 0.7$ .

It is assumed that all components are adiabatic and working under steady-state conditions. Changes in potential and kinetic energy of fluid streams are not considered. Piping losses are neglected as well, which means the fluid enters a component as it leaves the previous one.

### 6.1.2 Off-Design Model

The off-design model is set up based on the design model. Part load behaviour is calculated relative to design conditions.

The PB is operated in sliding pressure mode. This means that load variation is controlled by changing the pressure at turbine inlet at constant turbine inlet area. Usually this happens by varying the pressure in the drum and the evaporator. Load changes will follow with some delay due to the storage effect of the masses in the drum and the heat exchangers. Compared to constant pressure mode, where load changes are controlled by a throttle valve or partial admission to the turbine, sliding pressure mode does not offer a high flexibility to react to load changes in the power grid. The advantages of sliding pressure mode are a slightly higher efficiency, lower investment costs for the turbine because a control stage is not needed and a longer durability for highly stressed parts [Stro6].

The temperature difference between the HTF and the steam at the outlet of the superheater might fall below  $\Delta t_{SH,out} = 19^\circ\text{C}$  at little HTF mass flow rates. The TIT might also rise above  $t_{TIT} = 371^\circ\text{C}$ . This must be avoided. If necessary, liquid feed water is injected into the saturated steam before the super heater to maintain a temperature difference of  $\Delta t_{SH,out} = 19^\circ\text{C}$ . To avoid numerical problems with the solver, it is suggested to always inject a small mass flow, e.g.  $\dot{m} = 0.01\text{ kg s}^{-1}$ .

Pressure losses of pre-heaters, heat exchangers and the condenser in part load mode are a function of the pressure loss at design point  $\Delta p_{loss,0}$ , the mass flow rate  $\dot{m}_0$  at design point and the current mass flow rate  $\dot{m}$ .

$$\frac{\Delta p_{loss}}{\Delta p_{loss,0}} = \frac{\dot{m}}{\dot{m}_0} \quad (6.1)$$

The used part load characteristic for HTF-water heat exchangers, pre-heaters and the condenser is:

$$\frac{UA}{U_0A_0} = \left( \frac{\dot{Q}}{\dot{Q}_0} \right)^{0.8} \quad (6.2)$$

A detailed derivation of this relation can be found in [Grao2]. Because of a lack of more detailed information about the sub-cooling temperatures of the pre-heaters and the condenser they are assumed to follow the same relation presented in Equation 6.2.

$$\frac{\Delta t_{sub}}{\Delta t_{sub,0}} = \left( \frac{\dot{Q}}{\dot{Q}_0} \right)^{0.8} \quad (6.3)$$

For both part load relations above, all variables marked with the subscript 0 are from the design operating conditions of the plant.

Partial load mass flow rate and pressure drop in a multi-stage turbine can be calculated by Stodola's elliptic law [SL45]:

$$\sqrt{\frac{p_f^2 - p_d^2}{T_f}} = \frac{\dot{m}}{\dot{m}_0} \sqrt{\frac{p_{f0}^2 - p_{d0}^2}{T_{f0}}} \quad (6.4)$$

$p_f$  and  $p_d$  is the pressure at turbine inlet and turbine outlet respectively.  $\dot{m}$  is the mass flow rate through the turbine.  $T_f$  is the temperature at turbine inlet. 0 in the subscript indicates values of the design point. In this IPSEpro model the sections between the steam extractions are represented by a turbine. No matter if this turbine has one or multiple stages, Equation 6.4 is applied on each of them to calculate part load behaviour.

Off-design isentropic turbine efficiency is calculated as a function of the loading coefficient  $\psi$ .

$$\frac{\eta_{is}}{\eta_{is0}} = \frac{f(\psi)}{f(\psi_0)} \quad (6.5)$$

IPSEpro's built in standard turbine characteristic shown in Figure 6.2 is used for simulations. Further turbine part load characteristics for reaction and impulse turbines can be found in [Hub09].

It is assumed that mechanical losses of the generator-turbine system are constant because of constant speed. Neglecting electrical losses, the part load characteristic of the generator is [Trio4]:

$$\frac{P_{shaft}}{P_{shaft,0}} = \frac{1 - \eta_{gen,0}}{1 - \eta_{gen}} \quad (6.6)$$

Figure 6.3 shows generator efficiency at partial load for a generator efficiency of  $\eta_{gen,0} = 0.97$  at the design point. For pumps, no partload specific characteristics were used. Instead, the efficiency was kept constant at the design point efficiency.

## 6 Modelling the Power Plant

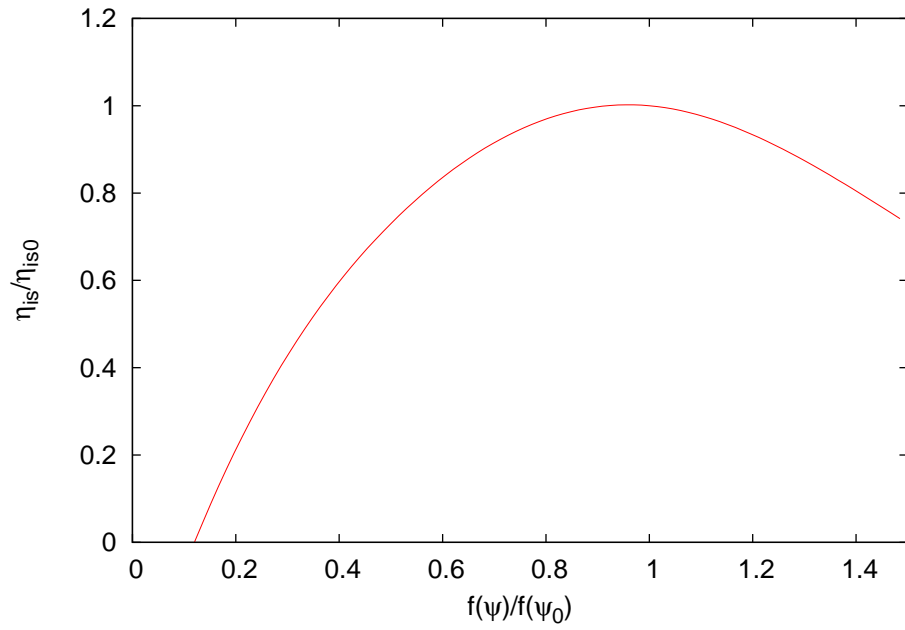


Figure 6.2: Isentropic turbine efficiency at partial load as a function of  $f(\psi)/f(\psi_0)$ .

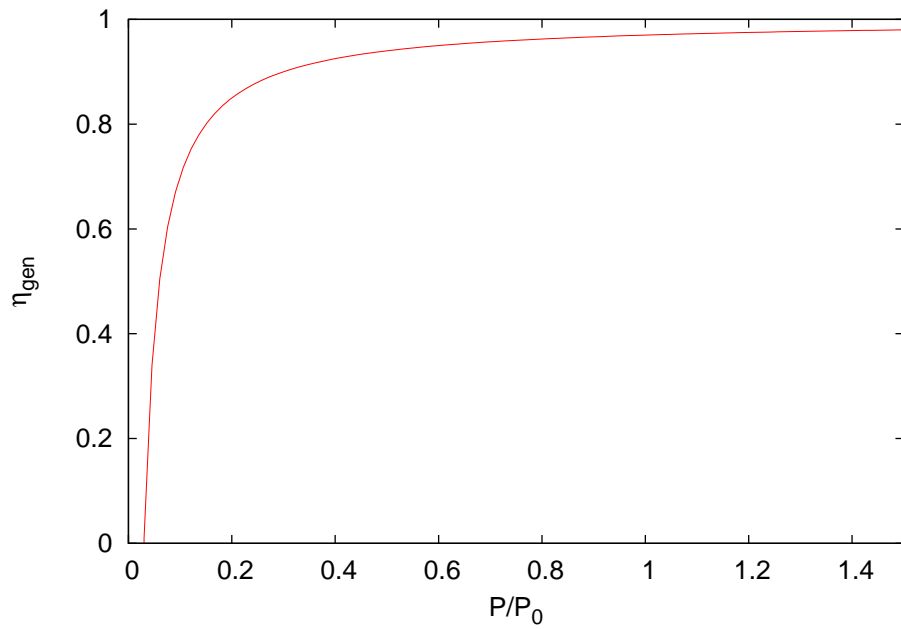


Figure 6.3: Generator efficiency at partial load as a function of  $P_{gen}/P_{gen,0}$ .



## 6.2 The Flow-Distributor

The Flow-Distributor connects the solar field, the thermal energy storage system and the power block. It replaces a set of mixers and splitters, which are merged into one component model. In this component the operating mode of the power plant can be set. Together with the script the Flow-Distributor plays an important role for transient time series analysis.

All operating modes presented in Section 2.5.1, except “Charging TES System Only” are implemented. For the sake of simplicity “Charging TES System and Serving PB”, “Serving PB Only from TES System” and “Serving PB from SF and TES System” are merged into an operating profile called “TES System and PB on”. In the “PB and SF Off, TES System Resting” mode a very easy PB warm-up model is included. Therefore this operating profile is called “PB off and Warm-Up”. Finally, the “Solar-Only” operating profile is realized as well.

Merging operating profiles demands many branched equations with “if - then” conditions. This type of equations need to be treated carefully. It is very easy to cause singularities in the solution matrix or solver oscillations around a discontinuity created with these equations. On the other hand, too many operating profiles demand many changes in the operation profile. For the transient simulations performed later, operation profiles are changed by an automation script, which is another error source. In the end the reduction to three operation profiles proved most convincing.

### 6.2.1 PB Off and Warm-Up

In times without or only little insolation and an empty TES system, the PB is shut off and disconnected from the rest of the system. During this period the HTF-fluid circulates through the solar field.

Even if the PB is disconnected from the rest of the power plant, all the equations of the PB model must be solved. A minimum temperature  $t_{min,PB}$  and minimum mass flow rate of the HTF  $\dot{m}_{min,PB}$  for the stream leading to the PB are specified. If either the mass flow rate or the temperature of the SF outlet stream exceeds these minima, it is set to the higher value. The SF mass flow rate is limited to the nominal mass flow rate to the PB  $\dot{m}_{PB,0}$ . The coupling of the SF and PB mass flow rates and temperatures is important especially when the SF and the PB are warmed up. In case of switching on the PB, the estimate values for all the PB values are close to the expected result values. This improves convergence and reduces calculation time.

## 6 Modelling the Power Plant

In addition, a simple warm-up model for the power block is integrated into this profile. In a heat sink the fluid coming from the solar field is cooled down to a certain temperature before it is sent back to the SF. The heat released is taken into account for the energy necessary to warm up the PB. If the SF outlet temperature exceeds a certain limit temperature  $t_{SF,PB,su}$ , the fluid is cooled down to this temperature. If the SF outlet temperature and mass flow rate exceed  $t_{min,PB}$  and  $\dot{m}_{min,PB}$ , the fluid is cooled down to the PB drain temperature  $t_{out,PB}$ . The heat released there is added up over the time, representing the energy  $H_{su,PB}$  used to warm-up the PB. If a certain limit  $H_{su,PB,l}$  is reached, the PB is ready to start.

A minimum HTF mass flow rate  $\dot{m}_{min,pl}$  is circulating through the charge and discharge streams of the TES system. The fluid from the discharge outlet is guided to the charge inlet and the fluid from the charge outlet to the discharge inlet. For all calculations carried out this mass flow rate is set to  $\dot{m}_{min,pl} = 0.01 \text{ kg s}^{-1}$ .

### 6.2.2 Solar-Only

In solar-only operation the PB is directly connected to the SF. No mass flow or heat exchange with the TES system takes place. A minimum mass flow rate is circulating through the charge and discharge streams, the same like in "PB Off and Warm-Up" operation mode. This operation mode is for times when the TES system is empty and solar irradiation is insufficient to reach the desired power output or the TES system is fully charged and more power is coming from the sun than necessary for the desired power output of the power plant. In the first case, all collectors are focused, in the second case some collectors have to be defocused to meet the PB's power demand.

### 6.2.3 TES System and PB On

In case there is excess power coming from the SF and the TES system is not full, the TES system is charged. If the power from SF is not sufficient to meet the PB's demand and the TES system is not empty, the lacking power is retrieved from the TES system.

If  $t_{out,SF}$  is below  $t_{min,PB}$ , the SF is disconnected from the PB and TES system. The fluid is circulating through the SF, while the PB is operated by energy retrieved from the TES system. The discharge stream from the TES system is split,  $\dot{m}_{min,pl}$  is sent to the charging inlet stream since the oil-to-salt heat exchanger cannot be operated at a zero mass flow rate, the rest is sent to PB. The discharge inlet stream is a mixture of the outlet stream of the PB and the charging outlet stream.

In periods when  $t_{out,SF}$  is higher than  $t_{min,PB}$ , the PB and the TES system are connected to the SF. If there is a surplus of power coming from the SF, the TES system is charged; if there is a lack of power, the TES is discharged. When charging, the discharge mass flow rate is  $\dot{m}_{min,pl}$  and when discharging it is vice versa. The stream leading to the PB is a mixture of the streams coming from the SF and TES discharge. The stream leading to the SF is a mixture of the streams coming from the PB and TES charge. The TES charge stream has the temperature of the SF inlet stream. The TES discharge stream has the temperature of the PB outlet stream

### 6.3 PB, SF and TES Info and Power Plant Statistics

For a better overview of the most important and interesting values of the solar field, the TES system and the power block, component models called SF Info, PB Info and TES Info showing this information at one glance, are devised. Most data are collected by free equations from the individual component models. A similar model is available for the power plant, PP Stat. Energy output and consumption over a certain period and performance key values are calculated there.

The SF Info contains information about the collector inlet and outlet temperatures  $t_{coll,in}$  and  $t_{coll,out}$ , the SF inlet and outlet temperatures  $t_{SF,in}$  and  $t_{SF,out}$  and the HTF mass flow rates through the SF  $\dot{m}_{SF}$ . DNI on the aperture area and the DII on the receiver area are calculated for the whole SF and in case of defocused collectors for the active SF area as well. The thermal power transferred to the HTF-fluid in the SF  $\dot{Q}_{SF}$  is the sum of heat added to the fluid in the piping, the collectors and the expansion vessel, and the hydraulic power added by the SF-pump  $P_{hyd,SFpump}$ .

$$\dot{Q}_{SF} = \dot{Q}_{pipes} + \dot{Q}_{coll} + \dot{Q}_{EV} + P_{hyd,SFpump} \quad (6.7)$$

$\dot{Q}_{SF,max}$  is calculated as well; there it is assumed that all collectors are focused. Thermal losses  $\dot{Q}_{loss}$  in the SF are calculated as the sum of thermal losses for the individual parts.

$$\dot{Q}_{loss} = \dot{Q}_{loss,pipe} + \dot{Q}_{loss,coll} + \dot{Q}_{loss,EV} \quad (6.8)$$

And the thermal energy stored in SF equipment  $Q$  is calculated the same way:

$$Q = Q_{pipe} + Q_{coll} + Q_{EV} \quad (6.9)$$

## 6 Modelling the Power Plant

In the PB Info model the nominal net-power  $P_{net,nom}$  and the minimum net-power  $P_{net,min}$  can be prescribed. The net-power is calculated

$$P_{net} = P_{gen} - P_{para} \quad (6.10)$$

where  $P_{gen}$  is the generator power and  $P_{para}$  is the power of all parasitic consumers in the power plant. The thermal energy consumption of the PB  $\dot{Q}_{PB}$  and the condenser losses  $\dot{Q}_{cond}$  are presented there as well.

The TES Info component model provides information about the charging status  $C_{TES}$ , the stored energy  $H_{TES}$  and the charging or discharging heat rate  $\dot{Q}_{TES}$ . Storage hours  $C_{FLH}$  are calculated for current ( $Q_{PB}$ ) and nominal ( $Q_{PB,0}$ ) load.

$$C_{FLH} = \frac{H_{TES}}{Q_{PB}} \quad (6.11)$$

In the power plant statistics, the net output energy  $W_{el}$ , the energy delivered by the generator  $W_{gen}$  and the parasitic energy consumption  $W_{parasitics}$  for the investigated period are calculated. They are added up over the time  $t$  as following:

$$W^n = W^{n-1} + \dot{W}\Delta t \quad (6.12)$$

The thermal energy consumption of the PB  $Q_{PB}$ , the energy harvested by the SF  $Q_{SF}$  and charged and discharged energy to the TES ( $Q_{TES,C}$  respectively  $Q_{TES,D}$ ) are determined the same way, as well as the DNI on the total aperture area  $Q_{DNI}$ .

With these values the average net efficiency  $\eta_{net,avg}$  over the investigated time can be determined:

$$\eta_{net,avg} = \frac{W_{el}}{W_{DNI}} \quad (6.13)$$

The key figures described in Section 2.3.2, the storage factor  $\delta_{TES}$  (Equation 2.9), the capacity factor  $c_{el}$  (Equation 2.6) and the storage efficiency  $\eta_{TES}$  (Equation 2.8), are calculated here as well.

## 6.4 Power Plant Model - Script Interaction

With the SF, TES system and the PB connected by the Flow-Distributor a power plant model is established. Based on a design model a transient off-design model is set up. This off-design model is then used for calculations.

The IPSEpro model itself can only calculate one single calculation step. Transient calculations always cover one time increment and have a start and an end point. The result values of the previous step are used as start values for the following step. For this reason, the start values of the transient items have to be set as the result values of the previous step, before another calculation step can be carried out.

Since this calculation procedure stays the same over and over again, it is automated by a script. Therefore an external script as described in Section 3.2.3 is utilized. This script also performs some other tasks. It changes the operating mode if necessary due to the specifications. It modifies the time increment if no solution can be found at the current time increment. Calculation results of interest are saved to a file. These and some more tasks are repeated until an exit criterion is reached.

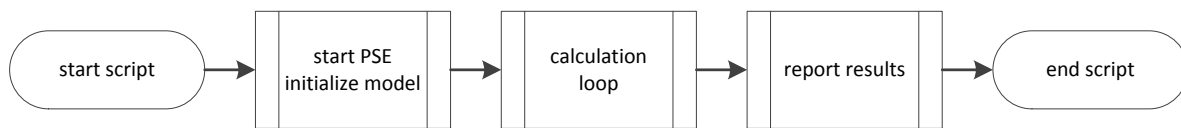


Figure 6.4: Basic flow sheet of the script procedure.

The detailed procedure of the script is described in the following sections. Figure 6.4 shows the basic procedure and the main parts of the script. First, PSE is started and the model is initialized, after this the calculation loop is entered. In the end the results are reported.

### 6.4.1 Starting PSE and Initializing the Model

Some preparations have to be made before starting a transient analysis. The power plant model must be adjusted to the desired starting point. Initial values for all transient items are provided. Afterwards a single calculation step is conducted and the project saved. This file is used for calculations.

Now the script enters procedure. It starts the PSE environment as described in Section 3.2.3, loads the component model library and the project file. Afterwards all necessary connections between the script and the project items are established. For

## 6 Modelling the Power Plant

example, these are all values which shall be saved or all transient items. Files to save simulation results are created.

Values for the most precise x- and y-tolerances of the solver and the exit criterion of the calculation loop are specified here. The standard time increment is defined here as well. The calculation result of the local time at the power plant's location is read from the project file, it becomes the starting time for the transient simulations. As a last step before the calculation loop is entered, the time of the local machine is checked. This allows measuring computation time.

### 6.4.2 Calculation Loop

The calculation loop is the most important part in the script. It executes the calculation steps in IPSEpro. The transient components are shifted one step further and the values of interest are saved. The loop can be subdivided into three main parts: the calculation part, the operation profile selection and the last part where the transient items are prepared for the next step and the results are saved.

The basic flow chart of the calculation loop can be found in Figure 6.5. At the begin of each loop run, a calculation step with a standard time increment is performed. At night the time-step size is doubled or tripled compared to daytime. This is possible since not so many rapid changes in temperature or mass flow rate occur during the night. In case the calculation is not successful, the script undertakes some measures to find a valid solution. If a solution is found, the model is prepared for the next calculation step, e.g. the proper operation profile is selected, collectors are defocused or focused and transient model items are updated. After this, the calculation results are saved. As a last step the exit condition is checked. If it is fulfilled, the calculation stops, otherwise the same procedure is repeated in the next calculation step. If no solution can be found, the calculation is terminated.

#### Calculation of a Single Step

As a first step it is checked whether it is day or night. Then the time increment is set to the current maximum value. With the help of time of the last successful calculation step, the time for the current calculation step is calculated and set. The procedure is depicted in Figure 6.6. Afterwards the script runs a calculation in IPSEpro.

If no solution can be found, the script enters some convergence improvement measures. The same step is repeated with higher x- and y-tolerances. If no solution can be found either, time increment is reduced to half of its previous value. Date

## 6.4 Power Plant Model - Script Interaction

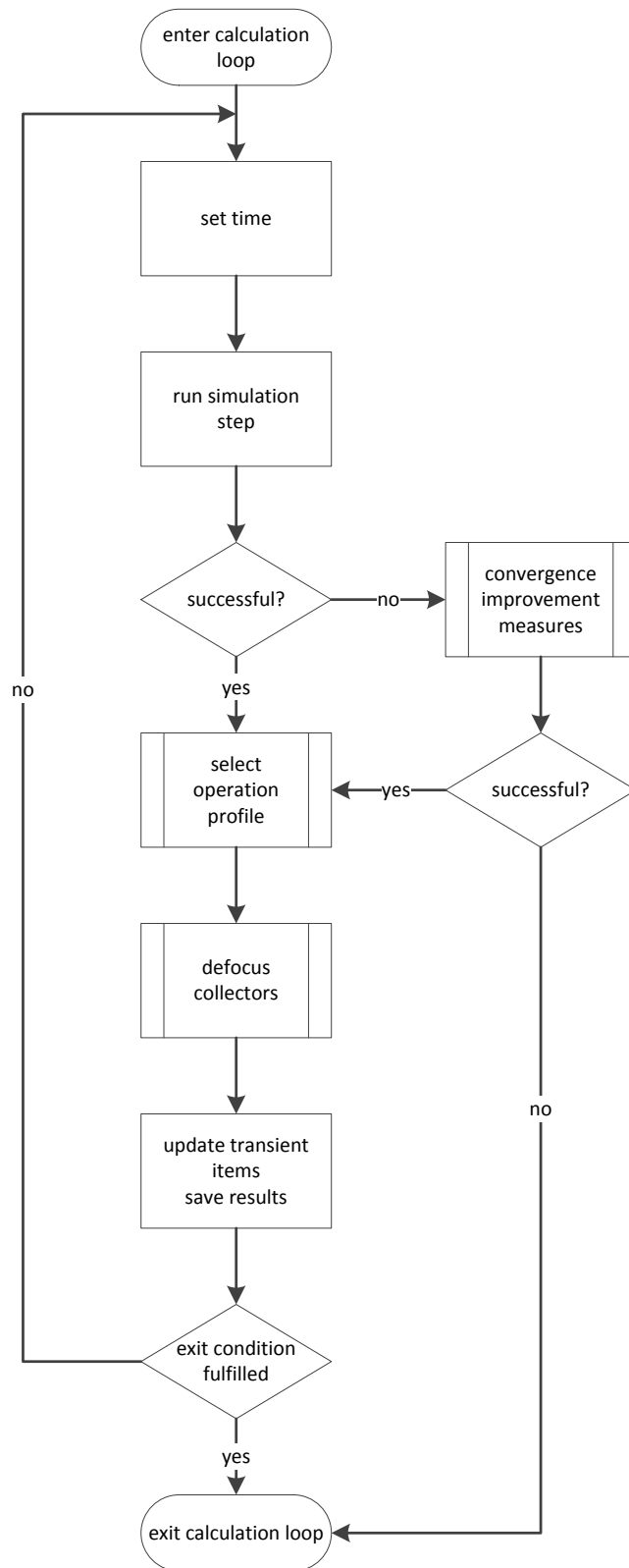


Figure 6.5: Basic flow sheet of the calculation loop.

## 6 Modelling the Power Plant

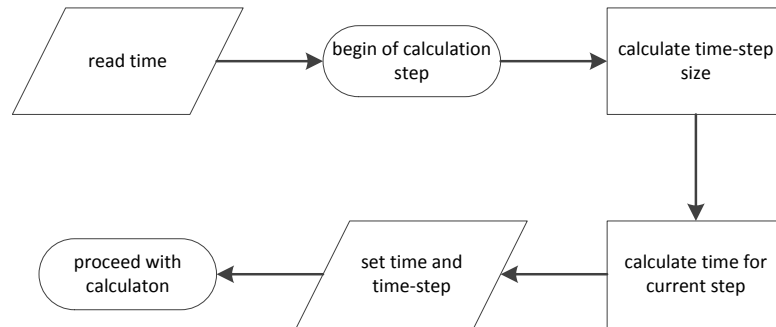


Figure 6.6: Procedure for setting the time for the current time step.

and time must be adjusted to the new time increment. This is necessary since the operation profile selected might not be appropriate for the new time instant. The solution process with the Newton-Raphson solver strongly depends on the initial values. Smaller time steps usually promise smaller changes to the prior step, and a solution might be found. The reduction of time step is repeated as long as neither the system converges nor a maximum number of steps is reached. In the scripts used in this work, the maximum number of steps is 15. If this happens, the script is paused for a manual check to find possible mistakes and proper settings for a solution. If the system converges, the  $x$ - and  $y$ -tolerances are set back to their original values and the script proceeds. If a converged solution cannot be achieved despite these measures, the calculation loop exits here. For a detailed flow sheet of this procedure see Figure 6.7.

### Selection of Operation Profile

If a valid solution is reached, the script continues with the operating profile selection. It is checked whether the PB shall be switched off or on in the next step. The criteria whether to switch off or on depend on the power plant size and the type of TES system and the operation strategy. For the calculations carried out here it is switched on, if the solar field outlet temperature  $t_{SF,out}$  is higher than the minimum fluid temperature  $t_{min,PB}$  which can be fed to the PB. The PB warm-up must be completed as well. The PB is shut down, if the net power falls below the minimum net power. It is also shut off, if the PB is operated from the TES system only and the TES system becomes empty.

Afterwards, as shown in Figure 6.8, the proper operating profile in the Flow-Distributor is set. If the PB is shut down: the "PB off/Warm-Up" profile is chosen. In the other case, two options are available, "TES+PB on" and "Solar-Only". If the power from



## 6.4 Power Plant Model - Script Interaction

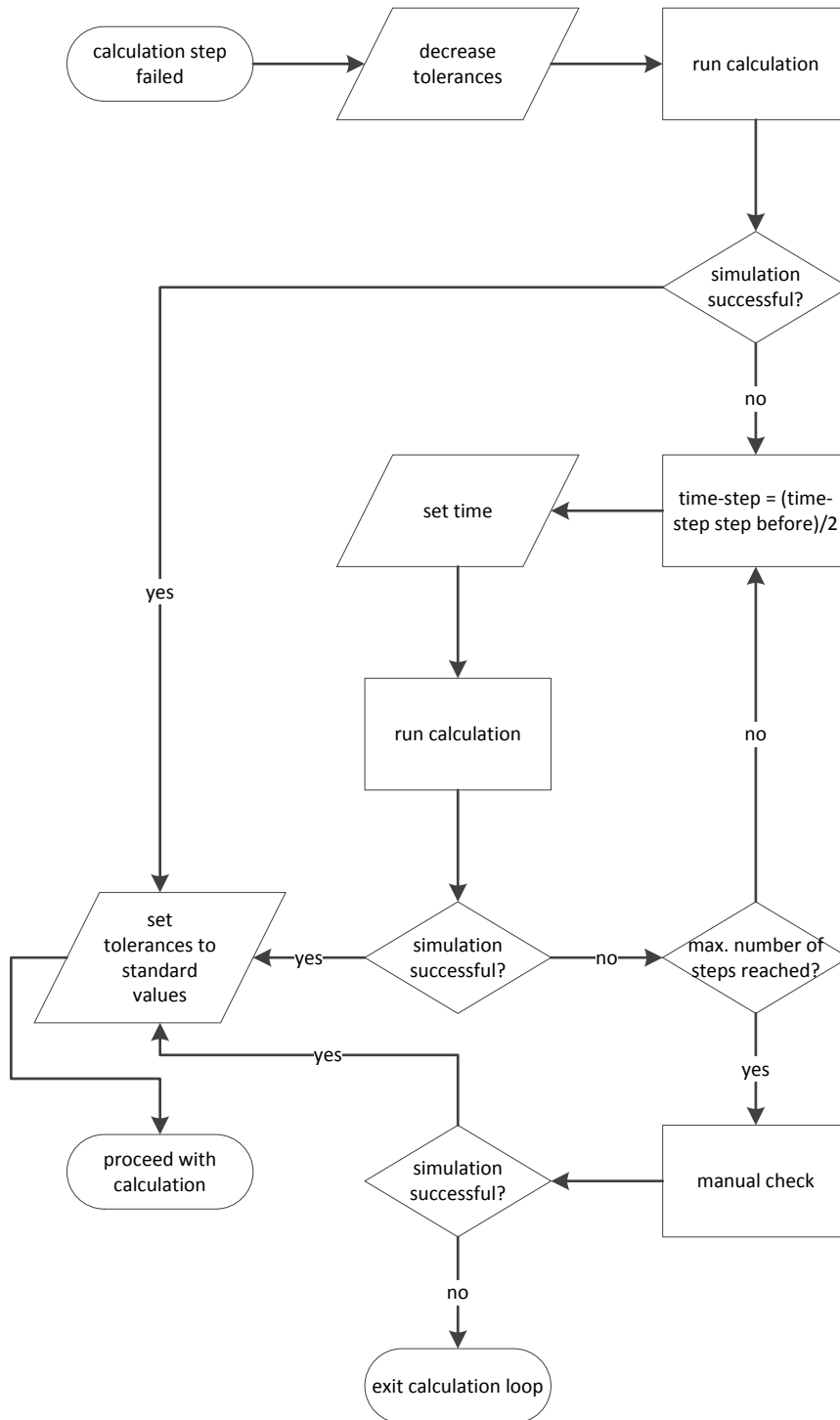


Figure 6.7: Detailed flow-sheet of the convergence improvement measures.

## 6 Modelling the Power Plant



Figure 6.8: Detailed flow sheet for selecting the appropriate operation profile.

the SF is too small to meet the PB's demand and the TES system is empty, "Solar-Only" operating profile is selected. In case the TES system is full and the SF could provide more power than necessary for the PB "Solar-Only" is also selected.

In all other cases the "TES+PB on" profile is selected. It can only be detected that the power plant shall switch to the "TES+PB on" operating mode when it already should operate in this mode. For this reason, if the operation profile is changed from any other profile to the "TES+PB on" profile, the calculation step is repeated at that time. The part at the right-hand side of the flow chart in Figure 6.8 shows this procedure. If no solution can be found, the operation profile is changed back to the previous one and the calculation is repeated. A valid solution is necessary at this point to proceed with the calculation. After this the operation mode is set to "TES+PB on" again. If no solution can be found, the script allows a manual check. In case a solution can be found, the script proceeds, if not it terminates. This procedure is illustrated on the right-hand side in Figure 6.8.

After this the number of collectors to defocus is determined and set. In case the PB is off all collectors are focused. In the other two cases the number of collectors to defocus is determined based on the thermal power consumption of the PB and the maximum thermal power  $Q_{Fluid,max}$  that can be delivered by the SF.

It is assumed that each collector contributes the same amount of thermal power  $Q_{coll,avg}$  to  $Q_{Fluid,max}$ . With  $N_{coll,row}$ , the number of collectors in a row, the necessary number of collectors focused  $N_{coll,focused}$  in the row with the defocused collectors is as following:

$$N_{coll,focused} = \frac{\dot{Q}_{PB} N_{coll,row}}{Q_{coll,avg}} - 0.3 \quad (6.14)$$

0.3 is subtracted to be on the safe side. It is always better to defocus one collector too many than one too few. No solution can be found with too few defocused collectors. First attempts has been made with Equation 6.14 without subtracting 0.3. In case  $N_{coll,focused}$  is only slightly higher than some integer, the next calculation step might fail due to too few defocused collectors. With too few collectors defocused the minimum heat rate that can be collected in the SF might be higher than the maximum heat rate allowed to the PB.

Considering this, the number of focused collectors in each row is calculated and then rounded to the next integer. Only whole collectors can be focused or defocused. Then the collectors are defocused in the SF model. They are always defocused beginning from the inlet at the collector row. The fluid temperature is lower and therefore heat losses are lower as well.

### Update Transient Items and Save Results

As a next step all calculation results are imported as estimate values. Afterwards the items which have a transient behaviour are prepared for the next calculation step. For example, for the absorber pipes and the piping the current drain temperature  $t_{drain}$  is saved as the drain temperature the step before  $t_{drain,before}$ .

The time of the current step is saved as initial time for the next step. Finally, the calculation results which are of interest are saved to a file. After several calculation steps a copy of the project file is saved. If a problem occurs and the script is terminated, one of these can be used to resume the transient simulation from a point shortly before the problem occurred. It is not necessary to repeat the simulation from the beginning.

Finally the loop's exit condition is checked. If it is false another calculation step is performed, if it is true the calculation is terminated here.

### 6.4.3 Report Results

After the calculation has finished, a summary file is written containing the values calculated in the PP Stat component. The project file is saved. As a last step the information about the computational time is written to a file.

## 7 Simulation Results

Power plant models with a two-tank and a thermocline TES system are set up with the component models described in Chapters 4, 5 and 6. A flow sheet of the plant with the two-tank TES system is presented in Figure 7.1. The SF on the left-hand side is set up as described in Section 4.8. The green and blue rectangles represent the TES system. Above them is the oil-to-salt heat exchanger. The big orange bar is the “Flow-Distributor”. The brown lines represent HTF and molten salt streams, the blue ones water and steam streams. In contrast to many other simulations like these, where the PB is replaced by some empirical relations, a detailed model is set up here. All the blue components are from the PB.

The investigated plant should be located at Harper Lake, California (Latitude: 35.03 North, Longitude: 117.35 West, Elevation: 632 meters AMSL), the same location as the SEGS VIII and IX plants. The design date is equinox, the 21<sup>st</sup> of March at 12 AM. The PB model with the steam parameters described in Section 6 is used. Rated net power output simulated is  $P_{net,0} = 80$  MW. The HTF is TherminolVP1 and the storage material is solar salt. Solar multiple and storage capacity differ for the different investigated configurations.

Solar irradiation is calculated by Hottel’s clear sky model. That means that all collectors are exposed to bright sunshine during the whole investigated period. No clouds are shading parts of the SF. The ambient conditions are assumed to stay constant throughout the whole year. Ambient temperature is  $t_{amb} = 30$  °C and ambient pressure is  $p_{amb} = 1.013$  bar. Wind speed is  $v_{wind} = 0$  km s<sup>-1</sup>.

### 7.1 Power Plant with Two-Tank TES System

Power plants with both two-tank TES models are created. First the basic two-tank model is used to show the ability of the whole simulation system to conduct transient time series analysis. A power plant concept with the detailed two-tank model is later used to carry out a performance prediction and annual yield analysis.

## 7 Simulation Results

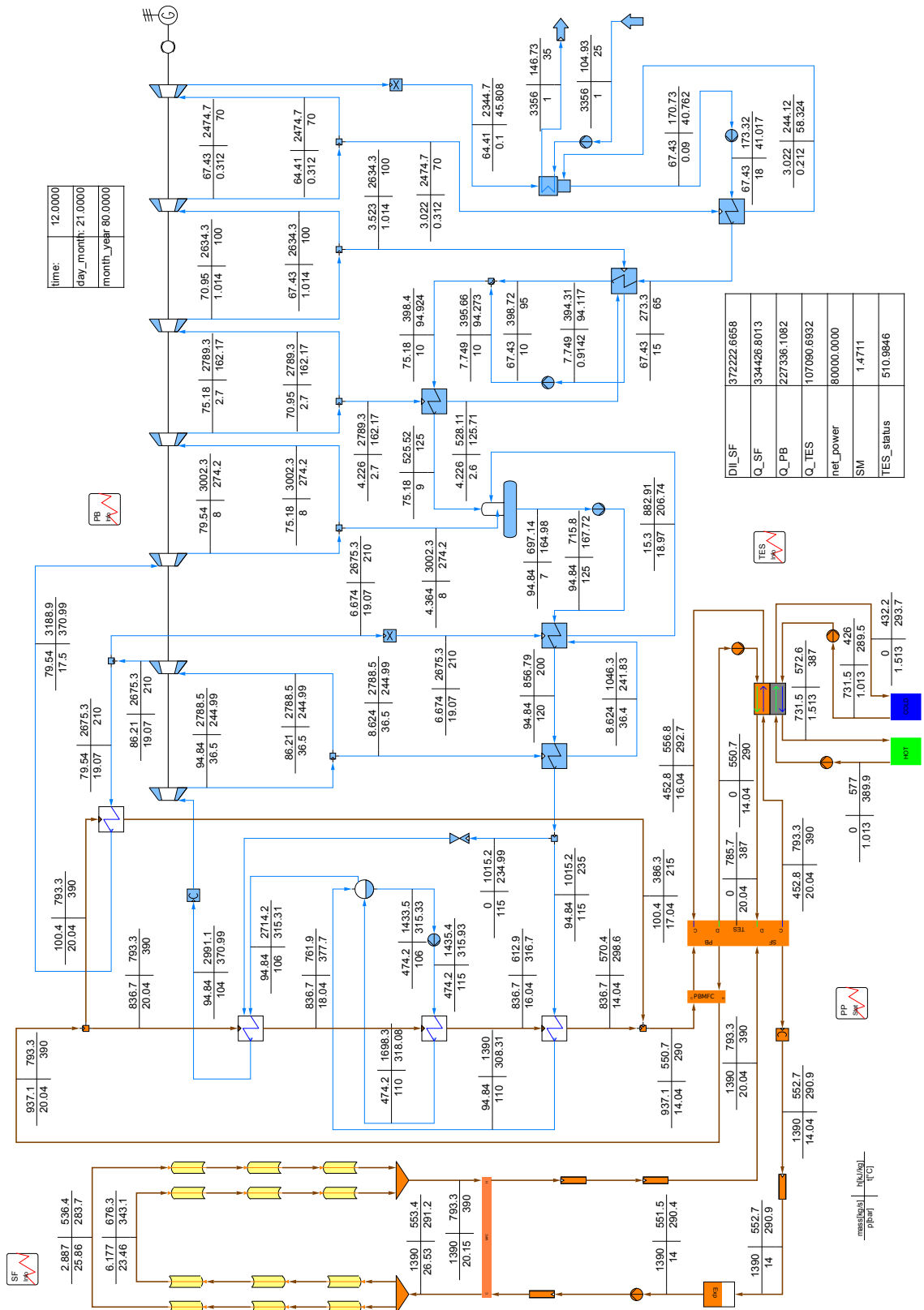


Figure 7.1: Flow sheet of the power plant with a two-tank TES system.

### 7.1.1 Power Plant with Basic Two-Tank TES System

A power plant with 310 collector rows, that is  $SM = 2$ , and a storage capacity  $C_{FLH} = 7.5$  full load hours and a rated power output of  $P_{net} = 80$  MW is assumed for the first simulations. Operation during March is simulated. Simulation starts at 4 AM at the 1<sup>st</sup> of March and ends 1<sup>st</sup> of April same time. 4 AM is a convenient start point, usually the TES system is empty and the PB is off at this time.

The power plant operation strategy is to provide a constant net power output  $P_{net,tar} = 80$  MW if possible. The HTF mass flow rate at design point is  $\dot{m}_{PB,0} = 950.9 \text{ kg s}^{-1}$ . The maximum mass flow rate allowed to the PB is  $\dot{m}_{PB,max} = 1100 \text{ kg s}^{-1}$ . In case of PB operation and TES charging all collectors are focused. In "Solar-Only" operation mode the number of focused collectors is adjusted to reach a net power output of  $P_{net,tar} = 80$  MW. The mass flow rate to the PB is still limited by  $\dot{m}_{PB,max}$ . If the collected heat in the SF is insufficient to reach  $P_{net,tar}$  and the TES system is empty, all collectors are focused and the PB is operated at maximum available power during this period.

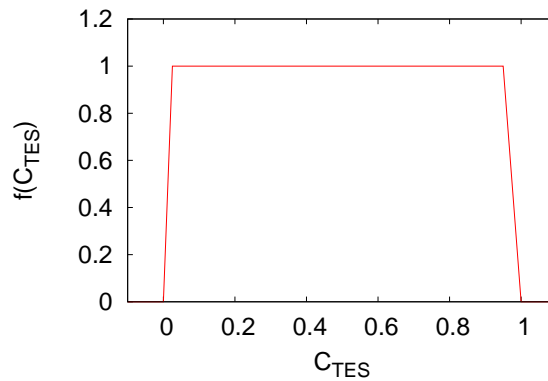


Figure 7.2: Ramp for smoothing transition in operation mode change.

If the operation profile is changed from one to another convergence problems might occur. To avoid these kind of problems the transition from one to the other operation profile must be smoothed. In case the TES system is close to fully charged (the charging state exceeds a certain limit  $C_{TES,lim}$ ) the heat flow to the TES system is decreased. From  $C_{TES,lim} = 0.95$  to  $C_{TES,full} = 1$  the heat flow rate is decreased according to the following relation:

$$\frac{N_{foc}}{N_{tot}} = \frac{\dot{Q}_{PB} + \dot{Q}_{TES} \cdot f(C_{TES})}{\dot{Q}_{SF,max}} \quad (7.1)$$

## 7 Simulation Results

$\dot{Q}_{SF,max}$  is the maximum heat rate that can be provided from the SF and  $C_{TES,lim,f} = 0.95$ .  $N_{foc}$  and  $N_{tot}$  are the number of loops with all collectors focused respectively the total number of collector loops.  $f(C_{TES})$  can be obtained from Figure 7.2.

When the TES system is close to empty (if  $C_{TES} < 0.05$ ,  $C_{TES,lim,e} = 0.05$ ), the net power output is linearly decreased from the target net power  $P_{net,tar}$  to the minimum net power output  $P_{net,min}$ :

$$\frac{P_{net,tar} - P_{net,min}}{C_{TES,lim,e}} = \frac{P_{net} - P_{net,min}}{C_{TES}} \quad (7.2)$$

Irradiation, power output and heat flow rates for the 21<sup>st</sup> and 22<sup>nd</sup> of March are shown in Figure 7.3. Every day approximately one hour after sunrise, the SF and the PB are warmed up so that power production can be started. At this time the provided heat flow rate is already high enough to start charging the TES system as well. Shortly after 3 PM the TES system is fully charged and from then, the PB is operated in "Solar Only" mode. At sunset the heat flow rate from the solar field is insufficient, heat is retrieved from the TES system to maintain the desired power output. The little drop in power output is caused by mixing the colder fluid from the SF with hotter fluid from the TES system. The PB operates at maximum mass flow rate. With the currently available power the target net power cannot be reached without exceeding the maximum mass flow rate. Shortly after the SF outlet temperature becomes too low and the PB is operated by heat only from the TES system. Around 1 AM the TES system is empty and the power plant is shut down. During the night the SF pumps are still working, consuming electricity from the power grid.

In Figure 7.4 simulation results for mass flow rate through the SF  $\dot{m}_{SF}$  and temperatures at SF and collector inlet and outlet are shown. In times when all collectors are focused the mass flow rate through the SF is predicted very accurate, SF outlet temperature is very close to the design value. When starting to defocus collectors the SF outlet temperature drops. The drop in DII compared to  $DII_0$  has a decreasing influence, the drop in  $\sum Q$  compared to  $\sum Q_0$  has an increasing influence on the mass flow rate. Obviously it is predicted too high to reach the design outlet temperature.

the DII decreases, which, in turn, decreases the mass flow rate but the stored heat in the piping decreases as well, which increases the mass flow rate.

Obviously then the predicted mass flow rate is too high to reach the design outlet temperature.

Figure 7.5 shows the fluid temperatures in the two tanks and the charging state in full-load-hours  $C_{FLH}$ . Temperature decrease in both tanks is quite high, the heat



## 7.1 Power Plant with Two-Tank TES System

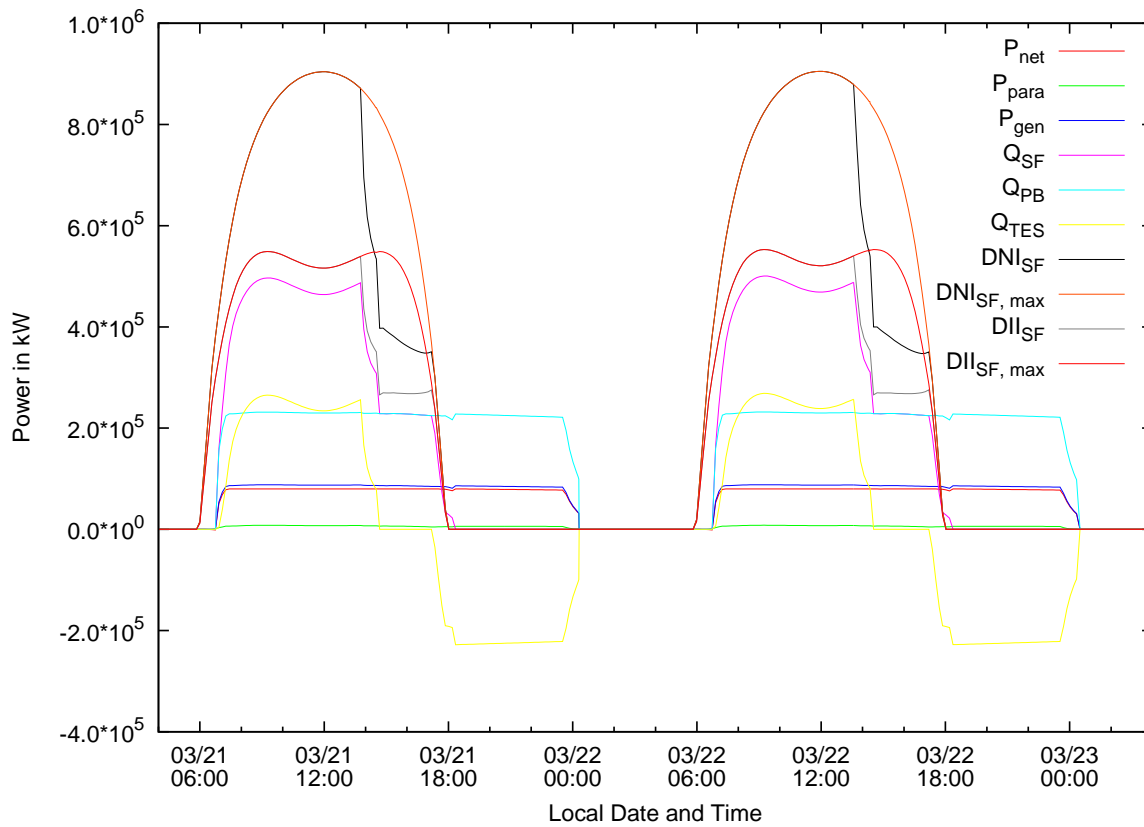


Figure 7.3: Simulation results for solar irradiation, heat-flow-rates and power output.

## 7 Simulation Results

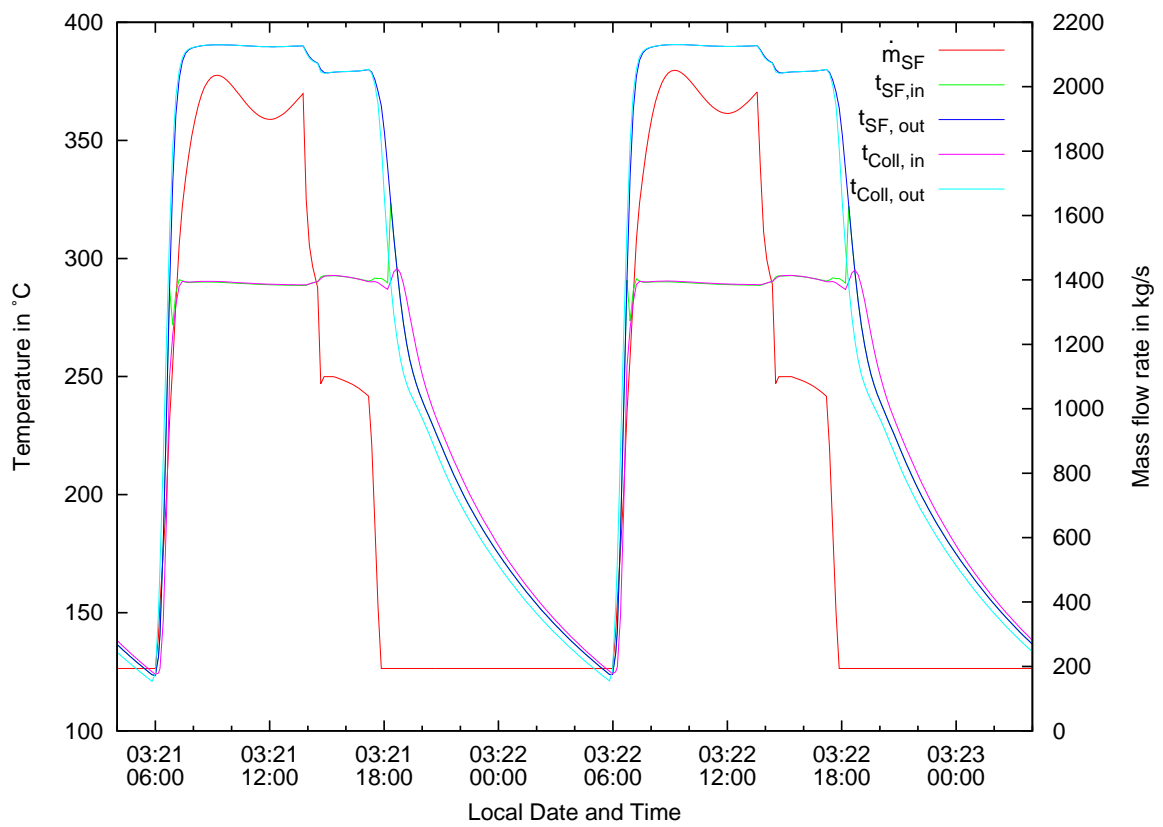


Figure 7.4: Simulation results for the HTF flow-rates through the SF and temperatures at SF and collector inlet and outlet.

## 7.1 Power Plant with Two-Tank TES System

loss factor  $k_{loss}$  has been anticipated too high. The large temperature drop at the beginning of the charging cycle is caused by fluid that has not reached design temperature.

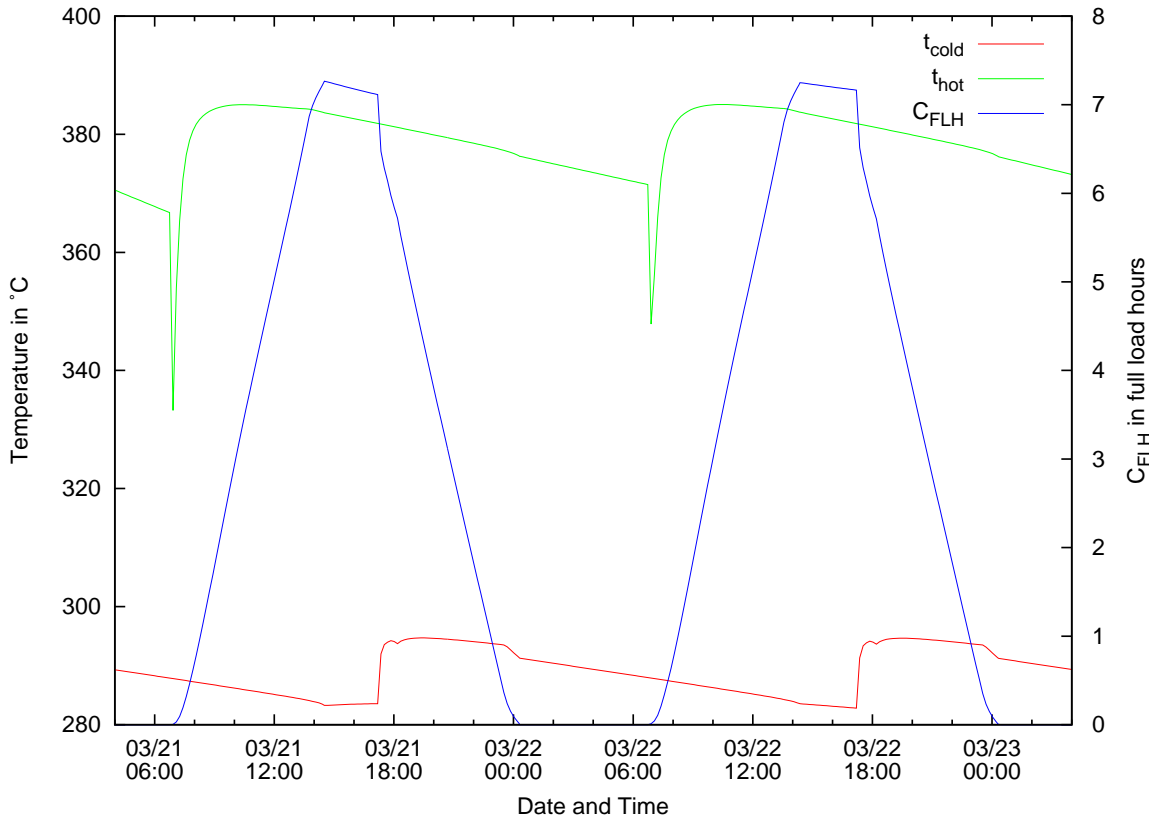


Figure 7.5: Simulation results for the TES system temperatures and the charging state.

In Table 7.1 results for the conducted performance prediction and yield analysis for March are shown. The rather low storage efficiency is caused by the high heat losses as described above. With a  $SM = 2$  and a storage capacity of  $C_{FLH} = 7.5$  full load hours, the predicted capacity factor is  $c_{el} = 0.7$  in March. With only 16% the average net efficiency is rather low, this can be explained by the large amounts of heat dumped when defocusing of collectors is necessary.

### 7.1.2 Power Plant with Detailed Two-Tank TES System

For three different power plant configurations with a detailed two-tank model a performance prediction and annual yield analysis is conducted. The first power

## 7 Simulation Results

Table 7.1: Calculation results for the performance prediction and yield analysis for March

Generator energy output	42 GWh
Net energy output	39 GWh
Parasitic energy consumption	3 GWh
Average net efficiency	16 %
Capacity factor	0.7
Storage efficiency	87 %
Storage factor	41 %

plant configuration has a  $SM = 1.5$  and  $C_{FLH} = 7.5$ , the second a  $SM = 2$  and  $C_{FLH} = 7.5$  and the third a  $SM = 3$  and  $C_{FLH} = 9$ . The design parameters for the tanks can be found in Table 7.2. The hot and cold tanks always have the same diameter, but the height is different. The tank walls are made of concrete. Wall and insulation thickness and heat transfer coefficients for the hot and cold tank are the same as well. Heat losses from the  $C_{FLH} = 9$  TES system are expected to be higher because of the larger surface area. Therefore a slightly better insulation material is used. All three plants have a net output of  $P_{net} = 80$  MW. The higher mass flow rates to the PB are caused by the higher power demand of the SF pump with higher SMs.

Table 7.2: Tank dimensions and storage mass at design point.

	$SM = 1.5$ $C_{FLH} = 7.5$	$SM = 2$ $C_{FLH} = 7.5$	$SM = 3$ $C_{FLH} = 9$
mass flow rate PB $\dot{m}_{PB,0}$	936.5 kg s <sup>-1</sup>	948 kg s <sup>-1</sup>	975 kg s <sup>-1</sup>
inner diameter $D_i$	36 m	36 m	36 m
inner height hot $H_{i,hot}$	22.3 m	22.6 m	27.8 m
inner height cold $H_{i,cold}$	21.6 m	21.8 m	26.9 m
wall thickness $x_{wall}$	0.3 m	0.3 m	0.3 m
insulation thickness $x_{ins}$	0.6 m	0.6 m	0.7 m
volume frac. PS $f_{PS}$	0.025	0.025	0.025
volume frac. empty $f_{empty}$	0.001	0.001	0.001
cond. coeff. wall $k_{wall}$	0.7 W m <sup>-1</sup> K <sup>-1</sup>	0.7 W m <sup>-1</sup> K <sup>-1</sup>	0.7 W m <sup>-1</sup> K <sup>-1</sup>
cond. coeff. insulation $k_{ins}$	0.09 W m <sup>-1</sup> K <sup>-1</sup>	0.09 W m <sup>-1</sup> K <sup>-1</sup>	0.06 W m <sup>-1</sup> K <sup>-1</sup>
conv. coeff. ambient $h_{amb}$	8 W m <sup>-2</sup> K <sup>-1</sup>	8 W m <sup>-2</sup> K <sup>-1</sup>	8 W m <sup>-2</sup> K <sup>-1</sup>
design temp. hot $t_{hot,0}$	386 °C	386 °C	386 °C
design temp. cold $t_{cold,0}$	286 °C	286 °C	286 °C
active mass $m_{act}$	$4.1 \times 10^7$ kg	$4.1 \times 10^7$ kg	$5.1 \times 10^7$ kg
total mass $m_{tot}$	$4.3 \times 10^7$ kg	$4.3 \times 10^7$ kg	$5.3 \times 10^7$ kg

This time the operation strategy has changed. Instead of the net power output the

## 7.1 Power Plant with Two-Tank TES System

HTF mass flow rate to the PB is prescribed. In the following simulations it is tried to maintain the design mass flow rate to the PB. If this is not possible, the maximum available mass flow rate is sent to the PB. When the TES system is full, the SF mass flow rate is adjusted to the PB mass flow rate by defocusing collectors.

Again, to avoid convergence problems caused by unsuitable estimate values from the step before, when changing the operation profiles the transition to the other operation profile must be smoothed. For this purpose the ramp function for the basic two-tank model is used (see Figure 7.2). If the TES is close to full ( $C_{TES} > 0.95$ ), the charging heat rate  $\dot{Q}_{TES}$  is decreased according following relation:

$$\dot{Q}_{TES} = \dot{Q}_{TES,max} \cdot f(C_{TES}) \quad (7.3)$$

$\dot{Q}_{TES,max}$  is the maximum power that can be currently sent to the TES if all collectors are focused. The relation used for the basic tow-tank TES system (see Equation 7.1) has turned out to be not so convenient. Therefore it is replaced by Equation 7.3.

When the discharging the TES system and it is close to empty, two cases can occur: in the first there is still power coming from the SF, and the second where the SF is already disconnected. For the first case a smooth transition to the other operation profile is reached with the following relation:

$$\dot{m}_{PB} = (\dot{m}_{PB,tar} - \dot{m}_{SF}) \cdot f(C_{TES}) \quad (7.4)$$

In the second case the HTF mass flow rate to the PB is reduced to shut it off when the TES system is empty. The following relation is used:

$$\frac{\dot{m}_{PB,tar} - \dot{m}_{PB,min}}{C_{TES,lim}} = \frac{\dot{m}_{PB} - \dot{m}_{PB,min}}{C_{TES}} \quad (7.5)$$

With a time increment of 10 minutes at daylight and 30 minutes during night-time almost 38000 single calculation steps are conducted for each power plant for an annual yield analysis. Dependent on the number of interruptions where a manual check has been necessary, computation time has been between 12 and 15 hours for one year of operation. The employed machines are 5-year-old office PCs with dual-core processor (processor frequency is 2 GHz). Since neither the script nor the PSE are optimized for parallel computing, on each core a script and PSE process has been running. The share of computational time needed for the calculations and the share of computational time needed for the script is not classified. The highest delay occurs if the script gets stuck and a manual check is necessary and when the solver runs into oscillations.

## 7 Simulation Results

Table 7.3 shows the calculation results for the three investigated power plants. Generator and net energy output rise with increasing SM. The capacity factor shows the same behaviour. Comparing the plant with the smallest and highest SM, doubling the SM and increasing the storage capacity by two full-load hours only raises the net power output by 27%. The net energy output increases only by 10% from the plant with the smallest SM to the plant with  $SM = 2$ . Average net efficiency decreases from the plant with the smallest to the highest SM. This shows that the TES system for the  $SM = 3$  plant is undersized, large amounts of heat must be dumped in case of full TES system and excess power from the SF.

Table 7.3: Calculation results for the performance prediction and yield analysis.

	$SM = 1.5$ $C_{FLH} = 7.5$	$SM = 2$ $C_{FLH} = 7.5$	$SM = 3$ $C_{FLH} = 9$
generator energy output $P_{gen}$	425 GW h	469 GW h	544 GW h
net energy output $P_{net}$	396 GW h	435 GW h	505 GW h
parasitic energy consumption $P_{par}$	29 GW h	34 GW h	39 GW h
energy from SF $Q_{SF}$	1135 GW h	1248 GW h	1454 GW h
energy to PB $Q_{PB}$	1135 GW h	1246 GW h	1458 GW h
energy to TES $Q_{TES,C}$	324 GW h	410 GW h	608 GW h
energy from TES $Q_{TES,D}$	325 GW h	412 GW h	612 GW h
average net efficiency $\eta_{avg}$	18 %	15 %	11 %
capacity factor $c_{el}$	56 %	62 %	70 %
storage efficiency $\eta_{TES}$	100.2 %	100.4 %	100.6 %
storage factor $\delta_{TES}$	29 %	33 %	42 %

Comparing stored energy  $Q_{TES,C}$  to retrieved energy from TES  $Q_{TES,D}$  the results seem to be surprising. More energy is discharged than charged. The energy sent to the PB is higher than the collected energy from the SF. This has a very simple explanation. Heat flow rates are calculated in the Flow-Distributor as the enthalpy difference of the inlet and outlet stream times the mass flow rate. The TES systems are very well insulated and the heat losses are low. In the power plant model in Figure 7.1 it can be seen that there are three pumps installed in the HTF and molten salt streams. The energy added from these pumps is also available as discharged energy. This compensates for heat losses or even exceeds them, and is the reason for a TES system efficiency of  $\eta_{TES} = 100\%$ .

For a  $SM = 1.5$  the TES system can be fully charged from the beginning of April to the end of August. In February, March, September and October it can be partly charged. From the beginning of November till the end of January it cannot be charged at all. During this period the plant can merely be operated in solar only mode. Figure 7.6 shows the heat and power flow rates of the plant at winter solstice. Power output has to follow the solar irradiation. The DNI and DII values

## 7.1 Power Plant with Two-Tank TES System

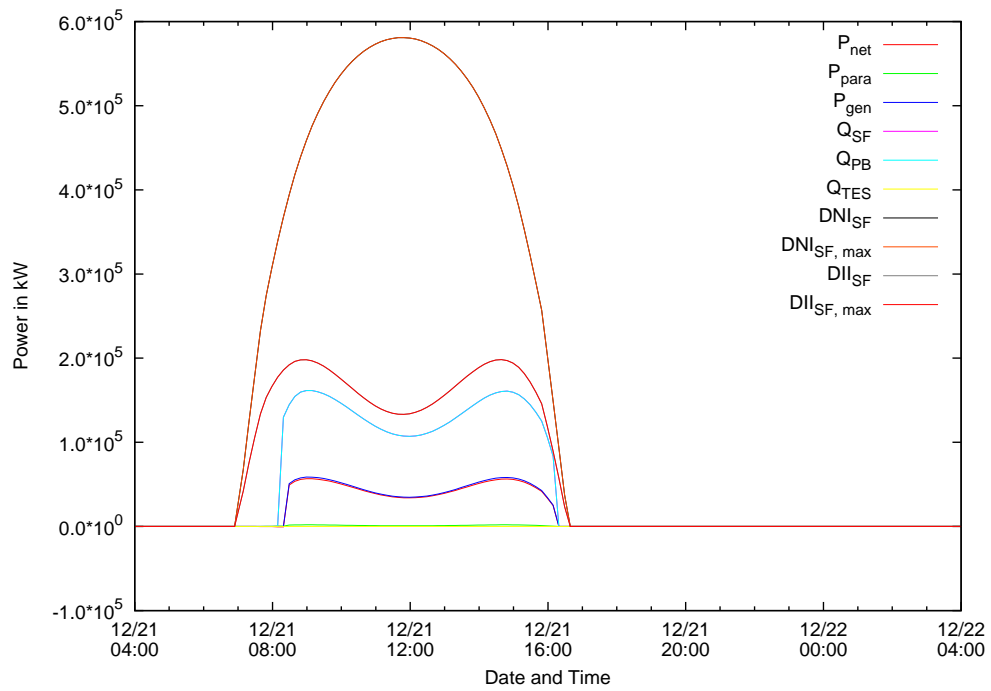


Figure 7.6: Heat and power flow rates for the  $SM = 1.5$ ,  $C_{FLH} = 7.5$  plant configuration on winter solstice.

## 7 Simulation Results

are identical with the DNI and DII maximum values since no collectors have to be defocused.

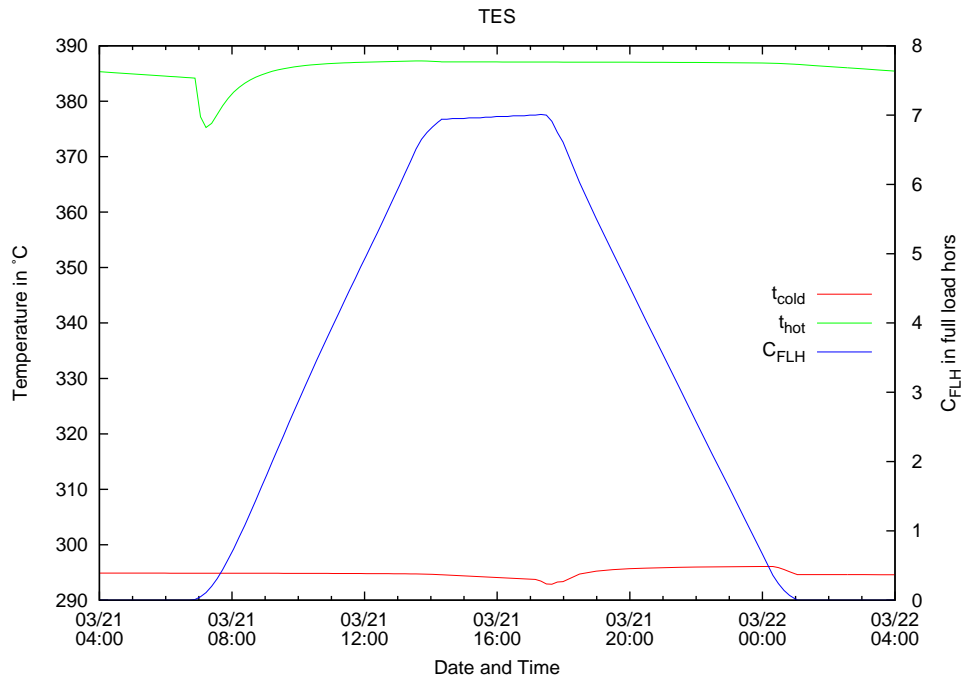


Figure 7.7: Hot and cold storage tank temperatures  $t_{hot}$  and  $t_{cold}$  and storage capacity of the  $SM = 2$ ,  $C_{FLH} = 7.5$  plant configuration on equinox.

For a  $SM = 2$  only a few weeks around winter solstice the TES system cannot be charged at all. From March to the mid-October it can be fully charged, but is accompanied with the need to defocus collectors as well. In Figure 7.7 it can be seen that already at equinox the TES system is fully charged at 1 PM. With a  $SM = 3$  the TES system can be charged all year long, from November to January only partly. This is also the only period where the whole solar field can be utilized. For the rest of the year, large parts of the collectors must be defocused. For example, on summer solstice the TES system is fully charged at 10 AM, for the rest of the day till sunset the plant must be operated in solar only mode. The heat and power rates of this plant on summer solstice are depicted in Figure 7.8. Only a small part of the SF can be utilized.

This already shows shortcomings when designing a solar thermal power plant with TES. If the SF is oversized compared to the TES system, this results in good utilization of the TES system but large amounts of damped energy. If it is the other way round, the TES system is poorly utilized.



## 7.1 Power Plant with Two-Tank TES System

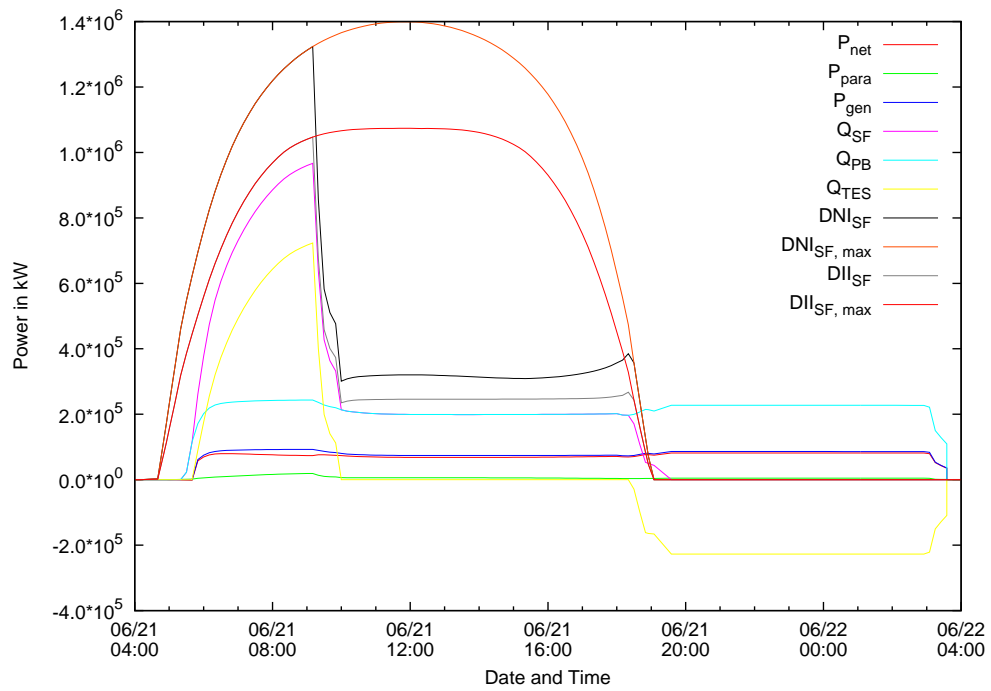


Figure 7.8: Heat and power flow rates for the  $SM = 3$ ,  $C_{FLH} = 9$  plant configuration on summer solstice.

## 7.2 Power Plant with Thermocline TES System

The PB configuration of before is connected with a thermocline TES system. Figure 7.9 shows the power plant with a  $SM = 1.5$  and a thermocline TES system with a storage capacity of  $C_{FLH} = 7.5$  full-load hours. The thermocline TES system is at the bottom in the middle, below the oil-to-salt heat exchanger. The power plant models are used to carry out a performance prediction and annual yield analysis again.

The design parameters for the thermocline tanks can be found in Table 7.4. The design temperature is a few degrees higher than compared to the two-tank systems. This leads to a slightly bigger tank size. The tank walls are made of concrete again. The insulation of the thermocline tanks is thicker compared to the two-tank tanks. The conduction coefficient is the same as for the smaller of the two-tank tanks.

Table 7.4: Tank dimensions and storage mass.

	$SM = 1.5$ $C_{FLH} = 7.5$	$SM = 2$ $C_{FLH} = 7.5$	$SM = 3$ $C_{FLH} = 9$
mass flow rate PB $\dot{m}_{PB,0}$	$936.5 \text{ kg s}^{-1}$	$950.5 \text{ kg s}^{-1}$	$977 \text{ kg s}^{-1}$
inner diameter $D_i$	20 m	20 m	20 m
wall thickness $x_{wall}$	0.3 m	0.3 m	0.3 m
insulation thickness $x_{ins}$	1 m	1 m	1 m
cond. coeff. wall $k_{wall}$	$0.7 \text{ W m}^{-1} \text{ K}^{-1}$	$0.7 \text{ W m}^{-1} \text{ K}^{-1}$	$0.7 \text{ W m}^{-1} \text{ K}^{-1}$
cond. coeff. insulation $k_{ins}$	$0.05 \text{ W m}^{-1} \text{ K}^{-1}$	$0.05 \text{ W m}^{-1} \text{ K}^{-1}$	$0.05 \text{ W m}^{-1} \text{ K}^{-1}$
conv. coeff. ambient $h_{amb}$	$8 \text{ W m}^{-2} \text{ K}^{-1}$	$8 \text{ W m}^{-2} \text{ K}^{-1}$	$8 \text{ W m}^{-2} \text{ K}^{-1}$
design temp. hot $t_{hot,0}$	$388 \text{ }^\circ\text{C}$	$388 \text{ }^\circ\text{C}$	$388 \text{ }^\circ\text{C}$
design temp. cold $t_{cold,0}$	$290 \text{ }^\circ\text{C}$	$290 \text{ }^\circ\text{C}$	$290 \text{ }^\circ\text{C}$
mass $m$	$4.2 \times 10^7 \text{ kg}$	$4.2 \times 10^7 \text{ kg}$	$5.2 \times 10^7 \text{ kg}$
mass node $m_N$	$2.1 \times 10^6 \text{ kg}$	$2.1 \times 10^6 \text{ kg}$	$2.6 \times 10^6 \text{ kg}$

The operation strategy is the same as for the two-tank power plants. For thermocline TES systems it is a little bit tricky to determine the charging status. For two-tank systems it is straight forward, if the hot tank is full, the system is fully charged, if it is empty, it is discharged. A proposal to determine charging status of a thermocline TES system is to compare the stored heat in the tank to the stored heat at design conditions. If the heat stored is higher than the heat stored in the tank at  $t_{hot,0}$ , the TES system is fully charged. If the heat stored is lower than the heat stored in the tank at  $t_{cold,0}$ , the TES system is discharged. This does not lead to satisfying results. The hot design temperature  $t_{hot,0}$  can never be reached throughout the whole tank. If the TES system is charged with fluid below design temperature, the temperature in the whole tank might be close to design temperature, but the calculated charging

## 7.2 Power Plant with Thermocline TES System

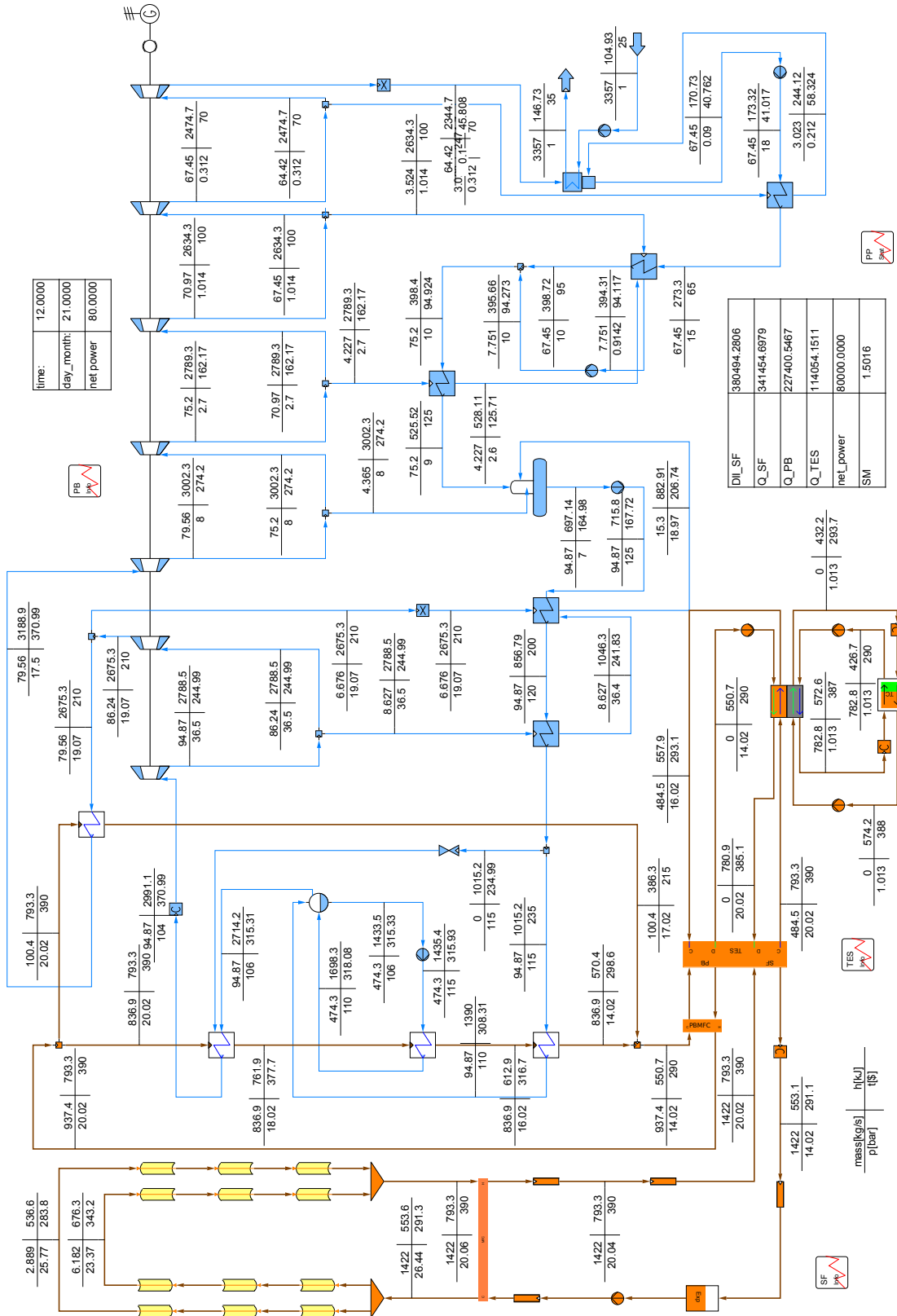


Figure 7.9: Flow sheet of the power plant with a thermocline TES system.

## 7 Simulation Results

status does not indicate a fully charged TES system. If at the bottom of the tank temperatures are below  $t_{cold,0}$ , but on top there is heat stored at temperatures suitable for discharging, the calculated charging indicates an empty TES system in case the heat stored in the whole tank is below  $H(t_{cold,0})$ . Therefore the use of  $C_{TES}$  and the transition relations used above is not convincing.

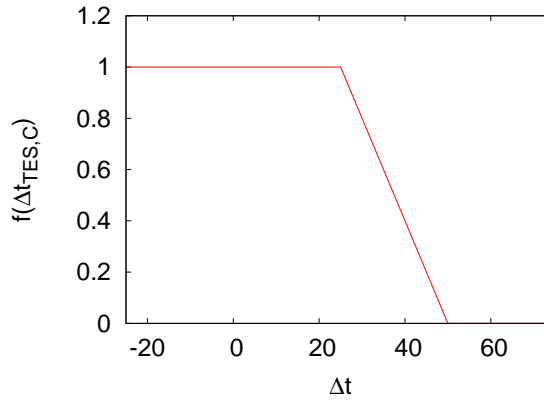


Figure 7.10: Decreasing ramp when the TES system becomes full.

If the TES is close to fully charged, the outlet temperature of the charging stream increases. The temperature difference between the PB outlet and the return stream from charging the TES system  $\Delta t_{TES,C} = t_{TES,C,out} - t_{PB,out}$  is a good indicator whether the TES system is fully charged or not. Therefore it is used in following relation to decrease the mass flow rate to the TES system:

$$\dot{m}_{TES,C} = f(\Delta t_{TES,C}) \cdot \dot{m}_{TES,C,max} \quad (7.6)$$

$\dot{m}_{TES,C,max}$  is the maximum flow rate that can be sent to the TES if all collectors are focused.  $f(\Delta t_{TES,C})$  can be found in Figure 7.10:

If the TES system is close to fully discharged, the fluid temperature decreases. The temperature difference between the minimum fluid temperature that can be fed to the PB and the discharge fluid temperature  $\Delta t_{TES,D} = t_{TES,D,out} - t_{PB,min}$  is used as an indicator of the TES empty. In case the TES is empty with still energy provided by the SF, the mass flow rate to the PB is determined as:

$$\dot{m}_{PB} = \dot{m}_{SF} + (\dot{m}_{PB,tar} - \dot{m}_{SF}) f(\Delta t_{TES,D}) \quad (7.7)$$

In case of power block shut-down with the SF disconnected, following relation is used:

## 7.2 Power Plant with Thermocline TES System

$$\dot{m}_{PB} = \dot{m}_{PB,min} + (\dot{m}_{PB,tar} - \dot{m}_{PB,min}) f(\Delta t_{TES,D}) \quad (7.8)$$

$f(\Delta t_{TES,D})$  can be found in Figure 7.11. The fluid temperature to the PB is allowed to decrease to  $t_{PB,min} = 330^\circ\text{C}$  and minimum mass flow rate to the PB is  $\dot{m}_{PB,min} = 300 \text{ kg s}^{-1}$ .

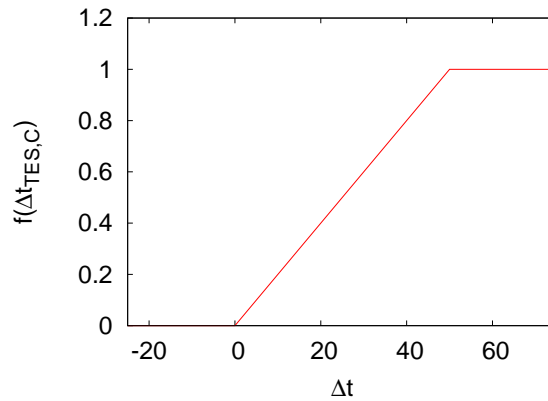


Figure 7.11: Decreasing ramp when the TES system becomes empty.

The same computers as for the two-tank calculations were employed here. During daylight the time increment is set to 10 minutes and to 20 minutes at night. It was not possible to set the increment to 30 minutes, because of the stability criterion of the thermocline tank nodes. Due to the smaller time step during the night more than 40000 calculation steps are necessary to complete the annual yield analysis. Computation time was a little bit shorter than for the two-tank systems. Some procedures in the script and equations in the power plant model which performed so well in the preceding simulations were improved. Nevertheless, it still took 12 to 14 hours to complete the task.

Table 7.5 shows the calculation results for the three investigated power plants. The observations which have already been made for the two-tank plants also apply here. Results are comparable to the results predicted for the two-tank storage system plants. Annual energy output is slightly lower than compared the plants with the two-tank TES system. Evaluation of annual performance of two-tank and thermocline thermal storage systems for trough plants carried out by Kolb [Kol11] showed similar results. He points out that thermocline systems can perform as well as two-tank system if degradation in temperature of the fluid sent to the PB is allowed. The higher the allowed degradation the higher the net energy output.

## 7 Simulation Results

Table 7.5: Calculation results for the performance prediction and yield analysis.

	$SM = 1.5$ $C_{FLH} = 7.5$	$SM = 2$ $C_{FLH} = 7.5$	$SM = 3$ $C_{FLH} = 9$
generator energy output $P_{gen}$	414 GW h	460 GW h	529 GW h
net energy output $P_{net}$	387 GW h	428 GW h	493 GW h
parasitic energy consumption $P_{par}$	27 GW h	32 GW h	36 GW h
energy from SF $Q_{SF}$	1119 GW h	1236 GW h	1438 GW h
energy to PB $Q_{PB}$	1121 GW h	1239 GW h	1440 GW h
energy to TES $Q_{TES,C}$	312 GW h	397 GW h	581 GW h
energy from TES $Q_{TES,D}$	314 GW h	400 GW h	583 GW h
average net efficiency $\eta_{avg}$	18 %	15 %	11 %
capacity factor $c_{el}$	56 %	61 %	70 %
storage efficiency $\eta_{TES}$	100.6 %	100.8 %	100.3 %
storage factor $\delta_{TES}$	27 %	32 %	41 %

For the same reason as described for the two-tank storage systems, more energy is retrieved from the thermocline tanks than added. Therefore more heat is sent to the PB than collected by the SF over the year.

The predicted changes in temperature profile in the thermocline tank of the  $SM = 1.5$ ,  $C_{FLH} = 7.5$  plant configuration for several charge and discharge cycles at the beginning of May are depicted in Figure 7.12. The temperature drop in the top node when the TES becomes full is caused by the temperature drop in SF fluid when defocusing collectors.

SF temperatures and the mass flow rate for the same plant for one of these days, the 4<sup>th</sup> of May, is shown in Figure 7.13. The rise in  $t_{SF,in}$  at 2 PM is caused by hotter fluid coming from the TES system. Defocusing or focusing collectors is the reason for the small fluctuations in SF mass flow rate and temperatures. Such a behaviour cannot be observed in a real SF.

In Figure 7.14 the heat flow and power rates on 15<sup>th</sup> of October of the  $SM = 3$ ,  $C_{FLH} = 9$  power plant configuration are depicted. The peak in  $\dot{Q}_{PB}$  is caused by the PB warm-up model. Transitions between the operating modes are realized much smoother than with the two-tank models.

## 7.2 Power Plant with Thermocline TES System

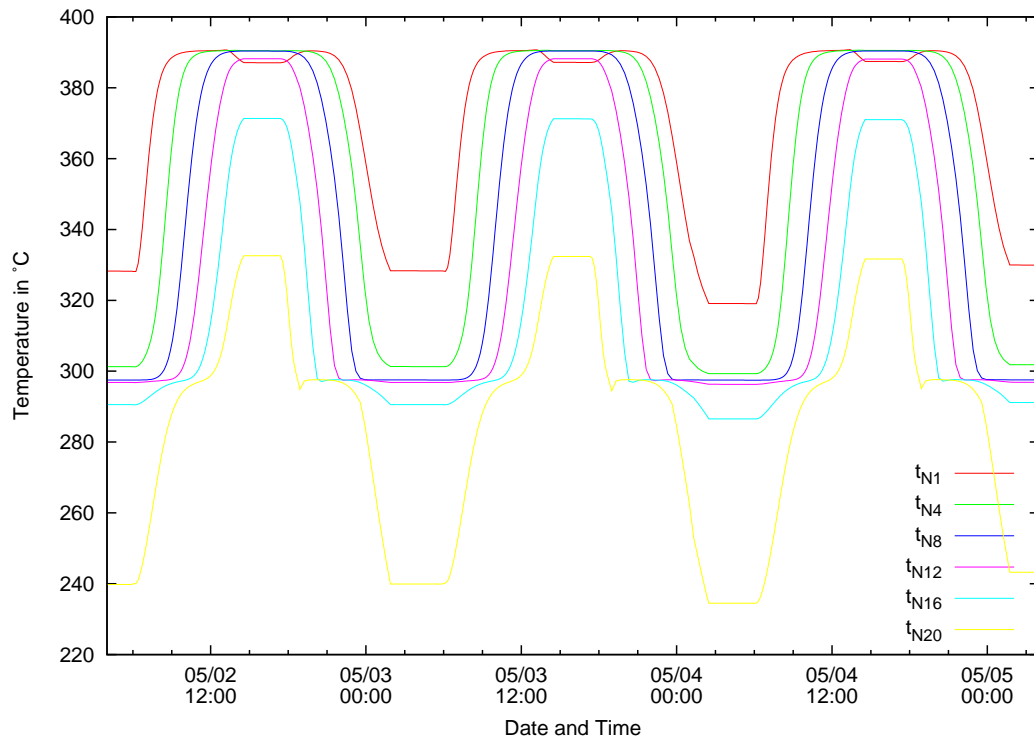


Figure 7.12: Simulation results of temperature profile throughout the thermocline tank of the  $SM = 1.5$ ,  $C_{FLH} = 7.5$  plant configuration on three days at the beginning of May. Node N20 is at the bottom of the tank and node N1 is at the top.

## 7 Simulation Results

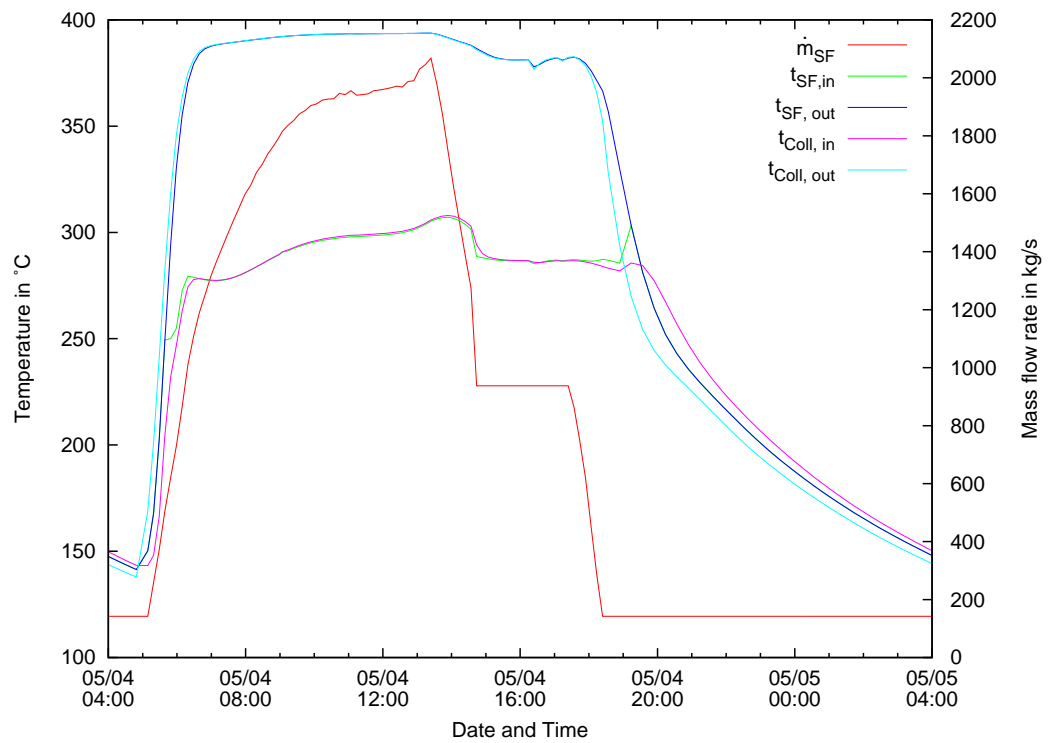


Figure 7.13: Predicted mass flow rates and temperatures in the SF of the  $SM = 1.5$ ,  $C_{FLH} = 7.5$  plant configuration on 4<sup>th</sup> of May.



## 7.2 Power Plant with Thermocline TES System

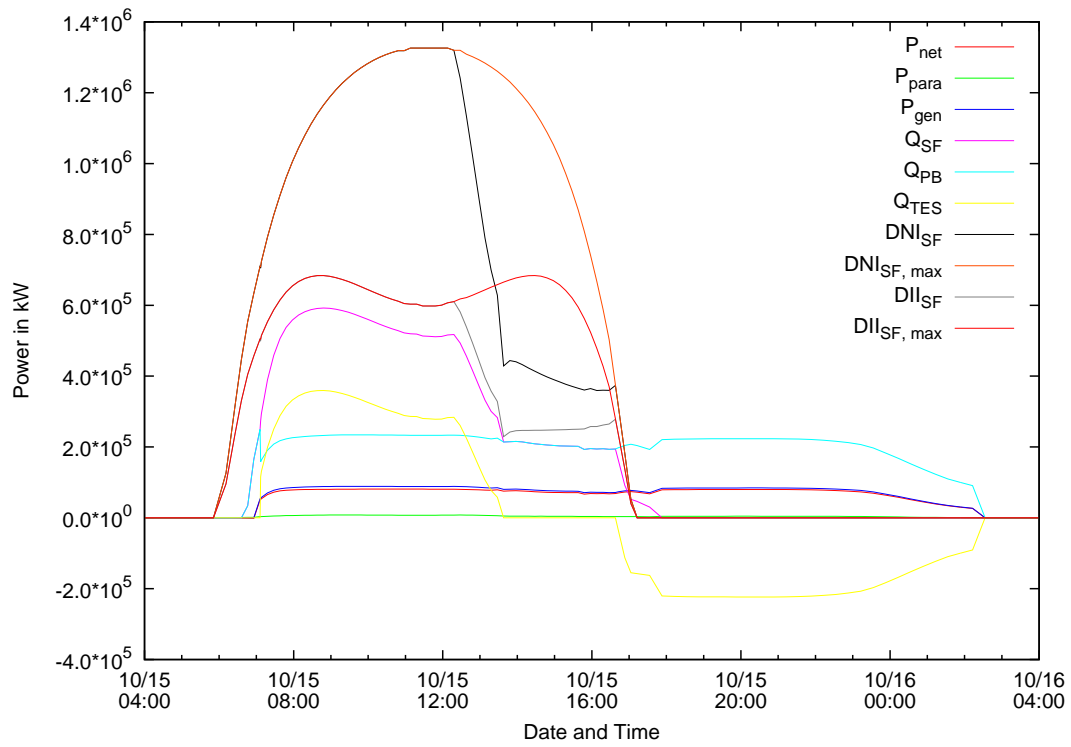


Figure 7.14: Predicted heat and power flow rates of the  $SM = 1.5$ ,  $C_{FLH} = 7.5$  plant configuration on 15<sup>th</sup> of October.



## 8 Conclusions and Outlook

A short summary of the work carried out is given here. The last section in this work gives an outlook on future work.

### 8.1 Conclusions

The goal of this work is reached. A simulation tool for transient time series analysis of solar thermal power plants with thermal energy storage was developed. Component models for a two-tank and a thermocline TES were developed. Solar thermal power plant models with the two-tank and the thermocline model were set up. The SF and the TES consist of transient component models except for the headers and the heat exchangers. These components are steady state models. The PB consists of steady state component models as well. The developed simulation tool was used to conduct a performance prediction and annual yield analysis for the power plant models with the two-tank and thermocline TES system.

The transient collector model was developed from an already existing steady state model. Transient models for piping and the expansion vessel were established. A header model that reflects the defocusing of collectors in a row was developed. New models of two-tank and thermocline storage systems were implemented.

The Flow-Distributor connects the SF, PB and the TES system. It replaces a set of mixers and splitters and makes the power plant model in IPSEpro more clearly.

An automation script which shifts the IPSEpro power plant model from one calculation step to the next was implemented. The script also changes the operation mode if any value falls below or exceeds a limiting value. Calculation values of interest are saved by the script as well.

The main aim of this work was not to create the most detailed solar thermal power plant model. Rather, the focus has been to show the possibility of carrying out a performance prediction and annual yield analysis with a power plant model in PSE using an automatizing script. The duration of computation time for this kind of simulations and the question whether this approach has advantages compared to

## 8 Conclusions and Outlook

the current approaches, where IPSEpro in combination with MS Excel is used, has been of interest as well.

The simulation results presented in Section 7.1 and 7.2 do not give a realistic prediction of annual performance for such a plant at the investigated location. No detailed weather and irradiation data were used. DNI was calculated by Hottel's clear sky solar radiation model and ambient temperature is assumed to stay constant.

All in all the feasibility to conduct transient time series analysis was shown delivering satisfying result: The use of the automation script allows a higher flexibility and gives more possibilities than the current approach where MS Excel is used. This method has the possibility to decrease computation time in such simulations compared to current methods and delivers accurate and very detailed results.

### 8.2 Outlook

For future development four main points have to be tackled:

- more realistic boundary conditions
- more detailed power plant model
- verification of TES models
- increase numerical calculation stability
- decrease computation time

To begin with the boundary conditions, the use of measured DNI and ambient temperature data is recommended. A SF model which depicts the reality better is necessary, especially when parts of the SF are defocused. The adaption of the SF mass flow prediction for the case of defocused collectors is also necessary. Together with a more detailed modelling of the SF hydraulics and a part load model for the SF pumps this allows a better estimation of pumping power parasitics.

The Flow-Distributor contains many branched equations. This makes the model a little bit confusing and negatively affects the stability of the solution system. The equations in this component might be simplified. Some of the equations might be moved to separate component models for a better clarity.

Potential to decrease computation time can be found in the script, the model equations and in the solver. If the solver was adapted for parallel computing, the computation time for a single calculation step can be decreased [Per12]. The use of fewer branched equations also improves calculation speed. The automation script shows potentials for improvements as well. Communication over the COM interface works slowly. Reducing the communication events to a minimum decreases computation time.

# Bibliography

- [Adi10] Roman Adinberg. “R15.1 Report on the Methodology to Characterize Various Types of Thermal Storage Systems: Project SFERA.” In: (2010). (Visited on 02/21/2012) (cit. on p. 5).
- [Bec09] M. Beckmann. *Skriptum - Kraftwerksanlagen für Elektrotechniker*. Dresden, 2009. URL: %5Curl%7Bhttp://tu-dresden.de/die\_tu\_dresden/fakultaeten/fakultaet\_maschinenwesen/iet/vws/Lehre/Kraftwerksanlagen\_E-Techniker%7D (cit. on p. 75).
- [BG84] G. Beckmann and P. V. Gilli. *Thermal energy storage: Basics, design, applications to power generation and heat supply / G. Beckmann, P.V. Gilli*. Topics in energy. Wien: Springer, 1984. ISBN: 0387817646 (cit. on pp. 10–12).
- [Bro+05] Doug Brosseau et al. “Testing of Thermocline Filler Materials and Molten-Salt Heat Transfer Fluids for Thermal Energy Storage Systems in Parabolic Trough Power Plants.” In: *Journal of Solar Energy Engineering* 127.1 (2005), p. 109. ISSN: 01996231. DOI: \url{10.1115/1.1824107} (cit. on p. 23).
- [CKK99] Gilbert Cohen, D. Kearney, and Gregory J. Kolb. *Final Report in the Operation and Maintenance Improvement Program for Concentrating Solar Power Plants*. 1999 (cit. on pp. 53, 54).
- [DB06] John A. Duffie and William A. Beckman. *Solar engineering of thermal processes*. 3rd ed. Hoboken and N.J: Wiley, 2006. ISBN: 0471698679 (cit. on pp. 43–45, 68).
- [DGT91] F. Dinter, Michael A. Geyer, and R. Tamme. *Thermal energy storage for commercial applications: A feasibility study on economic storage systems*. Berlin: Springer-Verlag, 1991. ISBN: 9780387530543 (cit. on pp. 17, 18, 20, 25).
- [DLB12] Rebecca Dunn, Keith Lovegrove, and Greg Burgess. “A Review of Ammonia-Based Thermochemical Energy Storage for Concentrating Solar Power.” In: *Proceedings of the IEEE* 100.2 (2012), pp. 391–400. ISSN: 0018-9219. DOI: \url{10.1109/JPROC.2011.2166529} (cit. on pp. 15, 26).
- [DR02] İbrahim Dincer and Marc Rosen. *Thermal energy storage systems and applications*. New York and Chichester: Wiley, 2002. ISBN: 0471495735 (cit. on pp. 9, 11).

## Bibliography

- [Eur11] European Academies Science Advisory Council. *Concentrating solar power: Its potential contribution to a sustainable energy future*. Halle (Saale), 2011. ISBN: 978-3-8047-2944-5 (cit. on p. 6).
- [Foro4] Martin Forster. "Theoretical investigation of the system SnO<sub>x</sub>/Sn for the thermochemical storage of solar energy." In: *Energy* 29.5-6 (2004), pp. 789–799. ISSN: 03605442. DOI: \url{10.1016/S0360-5442(03)00185-3} (cit. on p. 15).
- [Gey87] Michael A. Geyer. *Hochtemperatur-Speichertechnologie: Konzeption, Betriebsverhalten und Wirtschaftlichkeit eines modularen Gesteinsspeichers als Komponente in Solarturmkraftwerken*. Berlin: Springer, 1987. ISBN: 9783540180296 (cit. on pp. 5, 18, 20, 24, 29).
- [Gil+10] Antoni Gil et al. "State of the art on high temperature thermal energy storage for power generation. Part 1—Concepts, materials and modelization." In: *Renewable and Sustainable Energy Reviews* 14.1 (2010), pp. 31–55. ISSN: 13640321. DOI: \url{10.1016/j.rser.2009.07.035} (cit. on pp. 12–14, 22, 26).
- [GKo8] D. Yogi Goswami and Frank Kreith. *Energy conversion*. Mechanical engineering series. Boca Raton and Fla: CRC and London : Taylor & Francis [distributor], 2008. ISBN: 1420044311. URL: %5Curl%7Bhttp://www.loc.gov/catdir/enhancements/fy0727/2007017629-d.html%7D (cit. on pp. 2–4, 49–51, 60, 61, 73).
- [Grao2] Bernd Graf. "Untersuchung der Kopplungsmöglichkeiten von Parabolrinnenkollektoren mit GuD - Kraftwerken." PhD thesis. Stuttgart: Deutsches Zentrum für Luft- und Raumfahrt e.V., 2002 (cit. on p. 76).
- [Hado6] Jean-Christophe Hadorn, ed. *Thermal energy storage for solar and low energy buildings: State of the art by the IEA Solar Heating and Cooling Task 32*. IEA, 2006 (cit. on p. 15).
- [HKPo4] Ulf Herrmann, Bruce Kelly, and Henry Price. "Two-tank molten salt storage for parabolic trough solar power plants." In: *Energy* 29.5-6 (2004), pp. 883–893. ISSN: 03605442. DOI: \url{10.1016/S0360-5442(03)00193-2} (cit. on pp. 13, 21–24).
- [Hot76] Hoyt C. Hottel. "A simple model for estimating the transmittance of direct solar radiation through clear atmospheres." In: *Solar Energy* 18.2 (1976), pp. 129–134. ISSN: 0038092X. DOI: \url{10.1016/0038-092X(76)90045-1} (cit. on pp. 45, 46).
- [Hub09] C. Huber. *Modellbildung und Simulation des Wasser-Dampf-Kreislaufes eines solarthermischen Kraftwerkes*. Tech. rep. Graz, 2009 (cit. on p. 77).

- [Hun94] D. Hunold. *Zur Auslegung und Konstruktion von thermischen Energiespeichern mit einem fest-flüssig Phasenwechsel des Speichermaterials für Parabolrinnen-Solkraftwerke*. Düsseldorf and, 1994. ISBN: 9783183308064 (cit. on p. 11).
- [KMS08] Gerhard Knies, Uwe Möller, and Michael Straub, eds. *Clean power from deserts: The DESERTEC concept for energy, water and climate security ; [white paper]*. 3rd ed. Bonn: Protex-Verl, 2008. ISBN: 9783929118674 (cit. on p. 1).
- [Kol11] Gregory J. Kolb. "Evaluation of Annual Performance of 2-Tank and Thermocline Thermal Storage Systems for Trough Plants." In: *Journal of Solar Energy Engineering* 133.3 (2011), pages. DOI: \url{10.1115/1.4004239} (cit. on pp. 23, 24, 107).
- [Lai+06] Doerte Laing et al. "Solid media thermal storage for parabolic trough power plants." In: *Solar Energy* 80.10 (2006), pp. 1283–1289. ISSN: 0038092X. DOI: \url{10.1016/j.solener.2006.06.003} (cit. on pp. 12, 13, 25).
- [Lai+08] Doerte Laing et al. "Solid Media Thermal Storage Development and Analysis of Modular Storage Operation Concepts for Parabolic Trough Power Plants." In: *Journal of Solar Energy Engineering* 130.1 (2008). ISSN: 01996231. DOI: \url{10.1115/1.2804625} (cit. on p. 25).
- [Mat12] Mathworks. *Matlab Product Documentation*. 2012. URL: %5Curl%7Bhttp://www.mathworks.de/help/techdoc/matlab\_external/f89715.html#f116268%7D (visited on 08/28/2012) (cit. on p. 42).
- [Med+10] Marc Medrano et al. "State of the art on high-temperature thermal energy storage for power generation. Part 2—Case studies." In: *Renewable and Sustainable Energy Reviews* 14.1 (2010), pp. 56–72. ISSN: 13640321. DOI: \url{10.1016/j.rser.2009.07.036} (cit. on p. 22).
- [Mic12] Microsoft. *Microsoft Developer Network*. 2012. URL: %5Curl%7Bhttp://msdn.microsoft.com/en-US/%7D (visited on 08/28/2012) (cit. on p. 41).
- [Milo4] D. Mills. "Advances in solar thermal electricity technology." In: *Solar Energy* 76.1-3 (2004), pp. 19–31. ISSN: 0038092X. DOI: \url{10.1016/S0038-092X(03)00102-6} (cit. on p. 4).
- [Mon+09] M.J Montes et al. "Solar multiple optimization for a solar-only thermal power plant, using oil as heat transfer fluid in the parabolic trough collectors." In: *Solar Energy* 83.12 (2009), pp. 2165–2176. ISSN: 0038092X. DOI: \url{10.1016/j.solener.2009.08.010} (cit. on p. 17).
- [Nato5] National Renewable Energy Laboratory. *National Solar Radiation Data Base: 1991- 2005 Update: Typical Meteorological Year 3*. 2005. URL: %5Curl%7Bhttp://rredc.nrel.gov/solar/old\_data/nsrdb/1991-2005/tmy3/%7D (cit. on p. 44).

## Bibliography

- [Nat12a] National Renewable Energy Laboratory. *Solar Radiation Research Laboratory: Baseline Measurement System BMS*. 2012. URL: %5Curl%7Bhttp://www.nrel.gov/midc/srrl\_bms/%7D (visited on 09/19/2012) (cit. on p. 47).
- [Nat12b] National Renewable Energy Laboratory. *Solar Resource & Meteorological Assessment Project (SOLRMAP) : Escalante*. 2012. URL: %5Curl%7Bhttp://www.nrel.gov/midc/ts\_escalante/%7D (visited on 09/19/2012) (cit. on p. 47).
- [NSo7] Bo Nordell and Kjell Skogsberg. "THE SUNDSVALL SNOW STORAGE-SIX YEARS OF OPERATION." In: *Thermal Energy Storage for Sustainable Energy Consumption*. Ed. by Halime Ö. Paksoy. Vol. 234. NATO Science Series. Springer Netherlands, 2007, pp. 349–366. ISBN: 978-1-4020-5290-3. doi: \url{10.1007/978-1-4020-5290-3\_21} (cit. on p. 11).
- [OMB96] S.D Odeh, G.L Morrison, and M. Behnia. *Thermal Analysis of Parabolic Trough Solar Collectors for Electric Power Generation*. Tech. rep. Sydney: University of New South Wales, 1996 (cit. on p. 50).
- [PBo6] E. Perz and S. Bergmann, eds. *A Simulation Environment for the Techno-economic Performance Prediction of Water and Power Cogeneration Systems Using Renewable and Fossil Energy Sources*. 2006 (cit. on pp. 35, 36).
- [Per12] E. Perz. : *personal communication*. Ed. by L. Kriechbaum. 2012 (cit. on p. 114).
- [Pla07] Plataforma Solar de Almeria. *Annual Report 2007*. 2007 (cit. on p. 21).
- [PSK01] J. Pacheco, S. Showalter, and W. Kolb. "Development of a Molten-Salt Thermocline Thermal Storage System for Parabolic Trough Plants." In: (2001). (Visited on 02/13/2012) (cit. on p. 24).
- [Rat95] Rainer Ratzesberger. *Regeneratoren in Parabolrinnen-Solarkraftwerken*. Als Ms. gedr. Düsseldorf: VDI-Verl., 1995. ISBN: 9783183330065 (cit. on p. 73).
- [RBE08] J. Rheinländer, S. Bergmann, and M. R. Erbes. "Technical and Economic Performance of Parabolic Trough Solar Power Plants - A Computational Tool for Plant Feasibility Studies." In: *14th SolarPACES International Symposium on Concentrated Solar Power and Chemical Energy Technologies*. 2008 (cit. on p. 18).
- [REB10] J. Rheinländer, M. R. Erbes, and S. Bergmann, eds. *Simulations of solar field start-up in a PTC-CSP plant*. 2010 (cit. on pp. 51, 58, 59).



- [RZo7] Manuel Romero-Alvarez and Eduardo Zarza. "Concentrating solar thermal power." In: *Handbook of Energy Efficiency and Renewable Energy*. Ed. by Frank Kreith and D. Yogi Goswami. Mechanical engineering series. Boca Raton and London: Taylor & Francis, 2007. ISBN: 0849317304 (cit. on p. 50).
- [Sim02] SimTech Simulation Technology. *IPSEpro - The Design Suite: Company Pamphlet*. Graz, 2002 (cit. on pp. 35, 36).
- [Sim11a] SimTech Simulation Technology. *IPSEpro Process Simulator - COM Interface*. 5.0.001. Graz: SimTech Simulation Technology, 2011 (cit. on pp. 40, 41).
- [Sim11b] SimTech Simulation Technology. *IPSEpro Process Simulator - Model Development Kit*. 5.0.001. Graz: SimTech Simulation Technology, 2011 (cit. on pp. 37–40).
- [Sim11c] SimTech Simulation Technology. *IPSEpro Process Simulator - Process Simulation Environment*. 5.0.001. Graz: SimTech Simulation Technology, 2011 (cit. on pp. 40, 41).
- [SL45] Aurel Stodola and Louis Centennial Loewenstein. *Steam and gas turbines*. New York: P. Smith, 1945 (cit. on p. 77).
- [Stro6] Karl Strauß. *Kraftwerkstechnik: Zur Nutzung fossiler, nuklearer und regenerativer Energiequellen*. 5th ed. Berlin u.a: Springer, 2006. ISBN: 978-3-540-29666-9 (cit. on p. 76).
- [Trio4] Franz Trieb. *SOKRATES-Projekt: Solarthermische Kraftwerkstechnologie für den Schutz des Erdklimas ; Zusammenfassung des Projektberichts ; Zukunftsinvestitionsprogramm des Bundesministeriums für Umwelt, Naturschutz und Reaktorsicherheit ; SOKRATES Z II 6(D)-46040-1/3.1*. Stuttgart [u.a.], 2004 (cit. on p. 77).
- [Zal+03] Belén Zalba et al. "Review on thermal energy storage with phase change: materials, heat transfer analysis and applications." In: *Applied Thermal Engineering* 23 (2003), pp. 251–283. ISSN: 13594311 (cit. on p. 14).
- [Zav+12] Fritz Zaversky et al. "Part Load Behavior of Oil-to-Molten-Salt Heat Exchanger Configurations for Active Indirect Storage Systems in CSP Applications." In: *Proceedings of the 18th SolarPACES International Symposium on Concentrated Solar Power and Chemical Energy Systems*. Marrakech, 2012 (cit. on p. 63).
- [Zav10] Fritz Zaversky. "Solar Thermal Power Plants: Modelling of Parabolic Trough Collector Concepts." MA thesis. Graz: TU Graz, 2010 (cit. on pp. 43, 45, 47, 50).